

**DYNAMIC PERFORMANCE OF TALL WOOD BUILDINGS WITH FLUID
VISCOUS DAMPERS**

by

Mohamed Elshamy

B.E., Jordan University of Sciences and Technology, 2016

THESIS SUBMITTED IN PARTIAL FULFILLMENT OF
THE REQUIREMENTS FOR THE DEGREE OF
MASTER OF APPLIED SCIENCE
IN
ENGINEERING

UNIVERSITY OF NORTHERN BRITISH COLUMBIA

March 2025

© Mohamed Elshamy, 2025

Abstract

As lightweight and slender tall timber designs gain popularity, seismic loads and wind-induced vibrations are becoming a prominent concern in modern structural engineering. The reduced mass and stiffness of these structures render them flexible and, consequently, more susceptible to dynamic oscillations, which can affect both life safety and occupant comfort. Moreover, knowledge of damping characteristics in tall timber buildings is limited because of the relatively small number of completed projects. Nonetheless, as building height increases, a corresponding decrease in damping values becomes evident, rendering tall structures more susceptible to lateral drift and occupant discomfort during seismic and wind events. In response, the British Columbia Building Code has recently limited timber buildings to 18 stories, underscoring the need for advanced seismic and wind mitigation strategies in such designs.

This thesis addresses these challenges by developing numerical models of three 18-story timber buildings and subjecting them to dynamic wind analysis and nonlinear time history seismic analysis to capture their complex oscillatory behaviour. Fluid viscous dampers (FVDs) were strategically integrated into each model to align overall performance with the National Building Code of Canada criteria. The findings indicate that using FVDs reduces lateral drift, particularly in regions prone to seismic activity, and significantly enhances occupant comfort under wind-induced vibrations. Moreover, comparative assessments of multiple damper configurations illuminate how these devices can effectively balance wind and seismic demands, offering more profound insight into optimizing tall timber structures.

In conclusion, this work confirms the viability of modern tall timber buildings as a resilient, eco-friendly solution while providing practical guidelines for damper integration to safeguard both structural integrity and occupant well-being in the face of multifaceted dynamic loads.

Table of Contents

Abstract.....	ii
Table of Contents.....	iv
List of Tables.....	iv
List of Figures	v
Dedication	ix
Acknowledgment.....	x
1 Introduction.....	1
1.1 Background.....	1
1.2 Motivation.....	3
1.3 Research Scope and Objectives	3
1.4 Organization.....	4
2 Literature Review	6
2.1 Modern Tall Timber Buildings.....	6
2.1.1 Dynamic Challenges in Tall Timber Buildings.....	8
2.2 Timber As a Structure Material.....	9
2.2.1 Wood Properties	10
2.2.2 Orthotropic Behavior	10
2.2.3 Weight of Timber	12
2.2.4 Influence of Moisture.....	13
2.3 Innovative Timber Products Suitable for Tall Buildings	14
2.3.1 Structural Composite Lumber (SCL).....	15
2.3.2 Mass Timber.....	15
2.4 Structure Systems for Tall Buildings	18
2.4.1 Frame System.....	19
2.4.2 Braced System	20
2.4.3 Shear-Wall System	21
2.4.4 Core System.....	22
2.4.5 Outrigger-Belt Truss System.....	23
2.5 Lateral Load Considerations	24
2.5.1 Wind Load on Tall Buildings	24
2.5.2 Seismic Loads on Tall Buildings	30
2.5.3 Ductility and Overstrength.....	37
2.5.4 Structure Irregularities	38

3	Dynamic Performance of Tall Buildings	40
3.1	Theoretical Basis	40
3.1.1	SDOF System	40
3.1.2	MDOF System	41
3.1.3	Natural Frequencies and Mode Shapes	43
3.2	Damping of Tall Wood Buildings	45
3.3	Passive Structure Control Techniques	49
3.3.1	Passive Rate-Dependent Dampers	51
4	Analysis of Tall Wood Buildings	57
4.1	Braced Frame Building	57
4.1.1	Structural Specifications	58
4.1.2	Numerical Modeling	60
4.1.3	Modal Analysis Results	62
4.2	Core System Building	62
4.2.1	Structural Specifications	63
4.2.2	Numerical Modeling	64
4.2.3	Modal Analysis Results	67
4.3	Outrigger-Belt Truss Building	68
4.3.1	Structural Specifications	68
4.3.2	Numerical Modeling	70
4.3.3	Modal Analysis Results	71
4.4	Seismic Analysis	72
4.4.1	Equivalent Static Load Analysis	72
4.4.2	Response Spectrum Analysis	73
4.4.3	Time History Analysis	75
4.5	Wind Analysis	78
4.5.1	Static Wind Analysis	78
4.5.2	Dynamic Wind Analysis	78
5	Response of Tall Timber Buildings	81
5.1	Seismic Load Cases	81
5.1.1	Equivalent Static Load Analysis	82
5.1.2	Response Spectrum Analysis	85
5.1.3	Time History Analysis	89
5.2	Wind Responses	94
5.2.1	Inter-Story Drift	94
5.2.2	Inter-Story Accelerations	98
6	Fluid Viscous Dampers in Tall Wood Building	100
6.1	Installing FVDs	100

6.2	Design and Modeling of FVDs	101
6.3	Effectiveness of FVDs in Tall Timber Buildings.....	106
6.3.1	Modal Analysis	106
6.3.2	Seismic Responses	107
6.3.3	Wind Responses	117
6.4	Practical Considerations.....	121
6.4.1	Connections.....	121
6.4.2	Availability and Cost.....	123
6.5	Sustainability.....	124
7	Conclusion	126
8	References	130

List of Tables

Table 4.1 Modal Fundamental Periods for The First Three Modes Shape of Mjøstårnet Building.....	62
Table 4.2 Modal Fundamental Periods for The First Three Modes Shape in (s) of Brock Commons Building.....	67
Table 4.3 Modal Fundamental Periods for The First Three Modes Shape of Outrigger Tall Timber Building.....	71
Table 4.4 Scaled Ground Motion Records With Associated Hazard Levels And Key Parameters.....	76
Table 5.1 Seismic Weight And Maximum Base Shear of Mjøstårnet, Brock Commons, And Outrigger Building.....	84
Table 5.2 Maximum Base Shear of Mjøstårnet, Brock Commons, And Outrigger Building Under RSA.	88
Table 6.1 Drift Ratios And Required Viscous Damping for Tall Timber Buildings.	103
Table 6.2 Fluid Viscous Damper Properties and Parameters.	106
Table 6.3 Fundamental Periods, Mass Participation Ratios, and Mode Shape Directions Before and After Installing FVDs.	107
Table 6.4 Maximum Overturning Moments Response With and Without FVDs for Tall Timber Buildings Under Northridge Earthquake in (KN.m x10 ⁵).....	114
Table 6.5 Embodied Energy of Structural Systems.	124

List of Figures

Figure 1 (a) Mjøstårnet in Norway, (b) Ascent in USA, (c) HoHo in Austria [8].	7
Figure 2 Three Principal Axes of Wood with Respect to Grain Direction and Growth Rings [19].	12
Figure 3 Cross-Laminated Timber Panel: (a) Layup and (b) Axis Directions [34].	17
Figure 4 Engineered Glulam Timber with Finger Joint [34], [39].	18
Figure 5 Structural Behaviour of Outrigger Structural System [54].	24
Figure 6 Canada Wind Resource Map at 100 m Height, Modelled at 3 Km Spatial Resolution[56].	27
Figure 7 Flowchart of the Performance-Based Design [59].	31
Figure 8 (A) Seismic Risk Map of Canada, Showing the Distribution of Seismic Hazards Across the Country [56].	34
Figure 9 Seismic Risk Map of British Columbia Near the Cascadia Subduction Zone [56].	34
Figure 10 Changes in Estimated $S_a(0.2)$ at a 2%/50-Year Probability Level For Site Class C Soil (X450 M/S) In Victoria, Vancouver, and Montreal [60].	35
Figure 11 Flowchart Depicting Levels and Objectives of Performance-Based Design.	37
Figure 12 SDOF Equation of Motion with Mass–Spring–Damper System[61].	41
Figure 13 MDOF Equation of Motion with Mass–Spring–Damper System[61].	42
Figure 14 Damping Mechanism Showing Vibration Amplitude Reduction and Energy Dissipation. ...	46
Figure 15 Passive Damper Configurations (a) Diagonal Brace Damper, (b) Chevron Brace Damper, (c) Toggle Damper, (d) Cantilever Truss Damper [13].	50
Figure 16 (a) A Typical Longitudinal Cross-Section of A Fluid Viscous Damper, (b) The Fluidic Control Orifice, (c) The Idealized Force-Displacement Relationship, and (d) The Force-Velocity Relationship [87].	54
Figure 17 Mjøstårnet Structural System [12].	58
Figure 18 (a) Elevation, (b) Cross-Section of The Building, and (c) Wooden Decks [12].	59
Figure 19 (a) Mjøstårnet 3D Model in ETABS, (b) Longitudinal Direction Elevation, and (c) Transverse Direction Elevation.	61
Figure 20 Structural Cross-Section of Brock Commons (source: naturally wood).	64
Figure 21 3D Model and Core Placement of Brock Commons [100].	64
Figure 22 Layered Shell Element Representation of CLT Slabs in ETABS.	66

Figure 23 3D Model of Brock Commons Showing CLT Core Placement in ETABS.	66
Figure 24 Structural Cross-Section and 3D view of Outrigger Tall timber building.....	69
Figure 25 3D Model of Outrigger Tall Timber Building Showing LLRS Placement in ETABS.	71
Figure 26 Equivalent Static Load Analysis (ESLA) Force Distribution for a 5-Story Building.	73
Figure 27 Response Spectrum Curves for Vancouver (Site Class C, $V_{s30}=480$ m/s) [56].	74
Figure 28 Selected Ground Motion Time-History Records.....	77
Figure 29 Matched and Unmatched records with Target Spectrum for Vancouver.	77
Figure 30 Dynamic Base Moments represent the Wind Tunnel Test Data Across The Buildings.....	80
Figure 31 Maximum Drift Ratio in X-Direction for Mjøstårnet, Brock Commons, and Outrigger Building Under Static Seismic Analysis.	83
Figure 32 Maximum Drift Ratio in Y-Direction for Mjøstårnet, Brock Commons, and Outrigger Building Under Static Seismic Analysis.	83
Figure 33 Maximum Overturning Moment for Mjøstårnet, Brock Commons, and Outrigger Building Under Static Seismic Analysis.	85
Figure 34 Maximum Drift Ratio in X-Direction for Mjøstårnet, Brock Commons, and Outrigger Building Under RSA.....	86
Figure 35 Maximum Drift Ratio in Y-Direction for Mjøstårnet, Brock Commons, and Outrigger Building Under RSA.....	87
Figure 36 Maximum Overturning Moment for Mjøstårnet, Brock Commons, and Outrigger Building Under RSA.....	89
Figure 37 Maximum Drift Ratio in X-Direction for Mjøstårnet, Brock Commons, and Outrigger Building Under Christchurch Earthquake.....	91
Figure 38 Maximum Drift Ratio in Y-Direction for Mjøstårnet, Brock Commons, and Outrigger Building Under Christchurch Earthquake.....	91
Figure 39 Maximum Drift Ratio in X-Direction for Mjøstårnet, Brock Commons, and Outrigger Building Under Mexico City Earthquake.	92
Figure 40 Maximum Drift Ratio in Y-Direction for Mjøstårnet, Brock Commons, and Outrigger Building Under Mexico City Earthquake.	92
Figure 41 Maximum Drift Ratio in X-Direction for Mjøstårnet, Brock Commons, and Outrigger Building Under Northridge Earthquake.....	93
Figure 42 Maximum Drift Ratio in Y-Direction for Mjøstårnet, Brock Commons, and Outrigger Building Under Northridge Earthquake.....	93

Figure 43 Maximum Drift Ratio in X-Direction for Mjøstårnet, Brock Commons, and Outrigger Building Under Static Wind Analysis.	95
Figure 44 Maximum Drift Ratio in Y-Direction for Mjøstårnet, Brock Commons, and Outrigger Building Under Static Wind Analysis.	95
Figure 45 Maximum Drift Ratio in X-Direction for Mjøstårnet, Brock Commons, and Outrigger Building Under Dynamic Wind Analysis.	96
Figure 46 Maximum Drift Ratio in Y-Direction for Mjøstårnet, Brock Commons, and Outrigger Building Under Dynamic Wind Analysis.	96
Figure 47 Maximum Lateral Displacement in X-Direction for Mjøstårnet, Brock Commons, and Outrigger Building Under Dynamic Wind Analysis.	97
Figure 48 Maximum Lateral Displacement in Y-Direction for Mjøstårnet, Brock Commons, and Outrigger Building Under Dynamic Wind Analysis.	97
Figure 49 Story Acceleration Response in X And Y-Direction for Mjøstårnet Building Under Dynamic Wind Analysis.	98
Figure 50 Story Acceleration Response in X And Y-Direction for Brock Commons Building Under Dynamic Wind Analysis.	99
Figure 51 Story Acceleration Response in X And Y-Direction for Outrigger Building Under Dynamic Wind Analysis.	99
Figure 52 Fluid Viscous Dampers in Diagonal Mega-Brace Configurations (Source: Taylor Devices).	100
Figure 53 Model for Damper in Series with an Extender Brace.....	101
Figure 54 Fluid Viscous Damper Configuration for Brock Commons Tall Timber Building.	104
Figure 55 Fluid Viscous Damper Configuration for Mjøstårnet Tall Timber Building.	105
Figure 56 Fluid Viscous Damper Configuration for Outrigger Tall Timber Building.....	105
Figure 57 Hysteretic Loop of a Damper in Brock Commons Building under Seismic Events.	108
Figure 58 Hysteretic Loop of a Damper in Outrigger Building under Seismic Events.	109
Figure 59 Hysteretic Loop of a Damper in Mjøstårnet Building under Seismic Events.	109
Figure 60 Maximum Drift Ratio for Mjøstårnet, Brock Commons, and Outrigger Buildings with FVDs Under Christchurch Earthquake.....	110
Figure 61 Maximum Drift Ratio for Mjøstårnet, Brock Commons, and Outrigger Buildings with FVDs Under Mexico City Earthquake.	110
Figure 62 Maximum Drift Ratio for Mjøstårnet, Brock Commons, and Outrigger Buildings with FVDs Under Northridge Earthquake.....	111

Figure 63 Time History Displacement Responses at Story 18 (With and Without Dampers).....	112
Figure 64 Time History Base Shear Response for Brock Commons Under Christchurch Earthquake.	113
Figure 65 Time History Base Shear Response for the Proposed Outrigger Under Christchurch Earthquake.	113
Figure 66 Time History Base Shear Response for Mjøstårnet Under Christchurch Earthquake.....	113
Figure 67 Cumulative Energy Plot for Brock Commons Building Under Christchurch Earthquake.	115
Figure 68 Cumulative Energy Plot for Outrigger Building Under Christchurch Earthquake.	116
Figure 69 Cumulative Energy Plot for Mjøstårnet Building Under Christchurch Earthquake.....	116
Figure 70 Hysteretic Loop of a Damper in Brock Commons Building under Wind Events.	118
Figure 71 Hysteretic Loop of a Damper in Outrigger Building under Wind Events.....	118
Figure 72 Hysteretic Loop of a Damper in Mjøstårnet Building under Wind Events.	118
Figure 73 Maximum Drift Ratio for Mjøstårnet, Brock Commons, and Outrigger Building With FVDs Under Dynamic Wind Analysis.	119
Figure 74 Story Acceleration Response for Mjøstårnet Building With FVDs Under Dynamic Wind Analysis.....	119
Figure 75 Story Acceleration Response for Brock Commons Building With FVDs Under Dynamic Wind Analysis.	120
Figure 76 Story Acceleration Response for Outrigger Building With FVDs Under Dynamic Wind Analysis.....	120
Figure 77 Damper Frame and Its Nonlinear Damping Force Path Mechanism.	121
Figure 78 Effect of FVDs on Column Axial Forces for Brock Commons Building under Mexico City Earthquake.	122
Figure 79 Effect of FVDs on Column Axial Forces for Outrigger Building under Christchurch Earthquake.	122
Figure 80 Effect of FVDs on Column Axial Forces for Mjøstårnet Building under Northridge Earthquake.	122

Dedication

"Family is not an important thing. It's everything."

— Michael J. Fox

This thesis is dedicated to my beloved wife, Asma Omar, and to my precious sons, Shahem and Karam, as well as the little girl we are excitedly expecting.

To my wife— your strength, patience, and quiet resilience have been my guiding light. Through every high and low, your unwavering love and support have given me the courage to move forward. I am endlessly grateful for you. I pray each day for your renewed strength, comfort, and healing. May the days ahead bring you the peace and well-being you so deeply deserve. This work is a reflection of your courage and the love that surrounds you.

To my sons, Shahem and Karam—you inspire me every single day. You are the reason I strive harder, dream bigger, and believe more. May this achievement be a reminder that anything is possible with dedication and heart.

And to our daughter, not yet in our arms but forever in our hearts—this is for the future we are excited to share with you, filled with love, laughter, and dreams waiting to be lived.

Acknowledgment

First and foremost, I would like to express my sincere gratitude to my supervisor, Dr. Asif Iqbal, for his invaluable support, guidance, and encouragement throughout the course of this thesis. His expertise, insightful feedback, and mentorship have been instrumental in shaping both the quality and direction of this work. I am equally grateful to my committee members, Dr. Mohammad Kamali and Dr. Shahria Alam, for their valuable time, constructive critiques, and thoughtful suggestions, all of which have significantly contributed to the strength and clarity of my research.

I would also like to extend my deepest gratitude to my father, mother, and sister for their unwavering psychological and moral support throughout this journey. Their belief in me and constant encouragement provided the foundation I needed to stay focused and resilient. Their love, sacrifices, and heartfelt prayers carried me through the most difficult moments, and for that, I am eternally thankful.

Lastly, I am deeply thankful to my fellow students and colleagues, whose companionship and support made this journey both enriching and memorable. The shared moments of discussion, reflection, perseverance, and laughter turned long hours into meaningful experiences and made this chapter of my life truly special.

Thank you all for being a part of this journey.

— Mohamed Elshamy

1 Introduction

1.1 Background

Advancements in engineered wood products (EWP) have enabled modern tall timber buildings to become longer, lighter, and slenderer, increasing their susceptibility to oscillations under lateral loads. Historically, timber buildings are linked with low-rise and traditional structures. Innovations in EWP, such as cross-laminated timber (CLT) and glulam laminated timber (GLT), have been hailed as a 'game-changer.' Recent research has facilitated the ability to design and construct tall timber structures, even in earthquake-prone regions. That leads to pushing the boundaries of timber construction to new heights. This is demonstrated by projects like the 73-meter-tall HAUT in the Netherlands [1] and the 54-meter-tall Brock Commons in Vancouver [2]. Another instance is Treet, a 14-story timber apartment building in Norway [3], and HoHo, 84 meters high [4].

As of its completion in August 2022, the tallest timber building in the world is Ascent in Milwaukee, USA, standing at 86.5 meters with 25 floors and surpassing Mjøstårnet in Brumunddal, Norway, which stands at 85.3 meters with 18 floors. As interest in timber buildings grows, high-rise structures are gaining more attention. This focus is partly due to their role in advancing the field of timber construction. Currently, the tallest timber building, Ascent, is roughly ten times shorter than the world's tallest building, Burj Khalifa, in Dubai, suggesting significant potential for advancements in tall timber structures. Furthermore, as mass timber becomes increasingly prevalent in design practices, advancements in structural timber technology are expected to enable the construction of taller timber buildings and reduce building height limits. This will continue to challenge existing codes and research. The development of these buildings is commendable, as high-rise timber buildings in Canada offer sustainability, utilize abundant local resources, and stimulate the economy.

This aligns with government policies promoting sustainable development and healthier living environments.

Over the past century, building codes worldwide have typically limited wood constructions to a maximum of three to six stories. However, recent BC Building Code updates now permit taller mass-timber structures, up to 18 stories from the previous 12, highlighting the urgency of addressing this gap. Consequently, the 2020 National Building Code of Canada (NBC) raised the allowable height for timber-based up to 12 stories. Moreover, an alternative performance-based design (PBD) approach has been utilized in practice for newer and innovative, taller timber-based buildings, with no specific height limit as long as the system is demonstrated to be safe and feasible[5]. However, beyond 10 stories, considerations such as lateral drift and stiffness became crucial in governing the serviceability limit state; the primary challenge for tall wood buildings is designing the lateral load resistant system (LLRS) due to a lower inherent damping ratio, modulus of elasticity, and overturning moment resistance capacity than other buildings [6].

In conclusion, this research aims to fill the gap by investigating high-rise timber buildings' seismic and wind performance by integrating fluid viscous dampers (FVD) through detailed analysis and numerical studies. This thesis seeks to provide critical data and insights to inform future building codes and design practices. By improving the understanding of how these advanced damping solutions can enhance tall timber buildings' seismic and wind performance, this research will support the development of safer, more sustainable high-rise structures capable of withstanding seismic and wind loads.

1.2 Motivation

The motivation for this research stems from the growing ambition to push the height limits of timber buildings driven by advances in engineered wood products (EWPs) and updates to the BC Building Code, which now permits mass timber construction up to 18 stories. However, as building heights increase, challenges like lateral drift and reduced damping capacity become critical. Addressing these issues is essential to ensure stability, safety, and comfort under seismic wind loads.

The question of how tall timber buildings can go has become a central focus among structural engineers and researchers, particularly from a wind and seismic engineering perspective. Using passive control devices, specifically fluid viscous dampers (FVDs), presents a promising approach to improving dynamic performance.

1.3 Research Scope and Objectives

This thesis investigates the seismic and wind performance of tall timber buildings in seismic-prone regions, specifically southwestern British Columbia, adhering to Canada's 2020 National Building Code. The study was expanded to incorporate three study structures with diverse structural systems to strengthen the credibility and depth of understanding. This analysis offers a comprehensive evaluation of the dynamic behaviour of tall timber buildings, contributing to the advancement of state-of-the-art knowledge in this field. Additionally, to enhance the lateral performance of these structures and address the last height limitations, fluid viscous dampers were implemented to mitigate seismic and wind demands and improve overall performance.

The primary objectives of this research are:

- Evaluating the seismic and wind performance of tall timber buildings and identifying key challenges in achieving code compliance.
- Investigating the effectiveness of passive fluid viscous dampers in enhancing seismic resilience and occupant comfort under wind loads.
- Developing an optimized approach for the design and placement of fluid viscous dampers, maximizing damping efficiency and structural performance.

1.4 Organization

This thesis is organized into six main chapters, each addressing key aspects of tall timber buildings' seismic and wind performance and the role of fluid viscous dampers (FVDs) in enhancing structural resilience.

The literature review in Chapter 2 provides an overview of modern tall timber buildings, covering dynamic challenges, material properties, innovative timber products, and structural systems while addressing lateral load considerations, including seismic and wind forces. Building on this, Chapter 3 discusses the dynamic performance of tall timber buildings, focusing on damping techniques and passive control devices like fluid viscous dampers (FVDs) to mitigate seismic and wind-induced responses. This is followed by Chapter 4, which introduces the modelling and analysis of tall wood buildings under seismic and wind loads, presenting three model buildings (braced frame, core system, and outrigger-belt truss) and outlining seismic and wind analysis methods, including static and dynamic analyses.

Chapter 5 presents the structural response of tall timber buildings under seismic and wind loads, focusing on drifts, base shear, overturning moments and accelerations for different load scenarios.

Finally, Chapter 6 explores the role of fluid viscous dampers (FVDs) in mitigating seismic and wind-

induced vibrations, with attention to their effectiveness, connection design, and cost. This structure provides a logical flow of information, progressing from foundational concepts to in-depth analysis and application. It ensures a clear presentation of the research and its contributions to tall timber building design.

2 Literature Review

A literature review was conducted to support critical decisions on improving the lateral load resistance system for high-rise timber buildings and reducing the height limitations of tall timber structures. The study covers existing high-rise timber buildings, timber as a structure material, lateral structural systems for tall buildings, the hazard map in Canada, and lateral load considerations.

2.1 Modern Tall Timber Buildings

The global urban landscape is experiencing a significant transformation in architectural planning and construction practices, spurred by the need for sustainability, resilience, and innovation. Moreover, the rapid growth of the urban population and associated environmental concerns challenged city planners to consider sustainable and cost-efficient building systems in this scenario. High-rise timber residential towers have surfaced as an innovative and promising solution, redefining traditional views on skyscraper construction [7].

With the growing demand for urban housing and increasing concerns about climate change and resource scarcity, it is essential to explore alternative building materials and methods. Furthermore, as mass timber becomes a more appealing and common material in the design team's repertoire, future high-rise timber buildings with advancements in structural timber technology enable construction at greater heights; it's anticipated that building height limits will decrease and continue to push the boundaries of existing codes and research.

Notable examples [8] of such transformative projects include Ascent Tower in the USA, currently recognized as the tallest timber building in the world, Mjøstårnet in Norway, which held the title

previously, and HoHo Tower in Austria, known for its innovative design and use of prefabricated timber components, as illustrated in Figure 1.

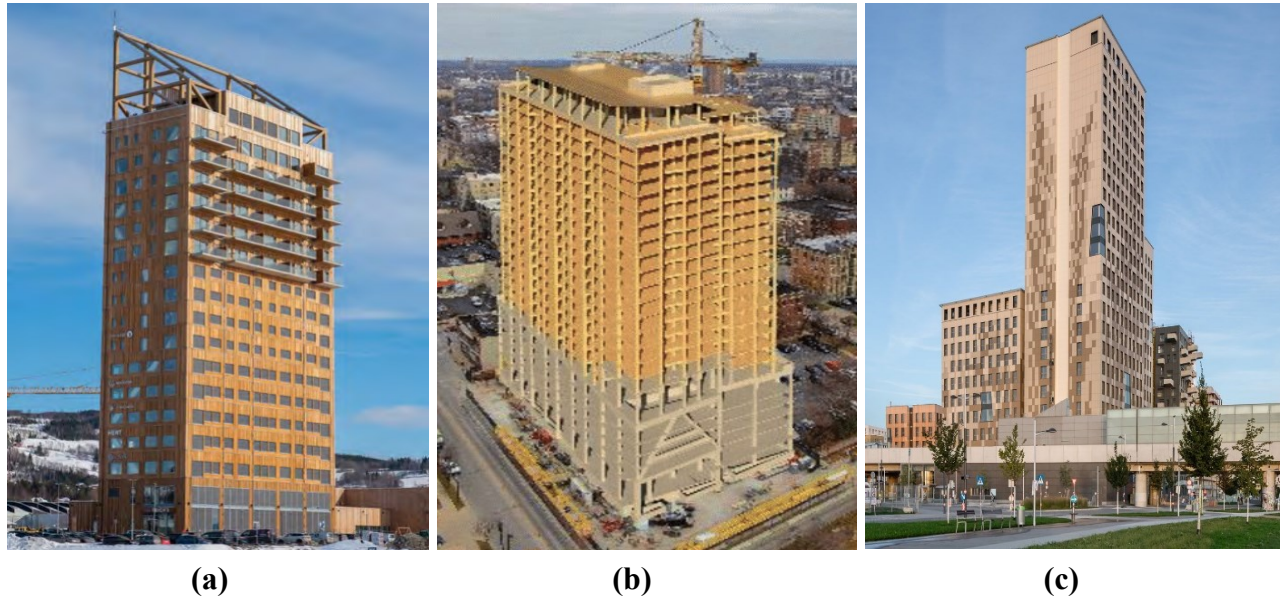


Figure 1 (a) Mjøstårnet in Norway, (b) Ascent in USA, (c) HoHo in Austria [8].

Several lateral resistance systems are suited for tall timber buildings, each tailored to meet the unique demands of height, seismic and wind hazard maps, and the structure's intended use. The appropriate system selection is critical for ensuring structural safety and performance under various loading conditions [9]. For instance, Brock Commons Tall Wood House, an 18-story student residence standing 54 meters tall, utilizes a hybrid mass timber structural system. While the foundation, ground floor podium, and cores are cast-in-place concrete, the floors and columns from levels 2 to 18 are made of mass timber. This timber construction includes five-ply cross-laminated timber (CLT) panels supported by glulam timber (GLT) columns or parallel strand lumber (PSL) columns in specific areas requiring higher compressive strength [10].

Similarly, the Ascent structure consists of a seven-level parking podium with 18 residential levels, including an amenity-level roof deck. The mass timber gravity superstructure, made up of glulam

beams, columns, and one-way spanning Cross-Laminated Timber (CLT) slabs, rises above the reinforced concrete podium at level 7. Reinforced concrete core walls form the structural lateral system, providing a safe means of egress for occupants and a secure access path for firefighters during construction and the building's lifespan [11]. Another instance is Treet, a 14-story timber apartment in Norway that employs diagonal glulam beams as its lateral-force resisting system. CLT was utilized for the elevator shaft and stairways, supplemented by concrete-topped floors to enhance wind performance [6].

Moreover, Mjøstårnet is an 18-storey timber building that reached its full height on September 4, 2018, exactly one year after the installation of the timber structures began in Brumunddal, Norway. The main load-bearing elements consist of large-scale glulam trusses along the façades, internal columns, and beams. These trusses manage the global forces in horizontal and vertical directions, providing the building with its necessary stiffness. CLT walls are used for the secondary load bearing of three elevators and two staircases, although they do not contribute to the building's horizontal stability [12].

2.1.1 Dynamic Challenges in Tall Timber Buildings

Space constraints and sustainability goals drive the rise of taller buildings in metropolitan areas. However, increasing building height reduces natural frequency and damping, making structures more susceptible to dynamic loads such as wind and earthquakes [13]. Timber buildings face heightened challenges [14] due to their inherently lower lateral stiffness than steel or concrete, resulting in more enormous lateral drifts and reduced overturning resistance under seismic loads. Additionally, timber's lightweight and flexible nature exacerbates wind-induced vibrations, leading to higher accelerations that can disrupt occupant comfort. Moreover, the viscoelastic behaviour of wood further complicates the dynamic response as its stiffness and damping properties evolve. Like

wind-induced forces, repeated loading degrades connection stiffness, impacting the overall dynamic performance. Studies emphasize notable changes in energy dissipation and stiffness, highlighting the importance of robust connection design. Reduced connection stiffness increases lateral drifts, affecting safety and serviceability[15].

As a result, developing effective lateral force-resisting systems (LFRS) is crucial for achieving performance beyond conventional life-safety criteria. Addressing these challenges necessitates a multidisciplinary approach integrating analytical methods, experimental data, and structural innovations. Key focus areas include enhancing damping mechanisms, optimizing connection performance, and maintaining occupant comfort. Thoughtful connection detailing and the incorporation of damping systems are essential to mitigate these effects. By addressing these issues, tall timber buildings can balance sustainability and structural resilience, facilitating their broader adoption in modern urban environments. This underscores the importance of a comprehensive understanding of the dynamic performance of tall timber buildings.

2.2 Timber As a Structure Material

Timber has been used as a construction material for centuries, serving both practical and structural purposes across different civilizations. While the specific ways timber has been utilized have varied by region and era, it has consistently remained one of the primary materials in building. In recent years, growing environmental awareness and the push for sustainable construction have revived interest in timber as a modern building material. With its low environmental impact, renewable nature, and production efficiency, timber is increasingly considered a viable alternative in the construction industry.

Timber's advantages include its non-toxic properties, renewability, minimal energy requirements during production, and potential for prefabrication. Combined with modern engineering techniques, these qualities make timber a competitive option alongside conventional materials like steel and concrete in various structural applications. When fully leveraged, timber has the potential to play a vital role in the development of future sustainable buildings [16].

2.2.1 Wood Properties

Timber has been noted as having an advantageous strength-to-weight ratio, making it practical for structural utilization considering its weight [17]. This implies that such materials are very convenient for application in small and large constructions where weight dictates the design. Since the strength and stiffness of wood are known to be anisotropic properties, careful attention is required while designing the vertical load and lateral support systems to harness maximum efficiency. However, a significant drawback of these materials is their hygroscopic nature, which causes the wood to swell or shrink as it gains or loses moisture. These variations will affect the timber's final mechanical properties, and questions about its feasibility for the structural design must arise. Another critical factor is viscoelasticity and creep deformation, whereby wood does not change its shape but yields under the application of a constant load over time. This is mainly of concern in structural applications where incessant loading conditions are experienced and may cause significant displacement to the stability of the building structure[18].

2.2.2 Orthotropic Behavior

Timber exhibits different mechanical properties as an orthotropic material along its three primary axes: longitudinal, radial, and tangential [19], as illustrated in Figure 2. The modulus of elasticity (MOE) is highest along the longitudinal axis due to the alignment of the wood fibers [20]. The MOE

in the longitudinal direction typically ranges between 4,400 to 15,700 MPa. However, the MOE is significantly lower in the radial and tangential directions, typically between 500 to 1,500 MPa radially and 300 to 850 MPa tangentially. Despite that, timber design codes such as the CSA O86 Standards do not differentiate between the radial and tangential axes due to their similar behavior and practical issues. As a result, this orthotropic behavior is typically simplified into two primary directions—either parallel to the grain or perpendicular to the grain.

Wood demonstrates Poisson's ratio, representing the relationship between the lateral and axial strains in a material when subjected to axial loading. In timber, Poisson's ratios vary based on the orientation of the applied stress and the resulting deformation. The Poisson's ratios are denoted by μ_{LR} , μ_{RL} , μ_{LT} , μ_{TL} , μ_{RT} , and μ_{TR} , where the first subscript indicates the direction of the applied stress (longitudinal, radial, or tangential), and the second subscript indicates the direction of lateral deformation. For example, μ_{LR} is the Poisson's ratio for deformation along the radial axis caused by stress along the longitudinal axis.

Typically, Poisson's ratio for timber along the longitudinal-radial (μ_{LR}) and longitudinal-tangential (μ_{LT}) planes is around 0.35, meaning that for a unit of strain in the longitudinal direction, approximately 35% strain occurs in the radial or tangential directions. Conversely, Poisson's ratios like μ_{RL} and μ_{TL} (stress along the radial or tangential direction causing deformation along the longitudinal direction) are much smaller, with minimal deformation, often around 0.035. These values are critical in designing timber joints and structural elements, as they help prevent excessive lateral deformation and potential brittle failure in the connections. [21], [22].

The shear modulus of timber varies between the planes. In the longitudinal-radial and longitudinal-tangential planes, it is approximately 1/20 of the longitudinal modulus of elasticity. In contrast, the radial-tangential shear modulus is much lower, about 1/100 to 1/200 of the longitudinal modulus.

Although the radial-tangential plane shows lower stiffness, it typically avoids brittle failures, leading to wood crushing as fibers are compressed. Conversely, shear in the other two planes often causes fiber slippage, leading to more brittle failures. Another potential failure mode is rolling shear, in which fibers roll relative to one another under transverse shear forces [23]. Understanding timber's orthotropic behavior is essential for ensuring it performs as expected under various load conditions. Designers must account for these variations in stiffness, shear response, and Poisson's ratio to maximize the material's potential while minimizing the risk of failure.

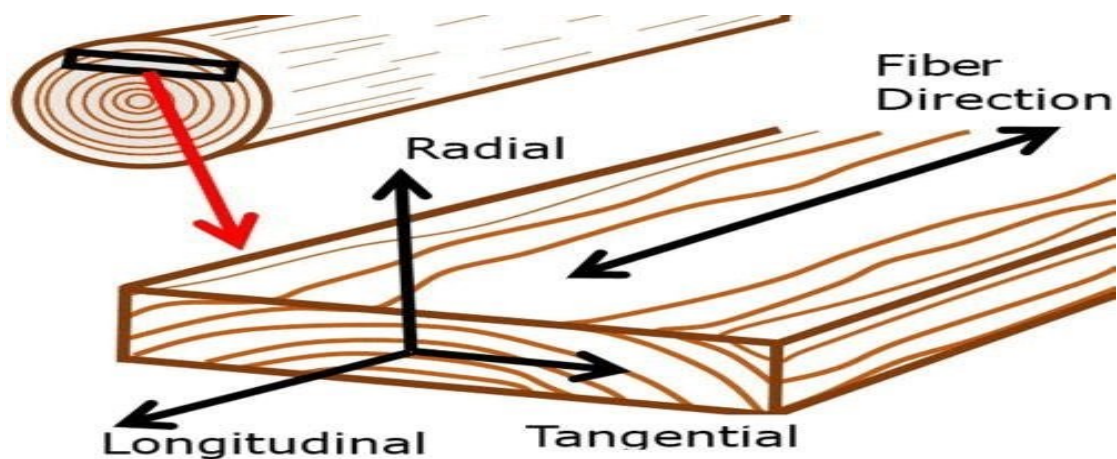


Figure 2 Three Principal Axes of Wood with Respect to Grain Direction and Growth Rings [19].

2.2.3 Weight of Timber

Timber's density can vary greatly depending on the species, falling between 175 and 1,250 kg/m³. Concrete typically has a density of around 2,400 kg/m³, but steel has a substantially greater density of about 7,850 kg/m³. For practical purposes, wood products typically weigh between 350 and 580 kg/m³, which makes them significantly lighter than steel and concrete [24]. There are several benefits to this significant weight differential, including more uncomplicated shipping, faster construction, and less foundation requirements. However, because there is less mass due to the reduced weight,

the building's inertia is reduced, which may affect the building's response to dynamic forces like wind or seismic activity, necessitating careful structural design to ensure stability.

2.2.4 Influence of Moisture

Timber is a hygroscopic material, continuously adjusting its moisture content to reach equilibrium with the surrounding environment. This process, known as adsorption or desorption, depends on the atmosphere's relative humidity, temperature, and moisture within the wood. As timber interacts with its environment, it gains or loses moisture to maintain balance. Processed timber products typically stabilize at around 12% moisture content in unheated indoor climates. This percentage is chosen to align the timber's moisture content with the expected conditions of its intended use, minimizing dimensional changes and improving material performance.

The fiber saturation point (FSP)—approximately 28-30% moisture content—marks the threshold above which changes in moisture content have little impact on timber's mechanical properties. Below the FSP, however, moisture fluctuations significantly affect properties such as strength and stiffness. As the wood dries, particularly below the FSP, its strength increases, with almost a threefold difference between wood near saturation and fully dried wood. Therefore, drying timber as much as possible before use is beneficial to maximize strength and stiffness [25].

As the timber dries, it undergoes shrinkage, primarily governed by its orthotropic behavior, which results in dimensional changes along the longitudinal, radial, and tangential axes. Modern processed timber products, which are typically dried during production, experience minimal shrinkage during construction. However, minor annual variations in moisture conditions can still impact timber. However, the effects are usually minor due to the slow diffusion of water through the material, especially in large cross-sections.

Moisture content also influences timber's modulus of elasticity (MOE), which measures its stiffness. Studies have shown an almost linear relationship between stiffness and moisture content below the FSP, with drier wood exhibiting higher stiffness [26], [27]. This is particularly important in the design of tall buildings, where even slight variations in moisture can have a significant impact over long distances. Ensuring a well-developed, moisture-safe design helps mitigate these effects and prevents structural issues caused by moisture fluctuations.

To further reduce the impact of moisture, surface treatments can be applied to timber, enhancing its resistance to moisture penetration and limiting dimensional changes over time [28]. This is especially critical in environments where timber is exposed to varying conditions, ensuring the long-term stability and durability of timber structures.

2.3 Innovative Timber Products Suitable for Tall Buildings

From conventional light-frame systems to more advanced heavy wood systems, the usage of timber in high-rise construction has changed dramatically. Engineered wood product (EWP) innovations have made it possible to construct multi-story structures which combine structural efficiency with sustainability. Wood is a good substitute for steel and concrete because of heavy timber systems like Structural Composite Lumber (SCL) and Mass Timber, which are made to increase wood's strength, stiffness, and load-bearing capability [29]. These products are made with innovative techniques that optimize the mechanical qualities of wood, such as laminating, bonding, and doweling. Thus, in high-rise applications, these advancements provide faster assembly times, lower carbon footprints, and more flexibility in design [30].

2.3.1 Structural Composite Lumber (SCL)

A type of engineered wood product known as structural composite lumber (SCL) is made to maximize the mechanical qualities of wood for usage in tall constructions. Wood fibers, strands, or veneers are bonded under pressure to generate these products to produce consistent, homogenous material with improved strength and stiffness. Laminated Veneer Lumber (LVL), Laminated Strand Lumber (LSL), Parallel Strand Lumber (PSL), and Oriented Strand Lumber (OSL) are common varieties of SCL. Due to its high strength-to-weight ratio and dimensional stability, SCL is becoming an excellent option for structural elements like beams, columns, and floor systems in tall wood structures [31], [32].

2.3.2 Mass Timber

Cross-laminated timber (CLT), glue-laminated timber (GLT), dowel-laminated timber (DLT), and nail-laminated timber (NLT) are examples of mass timber products. These engineered wood components are appropriate for vertical and horizontal loads in high-rise buildings because of their high strength and stiffness. Because mass timber products are usually prefabricated, waste and construction time are decreased in addition to labour costs on the job site. Mass timber's popularity in sustainable building projects is further contributed by its environmental advantages, which include carbon sequestration and renewability [33].

2.3.2.1 Cross-Laminated Timber (CLT)

High-strength adhesives join layers of timber boards arranged perpendicularly to create Cross-Laminated Timber (CLT), as shown in Figure 3, a mass timber product. The material's mechanical qualities—precisely its strength, stiffness, and dimensional stability—are greatly improved by this crosswise arrangement, which makes it the perfect choice for high-rise construction. Layers oriented

orthogonally offer balanced load-bearing capacity, which enables CLT to function remarkably well under lateral and vertical loads. Because of these characteristics, it is a strong option for structural applications like shear walls, floors, and roof panels in multi-story buildings [34]. CLT's strength is attributed to its multi-layer structure, which enables it to withstand tensile forces and support large compressive loads. Because the boards are aligned perpendicularly, the panel is more rigid and stable even when subjected to dynamic loading conditions, like earthquakes or strong winds. Because of its high load-bearing capacity and stiffness, which are on par with reinforced concrete, CLT can be used in shear walls, which offer the lateral stability and stiffness necessary to preserve the structural integrity of tall buildings [35].

One of the key mechanical advantages of CLT is its ability to distribute loads evenly across its layers, improving its resilience under pressure. The cross-lamination technique prevents splitting and enhances the panel's resistance to buckling, a common challenge in high-rise structures. CLT panels are especially beneficial when used as floor systems, as they provide strength and stiffness across long spans without additional support beams, simplifying the construction process and reducing material use [36].

Equally transferring loads among its layers and increasing its durability under strain are some of CLT's primary mechanical advantages. Bending is a common problem in large structures due to large spans that are prevented and improved using cross-lamination. Because CLT panels offer strength and stiffness over extended distances without extra support beams, they are particularly advantageous when used as floor systems. This streamlines the building process and uses less material [37].

Additionally, CLT performs exceptionally well in earthquake situations. Because of its high flexibility and stiffness, it can effectively absorb and dissipate energy during seismic occurrences,

reducing structural damage. CLT's ability to withstand large lateral forces while preserving stability and safety is demonstrated by its application as shear walls and floors in high-rise structures. This research demonstrated the feasibility of CLT in earthquake-prone areas by optimizing its mechanical qualities to give the required strength and flexibility [38].

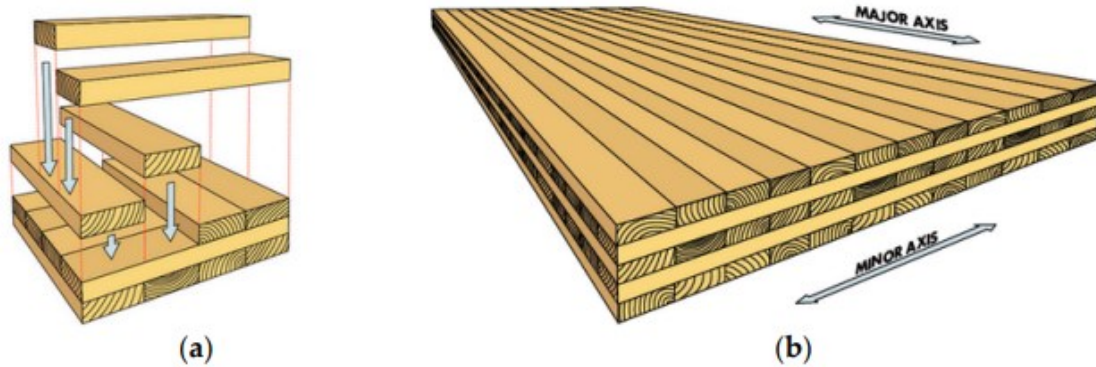


Figure 3 Cross-Laminated Timber Panel: (a) Layup and (b) Axis Directions [34].

Glulam Laminated Timber (GLT)

Commonly known as glulam, it is an engineered wood product that bonds several layers of timber boards with their grains running parallel. This process creates versatile and strong materials used extensively in tall building construction, as illustrated in Figure 4. GLT offers high load-bearing capacity and flexibility, making it suitable for structural applications such as beams, columns, and other framing components in multi-story buildings. The lamination process allows glulam to span longer distances than solid timber, essential for creating open spaces and flexible layouts in high-rise designs [39]. GLT's outstanding strength-to-weight ratio is one of its main benefits. Multiple layers are laminated to give GLT mechanical qualities similar to concrete and steel but at a fraction of the weight. This feature benefits tall structures since it can result in significant foundation and seismic design savings by lowering the overall weight. Creating long, slender beams and columns increases high-rise wood buildings' design potential due to GLT's strength and stiffness [40].

A notable feature of GLT is not just its structural performance but also its design flexibility. The product gives architects creative freedom while preserving structural integrity because it can be produced in various shapes, including arched and curved forms [41]. This adaptability helps create intricate and beautiful building shapes, becoming increasingly crucial in contemporary architecture.

Another critical factor in GLT's application in high-rise structures is its fire resistance. During a fire, the exposed GLT surface chars create an insulating layer that shields the interior timber from the heat. This charring tendency preserves the beams and columns' structural integrity for a considerable amount of time, satisfying tall buildings' strict fire safety requirements [42]. In hybrid wood structures, where it is mixed with other materials like steel. GLT frequently serves as the main load-bearing component in these arrangements, distributing forces through the building's frame and supporting vertical loads from several stories. Its versatility is increased by its compatibility with other materials, which enables it to be used with prefabricated parts to expedite and improve the efficiency of the building construction [43].

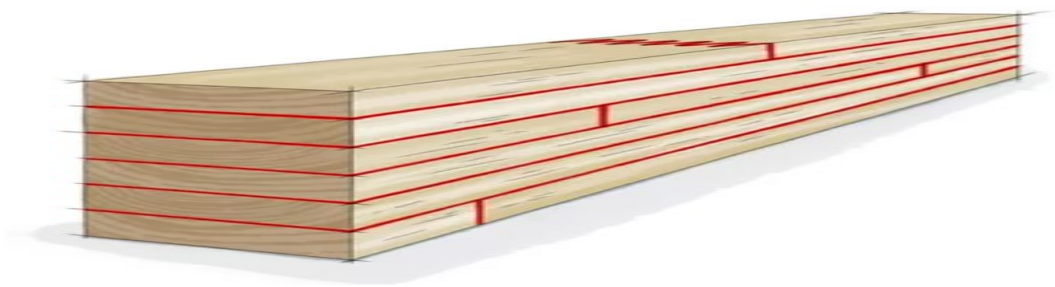


Figure 4 Engineered Glulam Timber with Finger Joint [34], [39].

2.4 Structure Systems for Tall Buildings

Lateral structural systems play a critical role in ensuring the stability and safety of tall buildings by resisting horizontal forces generated by wind, earthquakes, and other external loads. As buildings

rise in height, lateral loads increase in intensity, making these systems essential for maintaining structural integrity, controlling deflections, and minimizing swaying. Unlike low-rise structures, where gravity loads dominate, tall buildings' primary challenge is managing these lateral forces effectively through robust engineering solutions.

Various lateral systems, including frame systems, braced trusses, shear walls, core systems, and outrigger systems, are employed to distribute and resist these forces. Each system offers distinct advantages in terms of strength, flexibility, and efficiency, and they are often used in combination to achieve optimal performance. The selection of an appropriate lateral system depends on several factors, such as the height and geometry of the building, material choice, environmental conditions, and architectural design considerations.

Modern high-rise buildings increasingly rely on hybrid approaches, integrating multiple lateral systems to balance efficiency and aesthetics. These systems are essential for meeting stringent building codes and ensuring the comfort and safety of occupants, particularly in regions prone to seismic activity or strong winds. Through careful design and innovative engineering, lateral structural systems enable architects and engineers to push the limits of high-rise construction while maintaining resilience and stability.

2.4.1 Frame System

The frame system is a fundamental structural strategy that relies on interconnected beams and columns with moment-resisting joints to distribute vertical and lateral loads. These rigid connections resist bending forces under horizontal loads, making the system suitable for buildings that require flexibility in interior layouts. However, while frame systems are effective in mid-rise buildings, their

lateral stiffness diminishes in taller structures, leading to excessive drift if not supplemented with additional elements [44].

Steel frame systems are favored for their ductility in seismic zones, allowing them to deform without losing load-carrying capacity. Concrete frames are utilized where higher rigidity is required to limit sway. However, GLT beams and columns have gained traction in hybrid designs for their environmental benefits. GLT offers a high strength-to-weight ratio that spans long distances, providing a sustainable alternative to traditional materials like steel and concrete.

Despite these advantages, frame systems in timber are not considered the most efficient solution for lateral resistance. The primary challenge lies in the additional stresses induced in timber sections, particularly in beams and columns, under lateral loads. These stresses require larger cross-sections to ensure the system's structural integrity, increasing material usage and affecting the overall design efficiency. As a result, relying solely on timber frames for lateral resistance may not be practical in high-rise applications [45]

2.4.2 Braced System

The lateral bracing truss system enhances the structural stiffness of tall buildings by introducing diagonal braces that connect beams and columns, forming triangulated sections. These braces transform lateral forces, such as wind and seismic loads, into axial forces (tension or compression) that are efficiently transferred to the foundation [46]. This system is commonly used in steel and timber buildings, offering high stiffness without adding significant weight, which is especially valuable for tall structures where reducing the overall load is critical.

Braced frames are available in several configurations, including X-bracing, V-bracing, and K-bracing, each with distinct performance characteristics. X-bracing provides excellent resistance to

lateral loads by engaging tension and compression members, ensuring uniform force distribution. V-bracing offers more architectural freedom, allowing openings for doors or windows within the braced bays. K-bracing is used selectively where the design requires offset load paths [47]. These configurations can be adapted to meet specific architectural and structural needs.

Hybrid bracing systems have recently gained popularity, particularly in timber buildings [48]. These systems combine timber frames with steel bracing elements. Using steel braces enhances timber structures' stiffness and energy dissipation capacity, providing a practical solution for multi-story timber buildings. This integration ensures that buildings remain both structurally sound and environmentally friendly.

2.4.3 Shear-Wall System

Shear walls are vertical structural elements engineered to resist lateral forces by transferring them to the foundation through their in-plane stiffness. Commonly composed of reinforced concrete or cross-laminated timber (CLT), they are essential for enhancing the stability of high-rise structures, particularly under wind and seismic loads. To minimize torsional effects, shear walls are strategically positioned along the building's perimeter and often integrated around stairwells and elevator cores, ensuring continuity, structural integrity, and optimal performance during dynamic loading events [49].

Concrete shear walls provide exceptional stiffness and strength, making them ideal for high-rise structures. They limit lateral displacement by efficiently absorbing and distributing horizontal forces across multiple stories. However, timber-based shear walls, such as those made by CLT, offer structural performance and sustainability, making them increasingly popular in modern construction.

Timber shear walls are lighter than concrete, reducing the building's overall weight and foundation loads while maintaining the necessary stiffness to control sway and drift.

Shear walls are essential for controlling inter-story drift, preventing excessive movement between floors during dynamic loading events like earthquakes. In seismic regions, they absorb energy through controlled deformation, reducing the likelihood of structural failure [50]. To optimize performance, shear walls are often integrated with other systems, such as frames or outriggers.

2.4.4 Core System

The core system forms the structural backbone of many tall buildings, typically housing essential services such as elevators, staircases, and mechanical shafts. These vertical cores are constructed from reinforced concrete, steel, or CLT walls. Providing substantial resistance to both lateral and torsional forces. Core systems ensure the building remains stable by reducing sway and controlling rotational movement caused by wind or seismic loads [51].

Concrete cores are particularly valued for their high stiffness, durability, and exceptional fire resistance, making them the preferred choice in many high-rise projects. Their central placement ensures efficient access to essential services such as elevators, stairwells, and utilities and enhances structural performance by minimizing deformation and providing robust torsional stability [52].

However, with the incorporation of Encapsulated Mass Timber into the 2020 National Building Code of Canada (NBCC), a significant shift in structural design has emerged. CLT shear walls are now positioned as viable alternatives to traditional reinforced concrete (RC) shear walls or steel cores [53]. This development introduces new opportunities for sustainable construction by leveraging timber's environmental benefits while still meeting fire performance criteria through encapsulation techniques. Adopting CLT shear walls as part of the seismic force-resisting system

offers architects and engineers a versatile option that aligns with modern trends toward sustainability, reducing the carbon footprint of high-rise structures without compromising safety or performance.

2.4.5 Outrigger-Belt Truss System

Core systems are often combined with other structural components in tall buildings to enhance performance. For example, outrigger systems are frequently integrated with the core to distribute lateral loads more effectively. By connecting the central core to perimeter columns through horizontal trusses or beams, the building's stiffness is significantly increased, allowing it to resist greater lateral forces and enhancing the stiffness of tall buildings, as shown in Figure 5 [54]. Outriggers are placed strategically within the building to optimize load transfer, minimize sway, and control deflection. This hybrid approach ensures that the structure can withstand the demands of tall building design while maintaining architectural flexibility.

In addition to the outrigger system, belt truss systems play a crucial role in enhancing the structural performance of tall buildings. Belt trusses are horizontal truss systems that encircle the building's perimeter at specific levels, often coinciding with the outrigger floors. Their primary function is to tie together the external columns, increasing the overall rigidity of the structure and redistributing lateral loads more effectively. By forming a continuous frame around the perimeter, belt trusses enhance the capacity of perimeter columns to share seismic and wind loads, leading to improved load-sharing behavior between the core and the outer frame. This interaction further reduces lateral drift and enhances the building's torsional resistance. The strategic placement of belt trusses in conjunction with outriggers provides a dual-layer system of lateral force resistance, making the combined approach a highly effective solution for controlling deflection, increasing overturning resistance and improving overall structural stability.

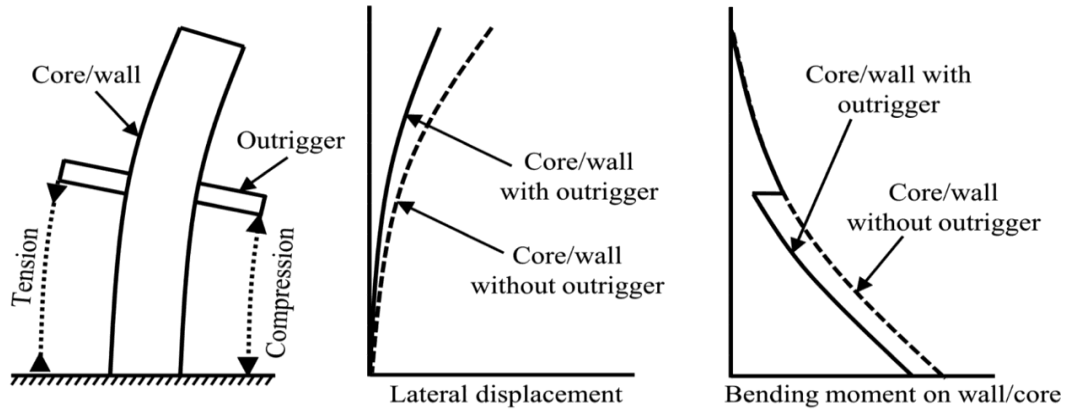


Figure 5 Structural Behaviour of Outrigger Structural System [54].

2.5 Lateral Load Considerations

2.5.1 Wind Load on Tall Buildings

Their structural characteristics strongly influence the response of buildings to wind loads. Key factors include the natural frequencies of the first few modes of vibration and the building's height, which determine whether a building is classified as rigid or flexible. High-rise buildings subjected to wind actions are generally treated as ‘vibrant bluff bodies,’ undergoing oscillations in multiple directions—along-wind, across-wind, and torsional. For slender structures, such as tall buildings, these oscillations can be dynamic, driven by buffeting, vortex shedding, galloping, and flutter. The susceptibility of such structures to dynamic response is mainly influenced by turbulence-induced buffeting, whereas vortex shedding and galloping are associated with transverse or crosswind responses. Flutter, a more complex phenomenon, arises from the coupled motion of bending and torsion, leading to instability [15].

Mass-timber buildings, especially tall ones, are characterized by low lateral stiffness and lightweight properties, which make them susceptible to wind-induced oscillations that can cause discomfort to occupants and lead to deflection-related serviceability issues. While significant advancements have

been made in understanding the seismic behavior of mass-timber structures, research on their performance under wind loads remains limited. As the height of mass-timber buildings increases, wind forces often become the controlling factor in their design, both for safety and serviceability. This is due to the low lateral stiffness and lightweight nature of timber systems used for gravity and lateral load resisting.

Under the National Building Code of Canada (NBCC), a building is classified as dynamically sensitive if it meets any of the following criteria: a lowest natural frequency between 0.25 Hz and 1 Hz, a height exceeding 60 meters, or a height greater than four times its minimum effective width. For such dynamically sensitive buildings, either the Dynamic Procedure or the Wind Tunnel Procedure must be applied to determine specified wind loads. However, current building code provisions, including the 2020 NBCC, often lack the accuracy needed to thoroughly evaluate wind-induced motions, particularly in cases where across-wind and higher-mode effects contribute significantly. These higher modes are vital to the overall dynamic response of mass-timber buildings, highlighting the need for enhanced precision in code requirements.

The design process for tall mass-timber buildings must also address serviceability performance, limiting excessive drift and ensuring occupant comfort regarding acceleration levels. Although ultimate limit state (ULS) design based on wind loads from building codes is often conservative, serviceability considerations become critical, particularly for taller structures where deformations are most pronounced in the along-wind direction. Using gust effect factors for drift checks is generally appropriate in these cases, and structural analyses are conducted to compute wind-induced peak drifts using 1-in-50-year wind loads.

Strategies to mitigate building motions include altering building shapes, increasing stiffness, and enhancing damping capacity. Increasing stiffness and inertia is beneficial for reducing along-wind accelerations, whereas increasing damping capacity effectively suppresses across-wind accelerations. Damping capacity can be enhanced using passive supplemental damping systems, which offer a practical approach to improving the performance of mass-timber buildings under wind-induced motion [55].

2.5.1.1 Wind Hazard Map in Canada

The Wind Hazard Map in Canada plays a crucial role in determining appropriate wind loads for structural design. Vancouver, for example, is generally classified as a rough terrain area due to its extensive urban development, which includes densely packed buildings and trees. This classification impacts wind speed profiles and turbulence intensity. Conversely, Victoria is classified as open terrain due to its coastal location,

Key parameters provided by the Wind Hazard Map include wind speed values representing estimated wind speeds for specific return periods derived from historical meteorological data; return periods that offer wind speed estimates for different return periods, such as 1-in-10 and 1-in-50 years, to assess extreme wind event risks; exposure categories that reflect different terrain types, such as open country, suburban, and urban, which influence wind pressures on buildings; regional variability showing wind speed variations across Canada considering diverse climate and geography; and wind zones and altitude effects, where Canada is divided into different wind zones and the map accounts for altitude, modifying wind speed values for specific geographic conditions.

The wind speeds and velocity pressures used in the Code are regionally representative values based on long-term observations at weather stations across Canada (as shown in Figure 6). The reference

wind speeds are nominal one-hour averages at a height of 10 meters above flat, open terrain. These values have been reviewed and updated over several editions of the Code to ensure accuracy.

Annual maximum wind speed data was analyzed via moments to establish wind speeds across various return periods. These values informed the development of reference maps for structural design purposes, with specific data points being abstracted and documented for locations listed in Table C-2 of the NBCC. For instance, the hourly wind pressures for Vancouver and Victoria at a 1/10-year return period are 0.34 and 0.46 (KPa), respectively, while for a 1/50-year return period, these values increase to 0.45 and 0.57 (KPa). This nuanced mapping allows for more precise and location-specific wind load assessments in structural engineering applications.

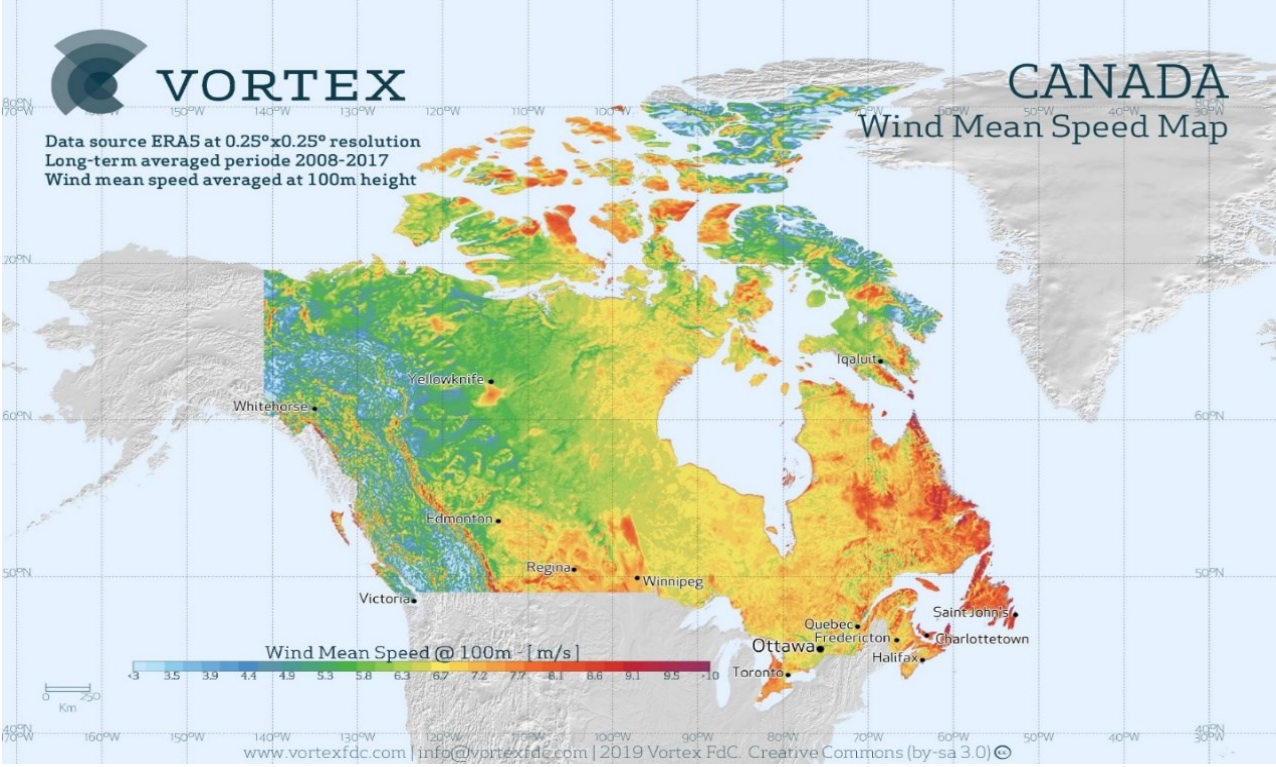


Figure 6 Canada Wind Resource Map at 100 m Height, Modelled at 3 Km Spatial Resolution[56].

2.5.1.2 Wind Performance Objectives

2.5.1.2.1 Comfort of Occupants

In high-rise buildings, wind-induced motion can significantly impact occupant comfort, particularly during moderate to high wind events. The perception of motion varies among individuals, with factors like frequency, amplitude, and duration of acceleration influencing how people experience movement. Studies show that occupants are more sensitive to certain frequencies and tend to notice higher accelerations more acutely. Therefore, ensuring occupant comfort often involves limiting these perceived accelerations to acceptable levels.

Occupants in residential buildings, in particular, experience discomfort more readily than those in commercial spaces, likely due to longer periods of occupancy and the expectation of stability in personal environments. Guidelines such as ISO6897:1984 and ISO10137:2007 emphasize the need for frequency-dependent criteria, acknowledging that human perception thresholds differ across frequencies. This frequency sensitivity necessitates more stringent controls for high-rise structures to limit accelerations in the range that occupants find most perceptible.

Therefore, practical wind performance objectives should balance structural resilience with occupant comfort considerations, especially as high-rise designs push the boundaries of traditional building height and slenderness. This balance helps minimize the adverse effects of perceptible motion, enhancing the quality of life for residents and the functionality of work environments in tall buildings.

2.5.1.2.2 Acceptable Movement

Understanding acceptable movement for wind and vibration, especially concerning serviceability in tall buildings, involves evaluating several criteria that balance structural stability, occupant comfort,

and non-structural element performance. Here's a comprehensive guide to navigating these key aspects, drawing from established engineering practices and standards, including the National Building Code of Canada (NBCC) and internationally recognized guidelines:

Serviceability limits for inter-story drift, or lateral sway between floors, are often specified to prevent excessive movement that could disrupt occupants or damage non-structural components, like walls, partitions, and cladding. The NBCC suggests a standard limit of 1/500 of the building height per story for wind loads. This limit means that the lateral displacement for each story should not exceed 1/500 of the total height of that story. However, deviations from this standard are sometimes permitted if justified through analysis, mainly when resilient non-structural components are used.

In addition to drift, building codes may specify overall deflection limits, which refer to the total horizontal displacement of the structure's top. These deflection limits are crucial to prevent noticeable sway that can cause occupants discomfort and control cumulative stress on materials and connections.

2.5.1.2.3 Acceptable Acceleration

Excessive motion in tall buildings due to wind events can lead to occupant dissatisfaction, particularly if accelerations exceed comfort thresholds. Building codes and guidelines worldwide aim to limit these serviceability accelerations, though the specifics vary by region and standard.

In D. Boggs' study [57], the nausea acceleration limit is 0.098 m/s^2 , while the perception limit is 0.049 m/s^2 for approximately 50% of the population and 0.020 m/s^2 for approximately 2% of the population.

The National Building Code of Canada (NBCC) provides some of the earliest and simplest guidelines, setting a peak acceleration range of 10 to 30 milli-g [58] based on a ten-year return

period, with lower values recommended for residential buildings. These criteria are grounded more in historical precedent than detailed research, assuming acceptable performance when wind tunnel results align with guidelines.

In Hong Kong and China, recent codes (e.g., JGJ 3-2010) implement stricter acceleration standards than NBCC, adopting a midpoint of NBCC's range for office (0.25 m/s^2) and residential (0.15 m/s^2) buildings, emphasizing occupant comfort.

ISO6897:1984 and its British equivalent BS6611:1985 introduced frequency-dependent guidelines, using root-mean-square acceleration over 10 minutes and a five-year return period. Developed from field data across varied structures, these standards apply a single curve for residential and commercial buildings, with more stringent limits at higher frequencies, which are more perceptible.

Each standard reflects regional priorities and varied assumptions about occupant sensitivity, occupancy patterns, and acceptable comfort thresholds, contributing to different approaches to managing wind-induced building motion.

2.5.2 Seismic Loads on Tall Buildings

Seismic design for tall buildings must address both safety and functionality. Modern approaches, particularly within performance-based earthquake engineering (PBEE), have advanced methods to ensure buildings meet specific performance objectives tailored to the expected seismic demands.

Performance-based design is inherently an iterative process [59], as outlined in the flowchart for PBEE (see Figure 7). The process begins with selecting performance objectives, which may be influenced by building owners, building codes, or jurisdictional requirements. These objectives define the expected structural response and resilience levels. Once objectives are established, the next step is to develop a preliminary design to meet these performance targets.

After creating the preliminary design, a performance assessment follows. The design is considered complete if the structure meets the selected performance objectives. However, if the goals are unmet, the design enters another iteration, requiring adjustments and reassessment until the desired performance is achieved. This iterative analysis defines the design in each cycle to meet the specified objectives and assures that the structure can achieve optimal performance under seismic conditions.

Two primary factors are essential for successful performance-based design in seismic applications: the seismic hazard map, which establishes design earthquake levels, and the performance objectives, which define the intended structural response and resilience. The seismic hazard map, discussed in greater detail in the next section, is critical for guiding design at the outset. It enables engineers to incorporate location-specific hazard information, grounding the design in accurate seismic risk assessments.

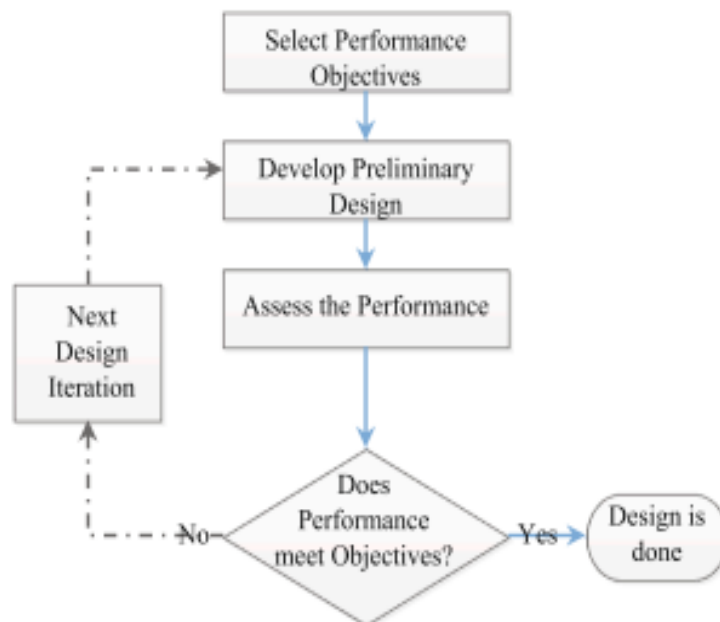


Figure 7 Flowchart of the Performance-Based Design [59].

In this context, performance objectives for tall buildings often encompass life safety and resilience against damage and functional downtime, which are crucial for minimizing societal impacts in urban centers. This shift reflects the need for structural systems sustaining major and minor seismic events while maintaining their integrity and operability.

Design frameworks such as displacement-based design (DBD) and direct displacement-based design (DDBD) have emerged as alternatives to traditional force-based methods. Unlike force-based design (FBD), which relies heavily on empirical estimates and behavior factors, DBD focuses on displacement limits as primary criteria. This approach is especially suited to PBEE objectives, where performance levels are linked directly to structural demands and potential damage under various seismic intensities, offering a more precise route to achieving desired performance outcomes.

2.5.2.1 Seismic Hazard Map in Canada

The seismic hazard map for Canada, which was developed as part of the 6th Generation Seismic Hazard Model (CanadaSHM6) [56], represents a significant advancement in assessing and visualizing earthquake risk across the country. This updated map builds on decades of seismic research and incorporates refined models for seismic sources, ground motions, site amplification, and aleatory uncertainty. CanadaSHM6 underpins the seismic design values proposed for the National Building Code of Canada (NBCC), addressing critical factors like the recurrence of significant earthquakes, ground shaking intensities, and site-specific amplification effects.

The Cascadia subduction zone is a key factor influencing seismic hazards in southwestern Canada, particularly in Vancouver and Victoria. Located off the Pacific coast, the Cascadia fault poses a substantial seismic risk due to its potential to produce megathrust earthquakes with magnitudes of 8.0 or greater, such as the M~9 event recorded in 1700. This fault spans from northern California to

central Vancouver Island and introduces considerable seismic hazard to Vancouver and Victoria's densely populated urban centers. CanadaSHM6 incorporates updated models for the Cascadia subduction zone, including refined geometry and recurrence intervals for megathrust events, increasing hazard estimates in these regions. These updates emphasize the critical need for designing buildings in Vancouver and Victoria to withstand high seismic forces, ensuring structural resilience and occupant safety during a major Cascadia earthquake.

Figure 8 illustrates Canada's seismic hazard distribution, while Figure 9 focuses on the British Columbia seismic risk map. These maps emphasize the elevated hazard in western Canada, particularly near the Cascadia subduction zone.

CanadaSHM6 also introduces new seismic hazard estimates derived from an improved understanding of seismic sources, including subduction interface earthquakes, particularly in regions affected by the Cascadia fault. For the first time, incremental rates for great megathrust earthquakes have been calculated directly from paleoseismic records, providing a historical perspective that enhances prediction accuracy. Combined with updated ground motion models and hybrid site amplification functions, these refinements result in an approximate 50% increase in estimated seismic hazard for many regions, especially in southwestern Canada.

CanadaSHM6 replaces separate amplification tables with hazard estimates calculated directly for a continuous range of VS30 values (140 to 3000 m/s), enhancing site-specific accuracy. This shift enables more precise assessments, reducing reliance on coarse Site Class categories (A to E) and simplifying the design process. The model also integrates a hybrid amplification approach considering "gradational" and "step-like" velocity profiles, addressing regional variations like glaciated central/eastern Canada and western regions such as Victoria, where resonance amplifies soft soil layers over bedrock.

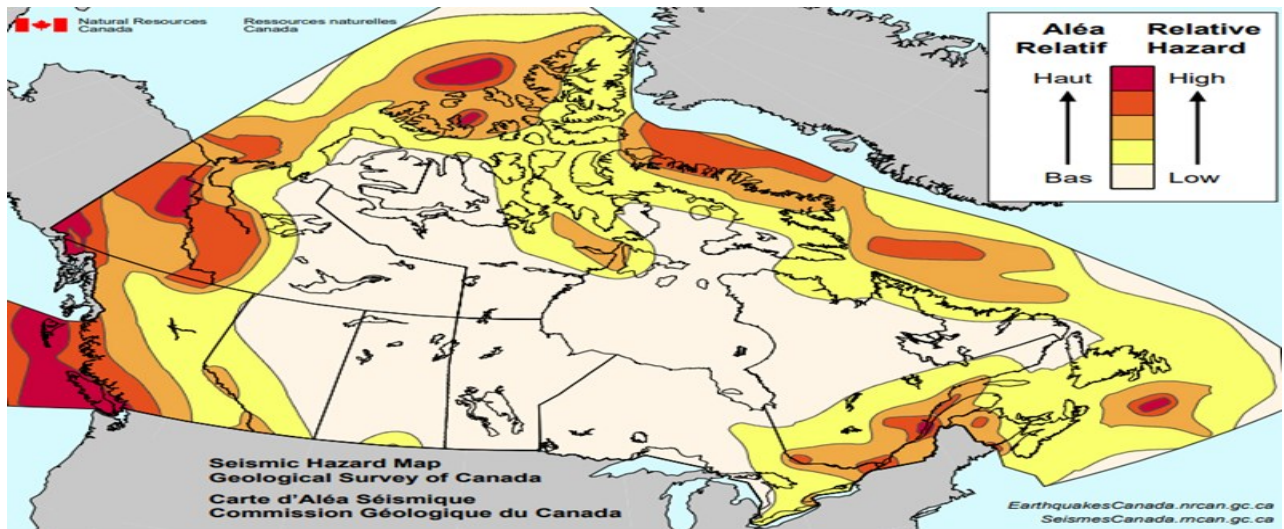


Figure 8 (A) Seismic Risk Map of Canada, Showing the Distribution of Seismic Hazards Across the Country [56].

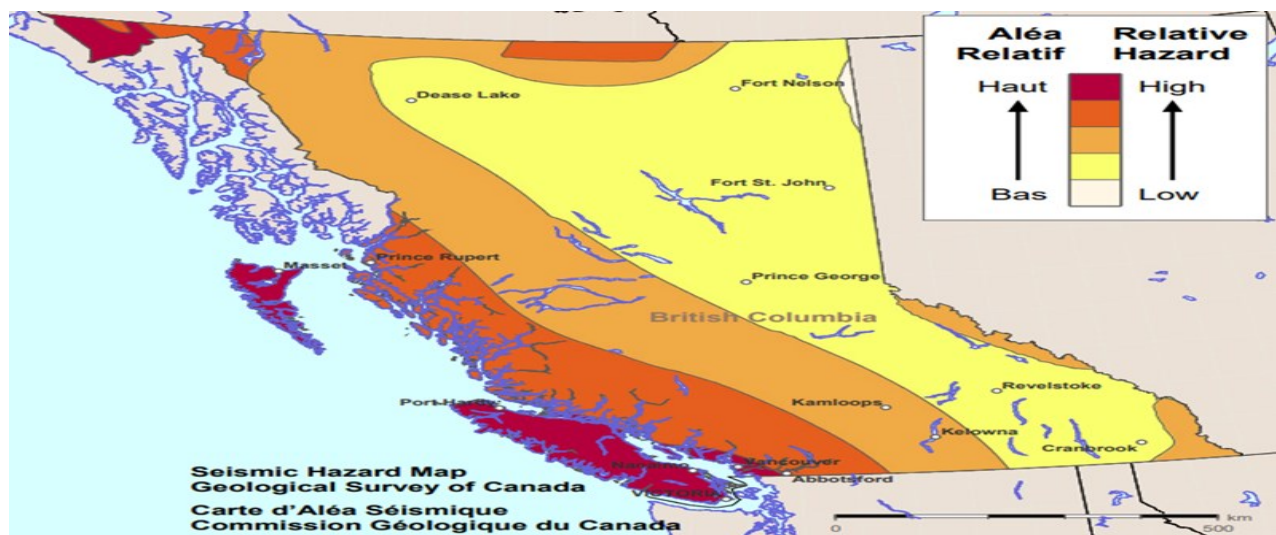


Figure 9 Seismic Risk Map of British Columbia Near the Cascadia Subduction Zone [56].

The historical evolution of seismic hazard estimates is illustrated in Figure 10, which compares hazard levels over time for cities like Montreal, Vancouver, and Victoria. In particular, Vancouver and Victoria have consistently increased hazards due to an improved understanding of seismic risks associated with the Cascadia subduction zone. Victoria’s hazard levels, for instance, have risen by 150% since the 1950s as the proximity of this city to an active plate boundary has become better understood [60].

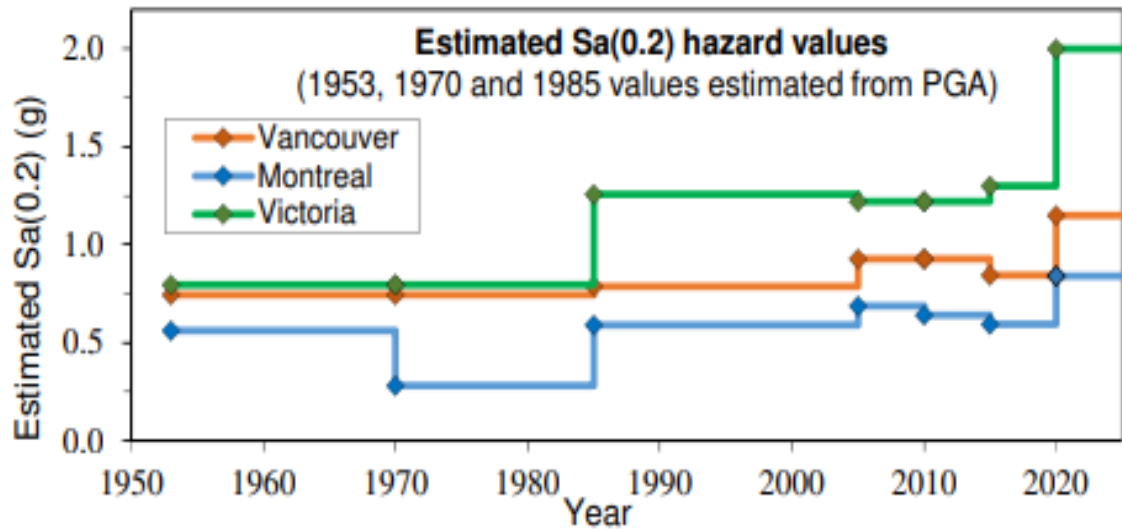


Figure 10 Changes in Estimated $S_a(0.2)$ at a 2%/50-Year Probability Level For Site Class C Soil (X450 M/S) In Victoria, Vancouver, and Montreal [60].

The 2020 National Building Code of Canada Seismic Hazard Tool is a valuable resource for estimating seismic risk at any location in Canada based on CanadaSHM6. This tool allows engineers and designers to input location-specific data and receive seismic design values tailored to the specific site conditions, facilitating more accurate and practical risk assessments nationwide [56].

2.5.2.2 Seismic Performance Objectives

Seismic performance objectives establish clear benchmarks for how a building should perform under seismic events, allowing engineers to design for specific outcomes beyond basic life safety. In the performance-based earthquake engineering (PBEE) framework, these objectives guide decisions on acceptable levels of damage, downtime, and resilience.

Advanced assessment tools, such as incremental dynamic analysis (IDA) and fragility curves, evaluate structural behaviour under realistic seismic loading, ensuring that buildings meet defined safety and functionality levels. Together, these methods enable a structured, objective approach to achieving performance objectives in seismic design.

The selection of earthquake levels and performance objectives plays a fundamental role in guiding the design process, ensuring that buildings are safe and resilient against seismic events' functional and economic impacts. For each level of earthquake intensity, engineers establish performance targets that align with the building's intended use, risk tolerance, and stakeholder requirements, as shown in Figure 11. For example, at the Service Level Earthquake (SLE), buildings designed with operational objectives prioritize minimal damage to both structural and non-structural components, allowing them to remain functional immediately after minor seismic events. This level is critical for buildings that must operate continuously, such as data centers, essential services, or laboratories with sensitive equipment, where even minor downtime could lead to significant disruptions.

The emphasis shifts to life safety at the Design Basis Earthquake (DBE) level. Here, structures are designed to handle moderate to severe earthquakes, sustaining some damage but maintaining stability to protect occupants. This level focuses on ensuring that people can safely evacuate the building if needed, with damage limited to repairable levels, minimizing risk to life and financial loss from repairs. This level is often applied to most residential and commercial buildings where the primary objective is to secure human life and support safe evacuation without necessarily maintaining full operability.

The design objective for Maximum Considered Earthquake (MCE) is collapse prevention. This approach ensures that the building structure will avoid catastrophic failure during rare and severe seismic events, preserving life safety even under extreme conditions. This level is vital for high-importance buildings, such as hospitals, emergency operation centers, and high-occupancy facilities, where structural integrity is paramount in scenarios that exceed typical design expectations.

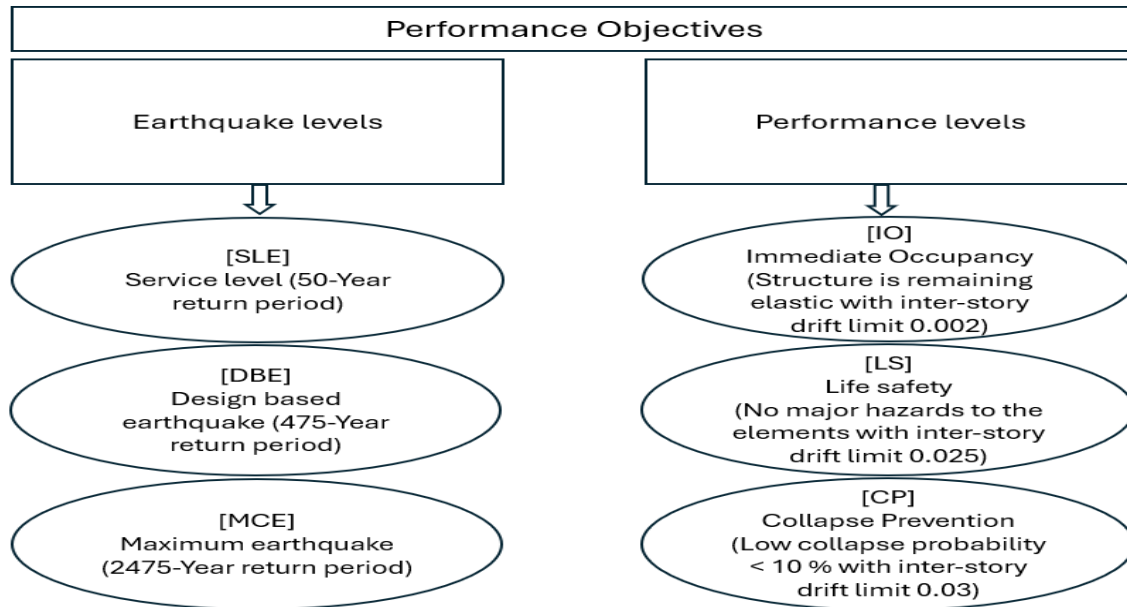


Figure 11 Flowchart Depicting Levels and Objectives of Performance-Based Design.

By selecting performance levels that align with each structure's intended use and risk profile, performance-based seismic design provides a comprehensive framework for achieving safe, resilient, and context-appropriate buildings that meet regulatory and stakeholder expectations.

2.5.3 Ductility and Overstrength

Ductility and overstrength are key attributes in seismic design that allow structures to endure earthquake forces without catastrophic failure. Together, these properties enhance a structure's resilience by enabling energy absorption and providing a strength reserve beyond code-specified seismic demands.

Ductility is the capacity of structural elements to undergo extensive plastic deformations without losing load-bearing ability. This flexibility allows buildings to absorb seismic energy and prevents brittle failure, especially in high-seismic regions. Overstrength represents the additional strength in a structure beyond what is required for essential code compliance, offering a buffer against

unexpected seismic forces. This inherent safety margin, often due to conservative design practices or material variability, helps protect non-ductile elements from damage.

In the NBCC (National Building Code of Canada), Table 4.1.8.9 specifies values for R_d and R_o , which guide calculating seismic forces based on a structure's ductility and overstrength characteristics. Together, ductility and overstrength support performance-based design by promoting control and ductile failure modes in specific elements, ensuring life safety and maintaining structural integrity during seismic events.

2.5.4 Structure Irregularities

Structural irregularities can significantly influence the seismic response of buildings, as they introduce variations in stiffness, strength, mass, or geometry that may concentrate stresses or amplify seismic demands in specific areas. The National Building Code of Canada (NBCC) classifies several structural irregularities in Table 4.1.8.6, defining conditions that may lead to unexpected behaviour under earthquake loading. Identifying and addressing these irregularities in the design phase ensures the building's stability and resilience during seismic events.

Vertical stiffness irregularity exists when there is a significant change in lateral stiffness between adjacent stories. This condition occurs for concrete and masonry shear walls if the lateral stiffness in a story is less than 70% of that in the adjoining story or less than 80% of the average stiffness of the three stories above or below. For other structural systems, it exists when the interstorey deflection exceeds 130% of that in the adjacent story. Sudden changes in stiffness can create weak points in the building's response to seismic forces.

Weight (mass) irregularity is identified when the weight of any story exceeds 150% of the weight of an adjacent story. Sudden increases in mass can cause a disproportionate concentration of seismic

forces, potentially leading to unexpected stresses. However, a roof lighter than the floor below is not a mass irregularity.

Vertical geometric irregularity is present when the horizontal dimension of the seismic force-resisting system (SFRS) in one story exceeds 130% of that in an adjacent story. Significant changes in the plan dimensions of the SFRS from one story to the next can disrupt the lateral load path and may amplify stress concentrations during an earthquake.

In-plane discontinuity in vertical lateral-force-resisting elements occurs when there is an offset or a reduction in the stiffness of a vertical lateral-force-resisting element between stories, except in braced or moment-resisting frames. Such discontinuities can lead to stress concentrations and increased vulnerability in the lateral force-resisting system (SFRS). Out-of-plane offsets are discontinuities in the lateral force path, such as offsets in the SFRS. They may introduce instability during seismic shaking by interrupting the alignment of the load path.

Discontinuity in capacity, or a weak story, describes a story with less shear strength than the story above. This weakness may cause the building to "hinge" at that story during strong seismic shaking, potentially leading to significant structural damage. Torsional sensitivity, another irregularity, occurs when diaphragms are not flexible, and the torsional ratio (B) exceeds 1.7. This condition can result in excessive building twisting during lateral motion, causing uneven stress distribution and increased deformation in some areas.

Finally, structural irregularities impact a building's stability and seismic performance. Recognizing and mitigating these irregularities ensures that lateral forces are managed effectively, reducing the risk of unexpected stress concentrations or weak points that could compromise structural integrity during an earthquake.

3 Dynamic Performance of Tall Buildings

3.1 Theoretical Basis

To understand the dynamic performance of tall buildings, it is essential to grasp the theoretical basis of structural dynamics. The dynamics of structure theories and equations provide a comprehensive framework for analyzing structural behaviour under dynamic loads, including wind and seismic excitations. This theoretical foundation encompasses the concepts of Single-Degree-of-Freedom (SDOF) and Multi-Degree-of-Freedom (MDOF) systems, as well as natural frequencies and mode shapes, which are critical for predicting the dynamic response of buildings.

3.1.1 SDOF System

A Single-Degree-of-Freedom (SDOF) system is the most straightforward representation of a vibrating structure. It is idealized as an oscillator consisting of mass and stiffness, which moves in a single direction. Consequently, only one coordinate is required to define the system's motion. The system oscillates when the mass is displaced and released without applying any external force. In an undamped scenario, the mass oscillates indefinitely as no frictional damping reduces the vibration amplitude. The equations of motion (EOM) describe the system's dynamics mathematically. Derived from Newton's second law, the dynamic equilibrium equation equates the forces acting on the mass (m) with spring (K) for a basic undamped SDOF system; this is expressed as:

$$ma(t) + Kx(t) = 0 \tag{1}$$

Where do $a(t)$ and $x(t)$ represent the acceleration and displacement of the object, respectively?

In cases where an external force acts on the system, the generalized equation of motion in terms of displacement and its second-time derivatives become:

$$m\ddot{x}(t) + kx(t) = P(t) \quad (2)$$

For actual structures, damping is always present to dissipate energy, causing the system to vibrate with decreasing amplitudes. Incorporating damping into the equation of motion gives the whole equation of motion, as illustrated in Figure 12, and the following equation:

$$m\ddot{x}(t) + c\dot{x}(t) + kx(t) = P(t) \quad (3)$$

where (c) represents the damping coefficient. The SDOF system provides a fundamental understanding of vibrational behaviour, forming the basis for analyzing more complex multi-degree-of-freedom systems.

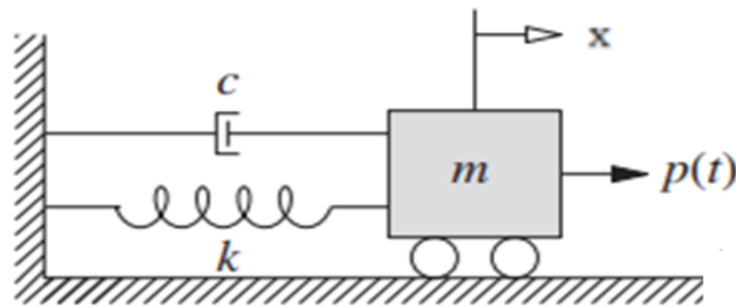


Figure 12 SDOF Equation of Motion with Mass–Spring–Damper System[61]

3.1.2 MDOF System

Unlike Single-Degree-of-Freedom (SDOF) systems, real-world structures distribute their mass and stiffness across multiple points, necessitating a more complex analytical approach. Multi-degree-of-freedom (MDOF) systems address this complexity by representing the dynamic behaviour of structures with multiple interconnected masses, as illustrated in Figure 13.

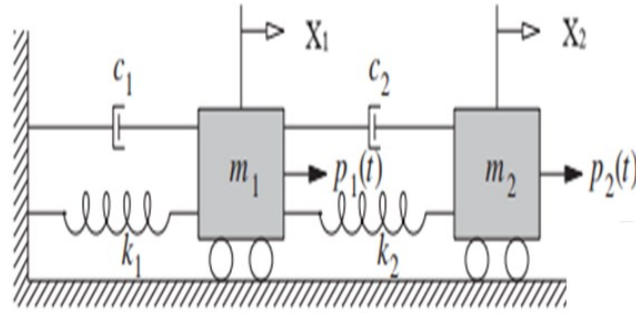


Figure 13 MDOF Equation of Motion with Mass–Spring–Damper System[61]

In an MDOF system, the number of independent coordinates required to describe the motion corresponds to the total number of degrees of freedom (DOFs). For example, in a two-story building, these coordinates represent the horizontal displacements of each floor. The dynamic equilibrium of each floor can be modelled using SDOF principles and extended to capture interdependencies between floors. The resulting equations of motion for each DOF are assembled into a coupled system of differential equations, expressed in matrix form as represented mathematically in Equation (4):

$$\begin{bmatrix} m_1 & 0 \\ 0 & m_2 \end{bmatrix} \begin{Bmatrix} \ddot{x}_1 \\ \ddot{x}_2 \end{Bmatrix} + \begin{bmatrix} c_1 + c_2 & -c_2 \\ -c_2 & c_2 \end{bmatrix} \begin{Bmatrix} \dot{x}_1 \\ \dot{x}_2 \end{Bmatrix} + \begin{bmatrix} K_1 + K_2 & -K_2 \\ -K_2 & K_2 \end{bmatrix} \begin{Bmatrix} x_1 \\ x_2 \end{Bmatrix} = \begin{Bmatrix} P_1(t) \\ P_2(t) \end{Bmatrix} \quad (4)$$

Where m_1 , c_1 , k_1 , m_2 , c_2 , and k_2 represent the mass, damping, and stiffness for story 1 and story 2, respectively.

The multi-story building exhibits interactions between floor-level vibrations, requiring evaluation as an MDOF system. The dynamic response of MDOF systems is influenced by the interactions among the degrees of freedom, resulting in coupled equations. Modal superposition techniques are often employed to simplify analysis. This method decouples the equations by transforming physical coordinates into modal coordinates, leveraging the orthogonality of mode shapes to analyze the dynamic behaviour more efficiently.

3.1.3 Natural Frequencies and Mode Shapes

The solution of an MDOF system under free vibration, when no external forces are applied, provides critical insights into the dynamic behaviour of a structure. It identifies the natural frequencies and corresponding displacement shapes, known as mode shapes (ϕ), which govern the structure's vibrational response. In the absence of damping and external forces, the equation of motion for free vibration simplifies to:

$$m\ddot{x}(t) + kx(t) = 0 \quad (5)$$

In general, the system's motion in free vibration follows a simple harmonic pattern depending on the oscillation frequency (ω), time (t) and phase angle (θ) expressed as:

$$x(t) = \phi \sin(\omega t + \theta) \quad (6)$$

By substituting this expression and its second-order derivative, the equation of motion is given as:

$$-M\omega^2\phi \sin(\omega t + \theta) + K\phi \sin(\omega t + \theta) = 0 \quad (7)$$

By simplifies it further and gives the undamped eigenvalue problem:

$$[K - \omega^2 M] \phi = 0 \quad (8)$$

The eigenvalues (ω^2) are the squares of the natural frequencies, and the eigenvectors (ϕ) represent the mode shapes. These mode shapes form an orthogonal set, enabling any arbitrary displacement to be expressed as a combination of the modes. Each mode corresponds to a specific deformation pattern occurring at its associated natural frequency. Additionally, the displacement vector is expressed as a sum of modal contributions:

$$x(t) = \sum_{n=1}^N \phi_n q_n(t) \quad (9)$$

Where $q_n(t)$ Represents the modal coordinate for the n^{th} mode. Substituting this expression into the equation of motion and utilizing the orthogonality of the mode shapes concerning the mass and stiffness matrices produces uncoupled equations of motion for each mode:

$$\ddot{q}_n(t) + 2\xi_n \omega_n \dot{q}_n(t) + \omega_n^2 q_n(t) = \frac{\phi_n^T F(t)}{M_n} \quad (10)$$

Where M , $2\xi \omega q(t)$, and $\omega^2 q(t)$ the generalized mass, damping, and stiffness for the n^{th} mode, respectively.

Finally, the participating mass ratio for a mode quantifies its significance in computing the structural response to acceleration loads in the global coordinate system (X, Y, and Z directions). This ratio is beneficial for evaluating the accuracy of response spectrum analyses and seismic time-history analyses. However, it does not provide information about the accuracy of time-history analyses under non-acceleration loads. The participating mass ratios for the n^{th} mode corresponding to translational and rotational acceleration loads (i) in or around the global axis X, Y, and Z are defined as:

$$r_{in} = \frac{f_{in}^2}{M_i} \quad (11)$$

Where f_{in}^2 is the participation factors, which represent the mode shape times the unit acceleration loads, and M_i is the total unrestrained mass acting in the direction of the participation factors. It is unnecessary in practical applications, including all modes in the summation. Generally, only the lower modes, which have the most significant impact on the dynamic response, are considered. The

selected modes should achieve over 90% mass participation to ensure accuracy. This approach balances computational efficiency with maintaining the required level of precision.

3.2 Damping of Tall Wood Buildings

Damping plays a crucial role in the structural behaviour of tall buildings, particularly in mitigating vibrations induced by dynamic loads such as wind and seismic events. Vibrations, if left uncontrolled, can result in discomfort for occupants or even structural damage. Initially developed for aerospace applications, vibration control technology has been adapted to protect buildings and bridges from external loads, improving structural resilience [62]. Damping refers to a building's ability to reduce vibration amplitudes while dissipating the absorbed energy, as shown in Figure 14.

The term "damping" in structural engineering can vary depending on the engineer's perspective. For a civil engineer, damping might be simply a reference noted on seismic or wind spectral maps, commonly annotated as 5% damped spectra.

On the other hand, structural engineers describe damping as variations in overall stress within a structure subjected to shock and vibration. This often leads to debates about the appropriate level of structural damping, typically ranging from 2%, 3%, and 4%, but not more than 5%. Given these definitions, a damper is an element that can be incorporated into a structure to provide resistive forces against motion, thereby allowing energy to be dissipated [63].

However, the damping ratio in tall buildings is typically lower than that of shorter structures. Equation 12 was developed by Anil K. Chopra [61] to predict the expected value of the first-mode damping ratio (ζ) for steel buildings based on the building height (H).

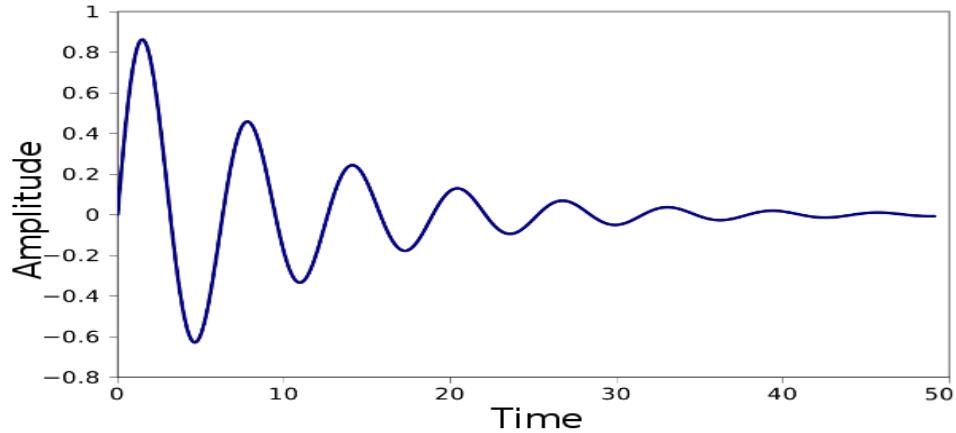


Figure 14 Damping Mechanism Showing Vibration Amplitude Reduction and Energy Dissipation.

$$\zeta = 1.2 + 4.26e^{2-0.013H} \quad (12)$$

Based on that, it is clear that tall steel buildings with heights ranging from 55 to 85 meters typically exhibit damping ratios between 1.5% and 2%. However, the understanding of damping characteristics in tall timber buildings is limited due to the relatively small number of completed projects [6]. However, as building height increases, a corresponding decrease in damping values becomes evident, rendering tall structures more vulnerable to lateral drift and occupant discomfort during seismic and wind loads. Additionally, FPInnovations’ research on mid- to high-rise timber buildings revealed damping ratios ranging from 1% to 2.5%, with an average of around 1.5% recommended for both wind and seismic design. However, ongoing monitoring of the Arbora and Origine buildings found damping ratios of about 2.5%, suggesting that the frequently assumed 1% value may be conservative for high-rise mass-timber buildings with CLT shear walls[64].

Recent research has emphasized the dynamic response of tall timber structures and the importance of incorporating energy dissipation mechanisms to enhance stability and reduce construction costs [65]. The challenges associated with low damping in timber buildings highlight the need for supplemental systems to ensure structural safety and serviceability.

Timber buildings often use hybrid timber-concrete or timber-steel systems to address vibration issues. The NBCC provides seismic force modification factors for braced timber frames but does not specify connection types for different ductility levels, limiting broader adoption. Using capacity-based design principles, connections are engineered to concentrate nonlinear deformations in the brace, thereby enhancing performance and preventing column failure [66]. However, recent research has underscored concerns regarding the seismic resilience of tall buildings, emphasizing the necessity for high-performance supplemental energy dissipation devices to enhance seismic resilience [67], [68].

Previous analytical investigations on coupled wall systems primarily focused on assessing natural vibration frequencies, often without integrating energy dissipation devices or dampers. The continuum approach is commonly adopted for its simplicity and applicability to tall buildings [69], [70]. Nonetheless, studies on shear walls coupled with dampers are quite limited. In one such study, Lavan et al. [71] used the continuum method to derive a fourth-order differential equation governing the response of shear walls with viscous dampers. This approach neglected the axial deformation of the walls and assumed that the entire system could be uncoupled into a stiffness medium and a damping medium. In a recent study, Moghadasi et al. [78] derived a fourth-order differential equation for analyzing shear walls coupled using viscous and viscoelastic dampers.

In recent years, significant efforts have been made to translate the concept of energy dissipation into practical technological applications. All vibrating structures inherently lose energy due to internal strain, friction, cracking, plastic deformation, and other factors. The greater the energy loss capability, the lower the vibrational amplitudes. Buildings with low inherent damping (typically about 1% of the critical value) can endure very high vibration amplitudes even when subjected to moderate earthquakes [72].

Enhancing energy dissipation capacity is essential for effectively reducing vibration amplitudes. A range of methods has been explored to achieve higher levels of damping, with additional approaches continually being proposed. These advancements broaden the scope and effectiveness of vibration control strategies in modern structural engineering, ensuring more resilient and stable structures [73].

Various types of devices are found in buildings worldwide, primarily recognized for enhancing energy dissipation within structural systems. This dissipation can occur by transferring energy between different vibrating modes or converting kinetic energy into heat. The first approach uses mechanisms based on principles such as fluid orifice, metal yielding, phase change in metals, deformation of viscoelastic materials, and frictional sliding. The second approach employs additional oscillators that act as dynamic vibration absorbers, effectively managing and reducing vibrations [74].

Employing timber-based hybrid buildings makes it feasible to overcome the height limitations typically associated with timber constructions. Three high-rise timber–reinforced concrete (RC) hybrid buildings, a 10-story uncoupled shear wall (10S-U), and 15- and 20-story coupled shear wall structures were investigated. The study noted that as building height increases, there's a corresponding need for enhanced energy dissipation. This study focuses on presenting the force modification factors. Seismic modification factors for timber hybrid buildings were developed by adapting the FEMA P695 (FEMA 2009) framework to Canadian seismic conditions and design parameters. Due to the influence of gravity load and the rocking response mechanism, the structure exhibits recentering capability in its response. Consequently, no residual drift was observed. Seismic modification factors of $R_o = 1.5$ and $R_d = 3$ were deemed acceptable following evaluation through Incremental Dynamic Analysis (IDA) and collapse margin ratio assessments. However, in the weaker direction, these factors exceeded the maximum drift ratio limit state of 2.5% CP outlined in

the National Building Code (NBCC). underscoring the critical importance of implementing structural control strategies [75]

3.3 Passive Structure Control Techniques

Seismic design based on performance highlights rising labour costs and other expenses for repairing structural and non-structural elements after typical earthquakes. Structural control systems are considered one of the most feasible and practical strategies to achieve performance-based design objectives. Serving as the first line of defence. Generally, structural control systems can be divided into four categories: passive devices with high energy dissipation density and no need for an external power source, active devices with force delivery devices and real-time processing sensors that require power for the actuator to generate a structural control force, semi-active that alter some structural parameters while consuming less power compared to active control systems, and hybrid control systems [76].

Among them, the passive system is the most commonly used as it is less expensive and can function without the need for an external source of energy, which might not be available during catastrophic earthquake events. The primary function of a passive energy dissipation device is to absorb or consume a portion of the input energy, thereby reducing the energy dissipation demand on primary structural members and minimizing potential structural damage.

Passive systems primarily include dampers and base isolators. However, base isolators, which effectively reduce seismic impacts by decoupling the building from ground motion, are less suitable for tall buildings due to their higher natural periods.

As a result, alternative damping solutions are preferred for high-rise structures to enhance stability and control lateral movements effectively. These supplemental damping systems safeguard people

and equipment against seismic forces. In addition, the dynamic response of high-rise buildings to earthquake ground motions and wind-induced excitations often dictates their structural design. It is widely recognized that tall buildings can experience amplified dynamic wind and seismic responses because of their relative flexibility and low damping, a characteristic that decreases with height [77].

Beyond conventional design approaches, such as capacity design to control seismic behaviour or increasing stiffness to limit wind and seismic effects, supplementary damping control systems provide an efficient, resilient, and low-damage design solution. In earthquake-resistant architecture, several types of seismic control systems are employed to mitigate the impact of earthquake forces on the primary structural framework [78].

Inter-story passive dampers are a structural engineering device created to reduce the impact of seismic forces on buildings. Typically installed between contiguous floors (inter-stories). When configured in locations where the main structure elements they replace are anticipated to endure severe damage under seismic loading, as illustrated in Figure 15 [13], these dampers dissipate energy and regulate relative motion between floors during an earthquake, such as fluid viscous damper and viscous elastic damper, and friction damper.

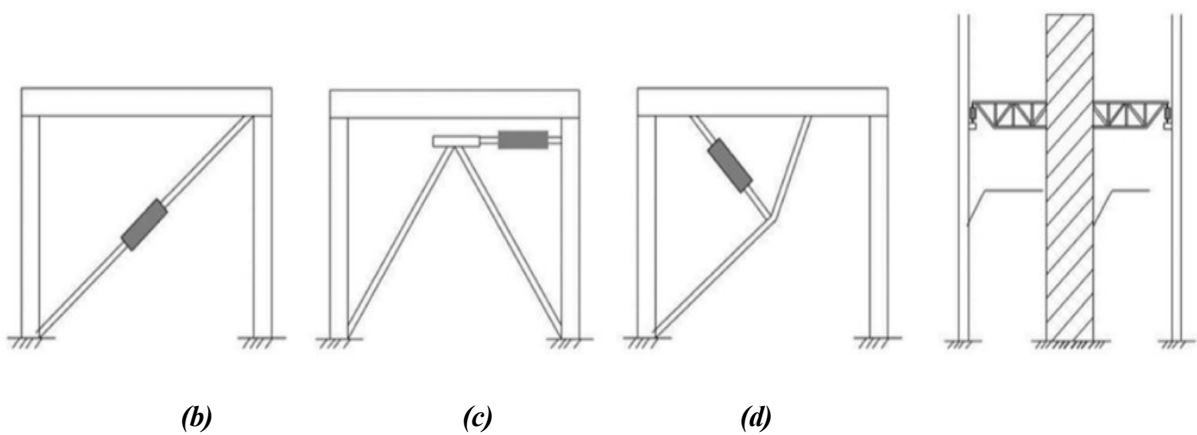


Figure 15 Passive Damper Configurations (a) Diagonal Brace Damper, (b) Chevron Brace Damper, (c) Toggle Damper, (d) Cantilever Truss Damper [13].

In terms of the control devices of the passive system, FEMA 274 classifies them into displacement-dependent dampers (rate-independent), velocity-dependent dampers (rate-dependent), and other types of dampers [79]. Displacement-dependent dampers, such as metallic and sliding friction dampers, dissipate energy through plastic behaviour within the dampers [80]. Additionally, velocity-dependent dampers include fluid viscous dampers and viscoelastic dampers. These dampers dissipate energy through forces relative to the deformation rate (i.e., velocity).

3.3.1 Passive Rate-Dependent Dampers

Rate-dependent passive dampers are crucial for mitigating seismic loads on structures. These advanced devices dissipate kinetic energy during an earthquake, reducing vibrations and enhancing structural stability. Unlike conventional dampers with constant resistance [81], velocity-dependent dampers adjust their force based on the structure's movement velocity. As seismic activity causes rapid and variable motion, these dampers increase resistance proportionally, offering superior control over the building's dynamic response. This adaptability ensures excellent safety and resilience against earthquakes.

Viscoelastic dampers (VEDs) and fluid viscous dampers (FVDs) are examples of such devices. They dissipate energy by exerting forces that vary proportionally with motion velocity. This characteristic enables them to offer effective damping across different levels of excitation [82], thereby enhancing structural performance and durability, especially in seismic environments. Rate-dependent passive dampers offer an attractive damping technology that addresses earthquake and wind loads. In the context of multi-hazard (MH) design, selecting the appropriate damper and its placement to satisfy MH performance limit states can be framed as an optimization problem [6].

3.3.1.1 Fluid-Viscous Dampers

FVDs are the most popular passive energy dissipation systems used in civil engineering and are commonly used in structural engineering [83]. These hydraulic devices dissipate mechanical energy by generating a damping force against motion. FVDs effectively mitigate transverse, longitudinal, and vertical displacements and can be installed in various structures.

FVDs have recently gained popularity due to several key advantages: 1) their significant energy dissipation capabilities and seismic performance enhancement; 2) their ability to generate forces independent of displacement; and 3) their capability to increase the damping ratio without substantially altering the stiffness characteristics. FVDs provide additional damping without significantly increasing the base shear, as they do not shift the fundamental period of the building [84]. This assists in reducing the overturning of the structure, making FVDs an effective solution to meet the stringent seismic design requirements for retrofitting existing structures [85].

Figure 16 (a, b) illustrates the components of an FVD, which include a cylinder, piston, hydraulic valve (orifices), piston rod, and silicone oil. When subjected to earthquake loads, the movement of the structure causes the piston to move relative to the cylinder, generating displacement. This reciprocating motion drives the flow of silicone oil within the cylinder. As the fluid moves, friction between the molecules and the cylinder's surface generates heat, converting seismic energy into thermal energy and producing a damping effect. FVDs are effective within a temperature range of 40 to 70°C, considered optimal operating for their best performance [72].

The simplest model of a viscous damper system, such as an oil damper, is the viscous type of model. When the damper is under compression, high-pressure liquid flows through the orifices from chamber 2 to chamber 1. Conversely, fluid flows from chamber 1 to chamber 2 when the damper is in tension. This movement of high-pressure fluid across the piston creates a pressure difference on

either side of the cap, generating the damping force. The piston has custom-designed orifices that create an optimized relationship, resulting in a pressure (force) that varies with velocity. The greater the velocity, the greater the resisting force produced. The following equation typically characterizes this relationship:

$$F = C \cdot V^\alpha \quad (13)$$

where (F) is the damping force, and (C) is the damping coefficient, which depends on the fluid properties, the piston's diameter, and the orifice areas. Changes in fluid temperature can affect the fluid properties, thereby influencing the damping coefficient. (V) is the velocity, and (α) is the velocity exponent, which can be set between 0.2 and 2.0 by selecting the appropriate shape of the piston head, depending on the specific application.

Values of α in the range of 0.3 to 0.5 are most common for building seismic applications. Wind-damping applications use exponents from 0.5 to 1.0, with the lower values used in structures subjected to wind and seismic inputs. Typically, a minor velocity exponent results in greater energy consumption. To protect diverse structures, it's necessary to employ different velocity exponents [86]. Figure 16 (c, d) depicts the force-stroking displacement and velocity diagram of an FVD with various α values while keeping the damping coefficient, energy dissipation, and displacement amplitude constant. A nonlinear FVD with a smaller α generates higher damper forces at lower velocity ranges (the hysteretic shape for $\alpha = 0.1$ is nearly rectangular) [87]. Furthermore, Martinez et al. [88] showed that the peak force of a nonlinear damper is approximately 35% lower than that of a linear damper, even though they have equal energy consumption.

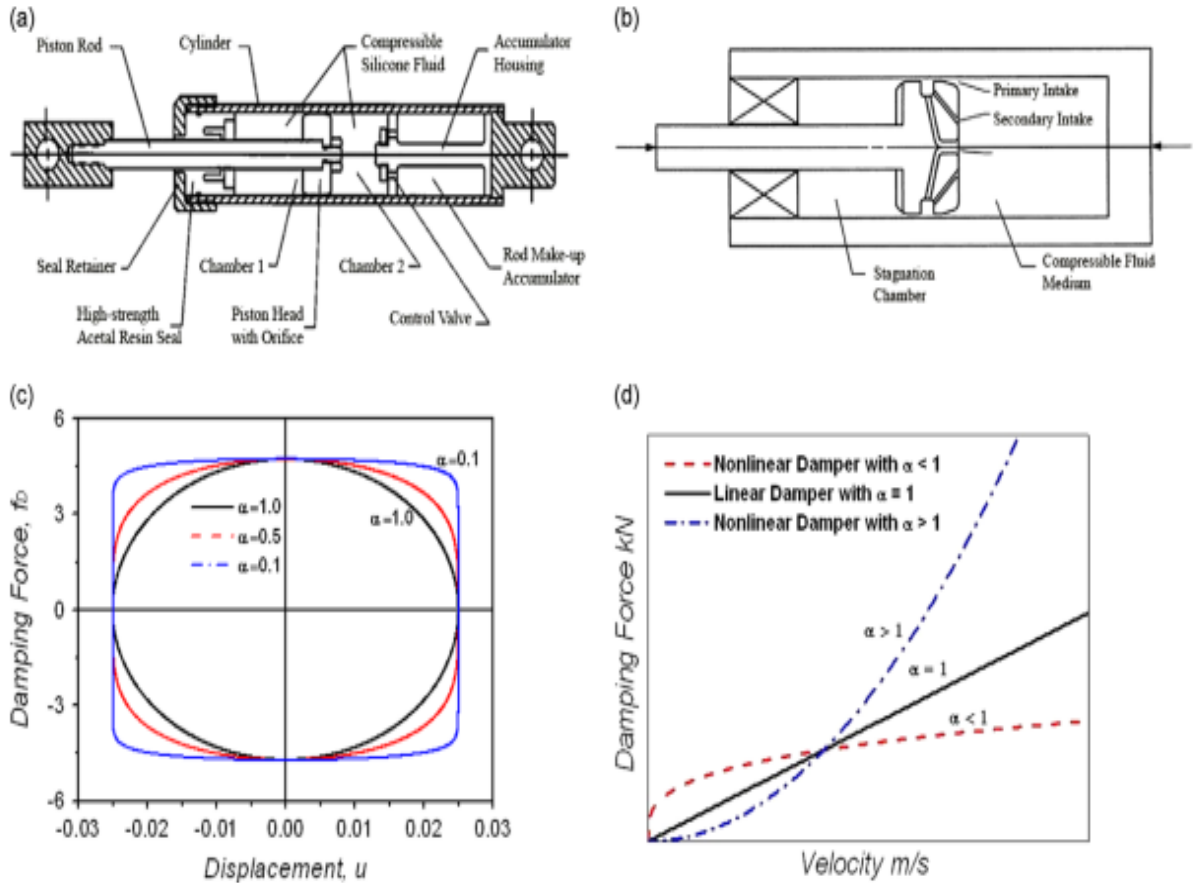


Figure 16 (a) A Typical Longitudinal Cross-Section of A Fluid Viscous Damper, (b) The Fluidic Control Orifice, (c) The Idealized Force-Displacement Relationship, and (d) The Force-Velocity Relationship [87].

Soong and Dargush (1997) [89] developed energy-based design approaches for buildings equipped with supplemental dissipative devices, including Fluid Viscous Dampers (FVDs). Sorace and Terenzi (2008) [90] extended these methodologies to systems with FVDs, determining damping coefficients to achieve specific energy dissipation capacities. However, the stiffness-proportional distribution method can reduce the efficacy of FVDs in taller buildings, especially when using a significant number of highly nonlinear dampers. This limitation stems from its disregard for flexural deformations and higher mode effects. As a result, energy-based distribution methods, which focus on maximizing the energy dissipation capacity of dampers, may provide a more effective approach for FVD design.

Several studies have demonstrated that selecting appropriate damping parameters for FVDs can effectively reduce seismic responses. Domenico et al. [91] investigated various combinations of damping coefficients and velocity exponents, and in a subsequent study [92], they determined the optimal damping coefficient for a fixed exponent to achieve the best energy dissipation behaviour. Wang [93] conducted a sensitivity study that aided in selecting values for the damping exponent and brace stiffness. Additionally, He et al. [94] determined that the optimal values for α and C were in the range of 0.4 to 0.5 and 10000 kN×(s/m), respectively. It's worth noting that employing smaller α values is more effective when the anticipated damper velocities are below 1 m/s.

This study [95] provided detailed insights into the behavioral benefits of the Integrated Damping System (IDS) approach and identified key parameters for its optimal application in tall buildings. The study found that an additional 6.2% of equivalent damping could be achieved, enabling the building to control wind-induced accelerations within user comfort levels and reduce both static and dynamic wind loads. Furthermore, the seismic performance of the building significantly outperformed that of a conventional counterpart without fluid viscous dampers.

Retrofitting buildings with FVDs can significantly decrease drifts and enhance the seismic performance of buildings. Braced steel frames are a prevalent design type that can also be adapted to accommodate dampers and integrate them with the main structure [90]. Unlike hysteretic devices, FVDs have been recognized as the most promising for nonstructural considerations because they can mitigate drifts and floor accelerations [96].

FVDs with $\alpha = 0.3$ are not recommended for relatively high-rise buildings due to their suboptimal performance [73]. The level of damping within a building substantially impacts its structural response during an earthquake. Occhiuzzi [97] conducted a comprehensive examination of damped buildings documented in previous literature and concluded that an optimal total damping of 20–25%

in the first mode is ideal. Beyond this level, additional damping was observed to increase accelerations, while further reductions in inter-story drift were deemed negligible. Further exploration in this area is essential. As highlighted by Christopoulos and Filiatrault [98], achieving a maximum total damping of 35% in the first mode appears feasible when utilizing FVDs.

Another study found that FVDs significantly improve seismic parameters such as displacement, drift, and period in G+30, G+40, and G+50 high-rise concrete buildings. A zigzag arrangement of FVDs outperforms a diagonal arrangement, with external corner placements reducing story displacement by up to 54% and central placements achieving up to a 28% reduction. [99].

In conclusion, selecting appropriate FVD properties is critical for effectively mitigating seismic and wind responses in tall timber buildings. By optimizing parameters such as damping coefficients, velocity exponents, and placement strategies, FVDs can significantly enhance structural performance, reducing drifts, displacements, and accelerations while ensuring safety and comfort.

4 Analysis of Tall Wood Buildings

This study involves a detailed analysis of three 18-story timber buildings with different structure systems selected to investigate their structural performance under seismic wind loads. The chosen structures include two iconic examples of tall timber construction, Mjøstårnet and Brock Commons. Additionally, a proposed 18-story timber building model is included to expand the scope of the analysis. Each building is meticulously modelled and analyzed using advanced structural analysis software ETABS. Based on the available documentation, comprehensive finite element models are developed to replicate the buildings' actual geometry, material properties, and design parameters. Detailed information on the buildings' specifications and the numerical modelling approaches is presented in the subsequent sections.

4.1 Braced Frame Building

Focusing on the braced frame system of Mjøstårnet [12], an 18-story timber building in Norway standing 85.3 meters tall, is a landmark in tall timber construction. As shown in Figure 17, the building glulam mega-brace system works as trusses along the façades, supported by columns and beams, to manage horizontal and vertical forces. Additionally, all the walls for the elevators and staircases do not contribute to horizontal stability. This system was designed to prioritize wind loads due to low seismic activity in Brumunddal; earthquake loads were excluded per Norwegian regulations. However, in seismic-prone regions like Vancouver, seismic forces govern design and must be accounted for. This study examines the feasibility of constructing this building in Vancouver, an area prone to high seismic activity, and proposes modern mitigation strategies to enhance its seismic and wind performance.

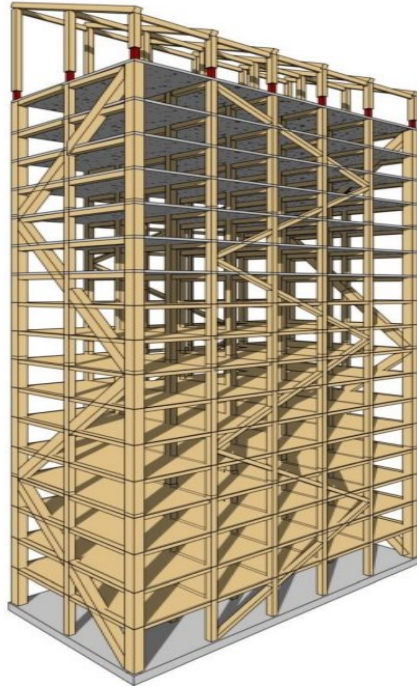


Figure 17 Mjøstårnet Structural System [12]

4.1.1 Structural Specifications

The building has a footprint of approximately 17 meters by 37 meters and incorporates a substantial concrete slab on the ground floor, supported by piles driven into the bedrock. These piles are designed to resist compression and tension forces, ensuring a robust foundation system for the tall timber structure. The structural framework features glulam columns with varying cross-sections depending on their location and demands. Figure 18 (a, b) shows the building's elevation and cross-section.

The corner columns, which have the most significant axial forces, have cross-sections of 1485 mm by 625 mm, while the typical internal columns have dimensions of 725 mm by 810 mm and 625 mm by 630 mm. Floors 2 to 11 are constructed using prefabricated wooden decks, as shown in Figure 18 (c). In contrast, floors 12 to 18 consist of 300 mm composite concrete slabs, with a prefabricated base acting as formwork for the cast-in-place upper layer. Transitioning from timber to concrete

floors for the upper levels provides additional mass to address residential-use comfort criteria and ensure compliance with acoustic performance standards. The glulam beams supporting the timber floors have cross-sections of 395 mm by 585 mm and 395 mm by 675 mm, while those supporting the concrete floors are 625 mm by 585 mm and 625 mm by 720 mm. The diagonal element used in the braced frame system has a cross-section of 625 mm by 990 mm.

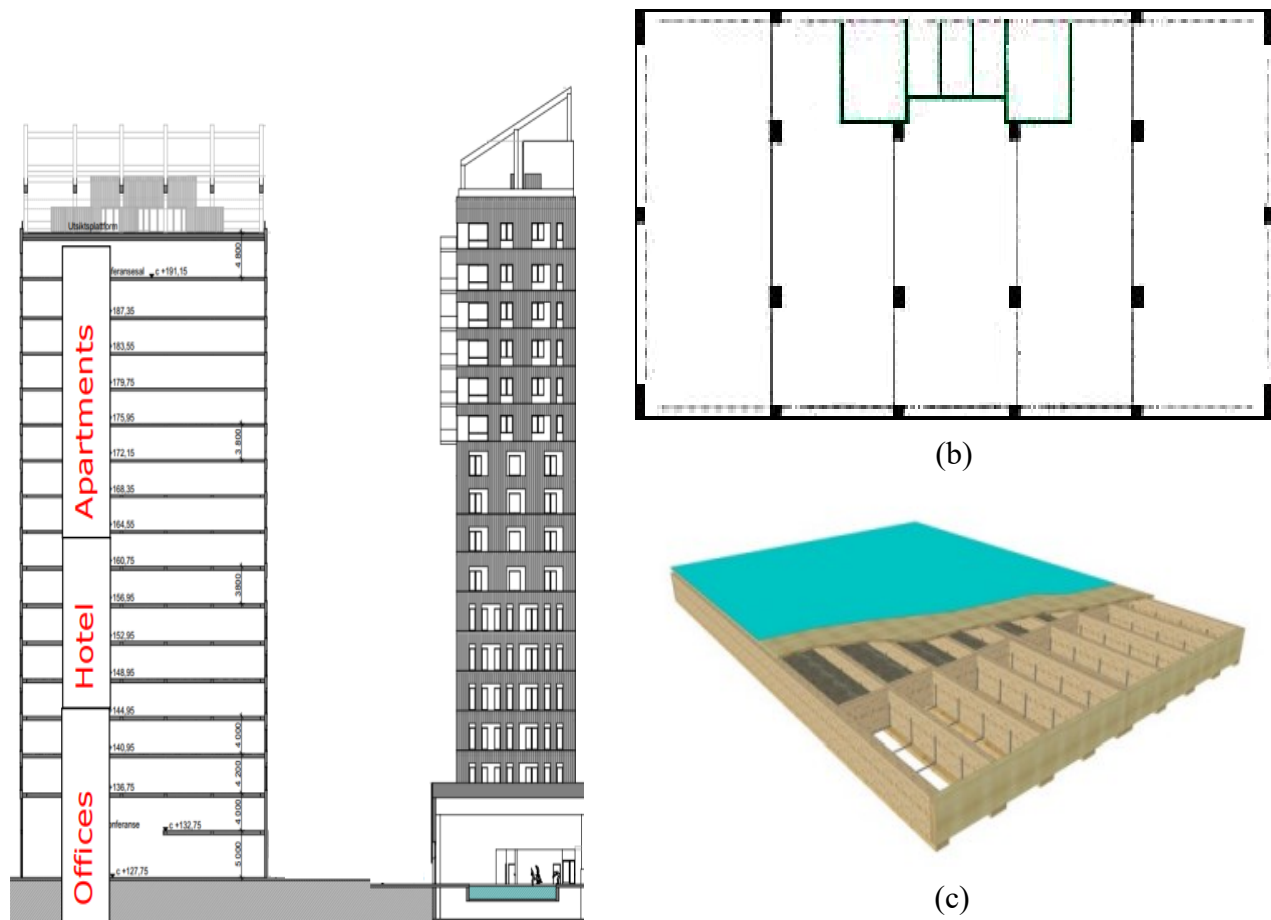


Figure 18 (a) Elevation, (b) Cross-Section of The Building, and (c) Wooden Decks [12].

The timber materials employed in the structure include glulam strength classes GL30c and GL30h, by EN 14080:2013, and cross-laminated timber (CLT) with a bending strength of $f_{mk} = 24\text{MPa}$. The wooden floor elements combine glulam from Moelven and laminated veneer lumber (LVL) from

Metsä Wood, showcasing the effective integration of advanced engineered wood products. The roof of the building includes a large glulam pergola fixed to the concrete deck on the 18th floor, adding a distinctive architectural feature. While enhancing the building's aesthetic identity, the pergola does not contribute to the building's stiffness.

4.1.2 Numerical Modeling

The numerical modelling of the Mjøstårnet building was conducted using ETABS, a commercial software widely utilized for advanced structural analysis. The structural components, including beams, columns, brace elements, and cross beams, were modelled as frame elements, as shown in Figure 19, with all aspects assumed to exhibit linear elastic behaviour. Additionally, both wood and concrete slabs were modelled as shell elements. This approach facilitated the precise calculation of the building's structural self-weight and stiffness while maintaining computational efficiency.

To account for the orthotropic nature of wood, the material properties of Douglas Fir-Larch 24f-Ex were defined with different elastic moduli in the longitudinal and transverse directions. A modulus of elasticity $E_1=12,800$ MPa was assigned in the longitudinal direction, while $E_2=750$ MPa was used for the transverse or radial direction. The density of wood was taken as $\gamma=4.5$ kN/m³. Moreover, standard properties were used for concrete elements, with a compressive strength of $f_c'=35$ and a density of $\gamma=24$ kN/m³. These definitions provide an accurate and consistent representation of wood and concrete materials, enabling precise structural system analysis.

The structural loads were distributed based on guidelines from the National Building Code of Canada (NBCC). Dead loads of 2.5 kPa were applied to the floors to represent typical finishes such as tiles, hardwood, or carpet with subfloor layers, as well as partitions, ceiling systems, and building services (mechanical, electrical, and plumbing). Live loads were specified as 1.9 kPa for residential floors

and 2.4 kPa for office floors. The weight of the prefabricated façades was modelled as a line load of 7 kN/m applied along the edge beams. Additionally, a snow load of 2.0 kPa was applied to the roof to account for environmental conditions.

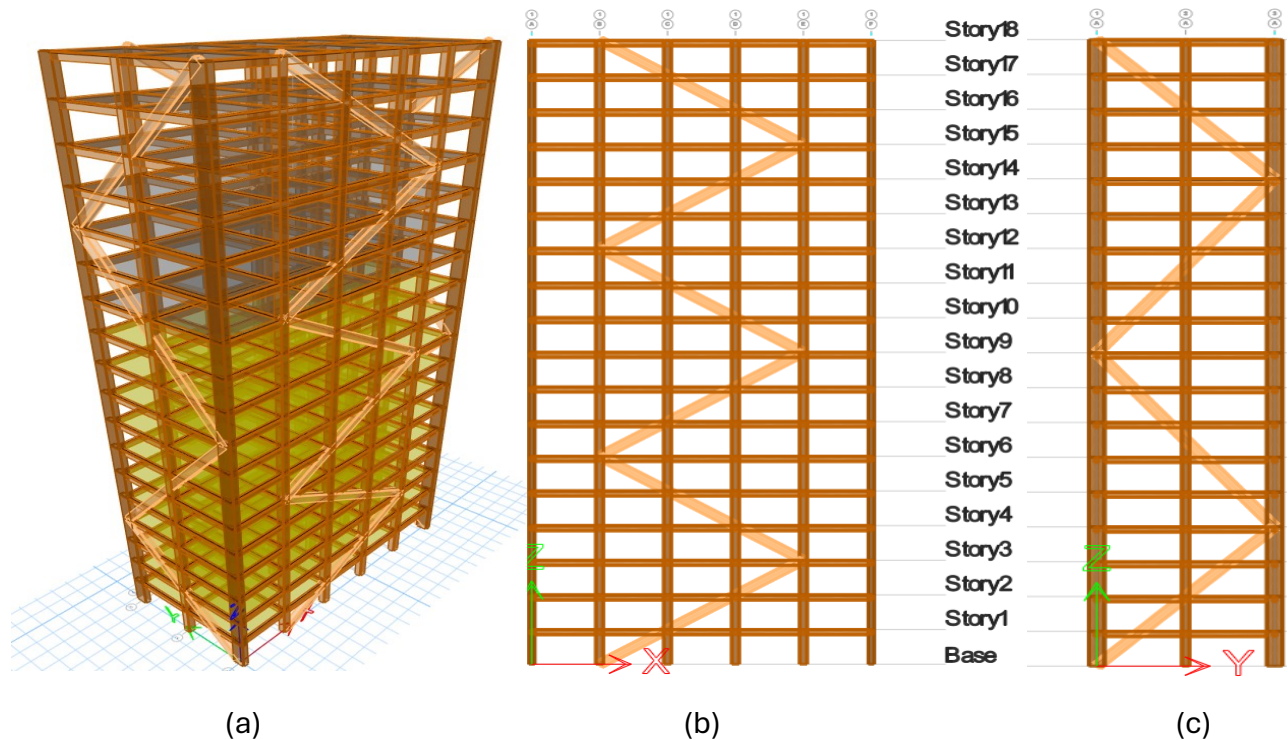


Figure 19 (a) *Mjöstårnet 3D Model in ETABS*, (b) *Longitudinal Direction Elevation*, and (c) *Transverse Direction Elevation*

The foundation system, including the concrete flat and piles, was excluded from the finite element model for simplification. This exclusion focuses the analysis on the superstructure, ensuring accurate results while minimizing computational complexity. Similarly, the walls for the elevators and staircases, as well as the pergola, were excluded from the model since they do not contribute to the overall stiffness of the structure. However, the interaction between structural and non-structural elements was incorporated to reflect the building’s overall behaviour under various loading scenarios. By combining detailed material modelling, load distribution, and advanced analysis tools,

the numerical model effectively captures the structural behaviour of Mjøstårnet, providing a reliable basis for further analysis and verification.

4.1.3 Modal Analysis Results

Without numerical data from the consultants and designers, determining the fundamental period (T_a) for braced frame systems is guided by the provisions outlined in Section 4.1.8.11.3 of the NBCC.

The empirical fundamental period is calculated using the following equation for such systems.

$$T_{emp} = 0.025 H \quad (12)$$

Where H is the total height of the building (meters), for the building under consideration, with a total height of H=81 m, the empirical fundamental period is computed to be 2.02 s. Additionally, the fundamental periods for the first three modes of the building, obtained through numerical analysis in ETABS, are presented in Table 4.1. These periods are within the expected dynamic behaviour of a braced frame system and are within the permissible range specified by NBCC $T_{lim}=4.05$ s.

Table 4.1 Modal Fundamental Periods for The First Three Modes Shape of Mjøstårnet Building.

Mode	Period (s)	Dominant Direction
1	2.47	Translational (Transverse)
2	1.97	Translational (Longitudinal)
3	1.35	Torsional

4.2 Core System Building

Brock Commons [10], the tallest timber building in Canada, was selected for this study as it exemplifies innovative tall timber construction. The 18-story structure, which stands 56 meters tall, serves as student housing at UBC's Vancouver campus. Considering Vancouver's high seismic

activity, it was designed to resist wind and seismic loads. Two reinforced concrete cores that house staircases and elevators provide lateral resistance to wind and earthquakes and transfer lateral loads from the floor and roof diaphragms to the foundations. Several research studies have investigated the feasibility of replacing the concrete core with a CLT core [100]. However, it was found that a CLT core with the exact dimensions and configuration is unstable under seismic loading for Vancouver, BC, as per the 2015 National Building Code of Canada. This study investigates the feasibility of replacing the concrete with a CLT core and proposes suitable modern mitigation strategies to improve seismic and wind performance.

4.2.1 Structural Specifications

Brock Commons, with a total floor area of 15120 m² and dimensions of 15 m by 56 m, features a mass timber superstructure designed for innovative and sustainable construction. The lateral force-resisting system (LFRS) was initially designed with a 450 mm concrete core. The building's cross-section is illustrated in Figure 20, while Figure 21 depicts its 3D model and core placement.

Structural connections are made of steel, and the building envelope comprises a prefabricated panel system that incorporates steel studs, fiberglass batt insulation, and a rainproof wood laminate cladding system. The foundations, columns, and transfer slabs utilize concrete with a characteristic strength of 35 MPa. The floors from Level 2 to Level 18 consist of 5-ply CLT panels, each 169 mm thick, topped with a 40 mm concrete layer, and assembled with 29 panels per floor.

GLT columns, grade D-Fir 16c-E, with dimensions of 265 mm by 265 mm, are used for levels 2 to 10, while smaller GLT columns measuring 265 mm by 215 mm are used for levels 11 to 18. PSL columns, grade 2.2E, with dimensions of 265 mm by 265 mm, are employed as middle columns on

Levels 2 to 5 due to their superior compression strength compared to GLT. All GLT and PSL columns rest on a 600 mm thick concrete transfer slab.

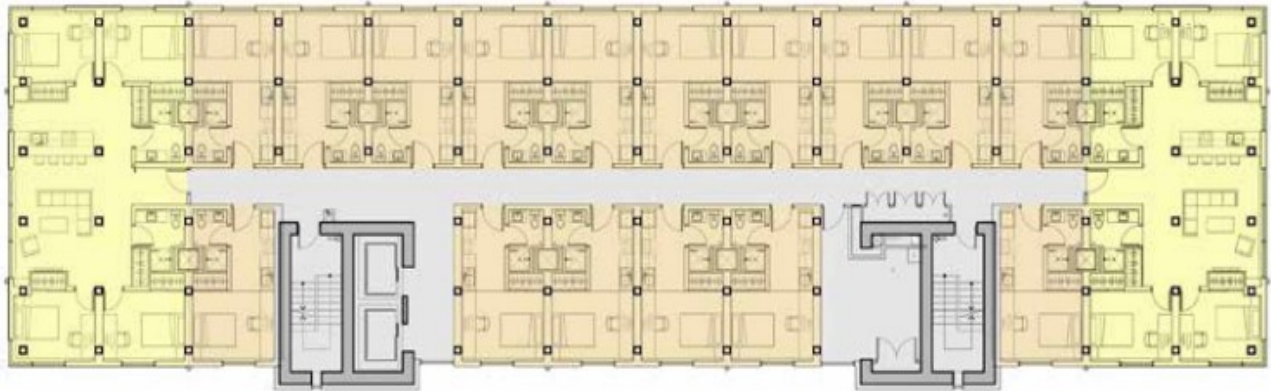


Figure 20 Structural Cross-Section of Brock Commons (source: naturally wood).

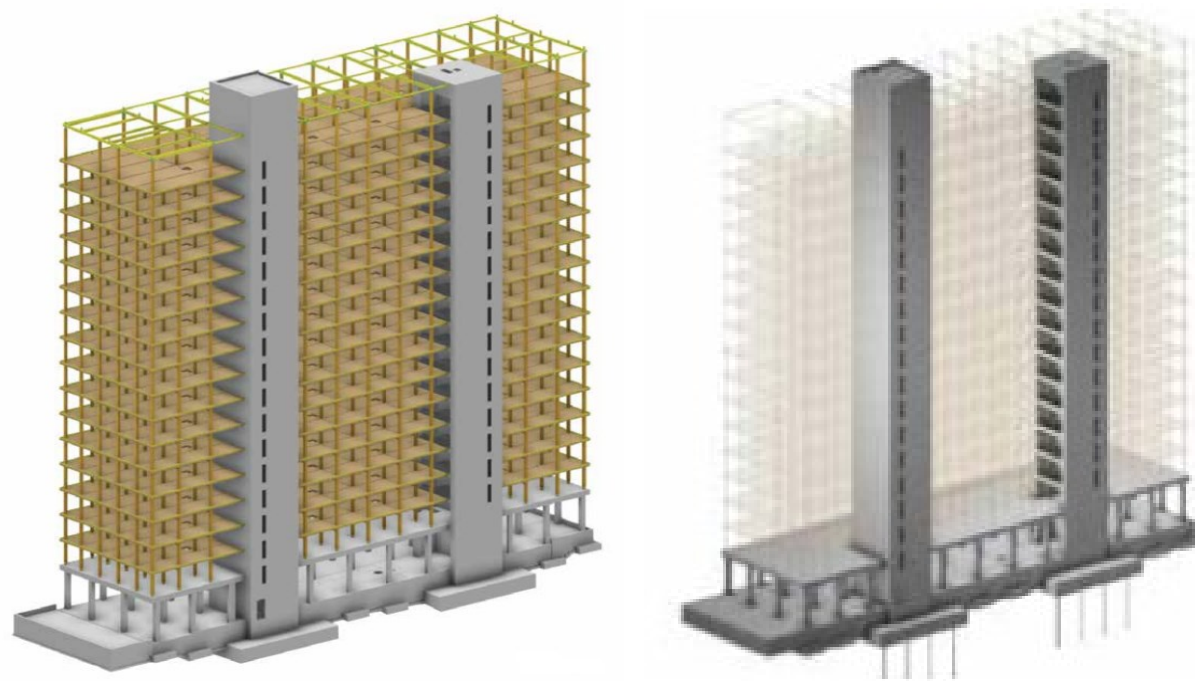


Figure 21 3D Model and Core Placement of Brock Commons [100].

4.2.2 Numerical Modeling

The numerical modelling of the Brock Commons building was conducted using ETABS, a widely utilized commercial software for advanced structural analysis. To simplify the model and enhance

computational efficiency, the study focused exclusively on the superstructure, excluding the foundation system, including the concrete flat and piles. Timber columns were modelled as frame elements, assuming linear elastic behaviour. In contrast, CLT elements were modelled as layered shell elements, as illustrated in Figure 22, to calculate structural self-weight and stiffness accurately.

Material properties were defined to account for the orthotropic nature of wood. For Douglas Fir-Larch 16c-E and PSL 2.2E, the modulus of elasticity in the longitudinal direction were set at $E_1=12,400$ MPa and $E_1=15,170$ MPa, respectively, while the transverse modulus was $E_2=750$ MPa for both materials. Similarly, the modulus of elasticity for the CLT elements was taken as $E_1=12800$ MPa and 1280 MPa in the longitudinal and the transverse direction, respectively. The density of wood was taken as $\gamma=4.5$ kN/m³. On the other hand, for concrete components, properties were defined with a compressive strength of $f_c'=35$ MPa and a density of $\gamma=24$ kN/m³. These definitions ensured accurate and consistent representation of wood and concrete materials in the structural analysis.

The load distribution was implemented following NBCC guidelines. Dead loads of 2.5 kPa were applied for typical finishes, such as tiles, hardwood, or carpet, along with subfloor layers, partitions, ceiling systems, and building services, including mechanical, electrical, and plumbing. Live loads were defined as 1.9 kPa for all floors except the roof. Prefabricated façades were modelled as line loads of 7 kN/m applied along edge slabs, and a snow load of 2.0 kPa was applied to the roof to account for environmental conditions.

As a built model, the lateral force-resisting system (LFRS) was initially modelled with a 450 mm thick concrete core. This study replaced the concrete core with a CLT core of equivalent thickness and placement to assess its performance under seismic and wind loads. Concrete columns were

modelled as frame elements, while the transfer slab was represented as a shell element. Figure 23 shows the 3D model in ETABS, highlighting the placement of the CLT core and other structural components. This numerical model combines detailed material definitions, precise distributions, and advanced modelling techniques to capture Brock Commons's structural behaviour effectively.

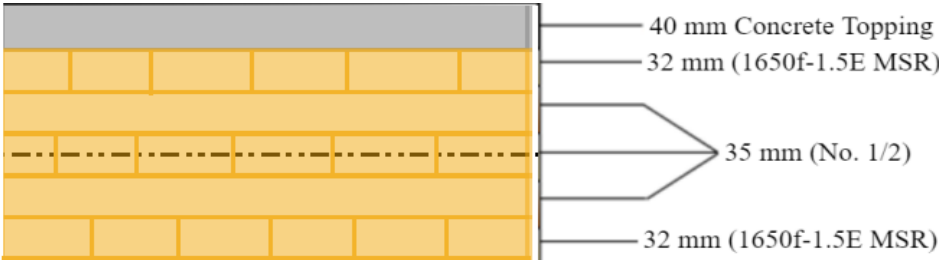


Figure 22 Layered Shell Element Representation of CLT Slabs in ETABS.

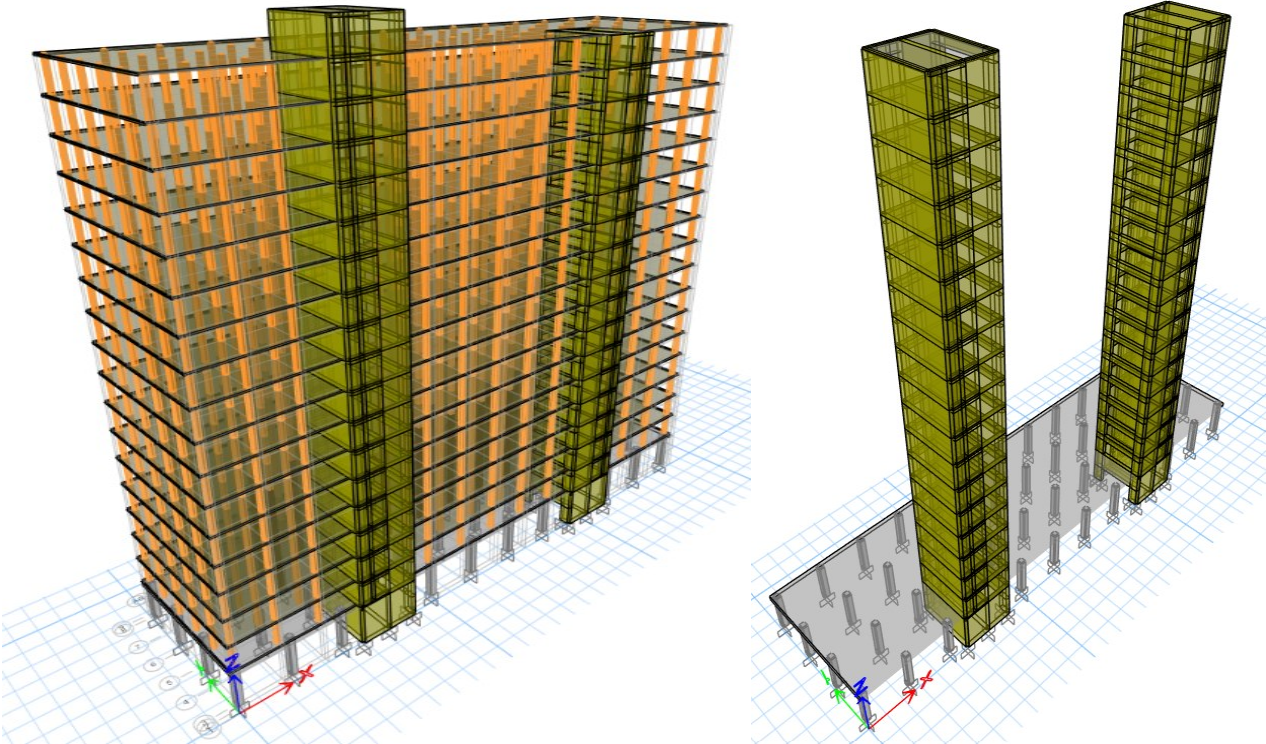


Figure 23 3D Model of Brock Commons Showing CLT Core Placement in ETABS.

4.2.3 Modal Analysis Results

With the availability of the numerical data from consultants and designers for the original building featuring as-built concrete cores [101], determining the fundamental period (T_a) for shear wall systems follows the provisions outlined in Section 4.1.8.11.3 of the NBCC. For such systems, the empirical fundamental period is calculated using the following equation:

$$T_{emp} = 0.05 H^{0.75} \quad (13)$$

For a building with a total height of $H=56$, the empirical fundamental period is calculated as 1.03 seconds, and the upper limit of fundamental period $T_{lim}=2.06$ s. Replacing the concrete cores with CLT cores increases the fundamental periods, altering the dynamic behaviour by shifting the torsion mode to the first mode and the translation modes in the transverse (X) and longitudinal (Y) directions for the second and third modes. Numerical results from this study and previous research [100] confirm these findings. The fundamental periods for the first three modes, compared across the as-built model, ETABS model, and prior research, are presented in Table 4.2.

Table 4.2 Modal Fundamental Periods for The First Three Modes Shape in (s) of Brock Commons Building.

Mode	Concrete Core	CLT Core	
		ETABS	[100]
1	1.99	2.13	2.13
2	1.85	1.90	1.87
3	1.32	1.69	1.76

4.3 Outrigger-Belt Truss Building

Given the limited number of tall timber buildings constructed worldwide, this study proposes an 18-story hybrid timber building utilizing a steel Chevron-braced core and glulam (GLT) belt-truss and outriggers as the primary lateral resistance system. This system aims to enhance credibility and depth of understanding of tall timber construction. The outriggers are strategically placed at the 6th and 12th stories based on findings from previous studies [102] to optimize their performance and maximize lateral load resistance efficiency. The outrigger-belt truss system is an effective lateral resistance mechanism for hybrid tall timber buildings, offering substantial improvements in global stiffness and resistance to lateral forces. However, it introduces stiffness irregularities between stories due to the concentrated rigidity at the outrigger levels. This study emphasizes addressing these irregularities by incorporating enhanced damping systems.

4.3.1 Structural Specifications

The proposed building's total floor area is 13,500 m² with dimensions of 25 m by 30 m and a total height of 63 m, designed as a sustainable and efficient hybrid structure. Pin connections were used between GLT beams and perimeter columns to prevent the formation of a moment-resisting frame, allowing the steel core and outrigger system to act as the primary lateral resistance system. This approach avoids oversized timber cross-sections, achieving an economical design. The building's cross-section and 3D model with core placement are illustrated in Figure 24.

Floors are constructed from 5-ply CLT panels, each 169 mm thick, topped with a 40 mm concrete layer to provide stability, acoustic performance, and stiffness.

GLT columns, graded as Douglas Fir 16c-E, were 450 mm by 450 mm, 400 mm by 400 mm, and 300 mm by 300 mm for stories 1 to 6, 7 to 12, and 13 to 18, respectively. Similarly, the core columns were designed as W14X145, W14X74, and W14X48 for the same story ranges, respectively, with W12X30 sections used for all beams. Steel double channels were used for core braces, with cross-sections varying based on demand.

GLT beams with a cross-section of 400 mm by 400 mm support CLT panels and transfer gravity loads to perimeter beams and the core. GLT belt truss and outrigger elements are sized at 265 mm by 265 mm to ensure stiffness and effective load transfer.

The core was modelled and designed in ETABS under ultimate limit state principles, adhering to NBCC load combinations with demand-to-capacity ratios below 1.0. This process ensures compliance with strength and stability requirements under various loading conditions.

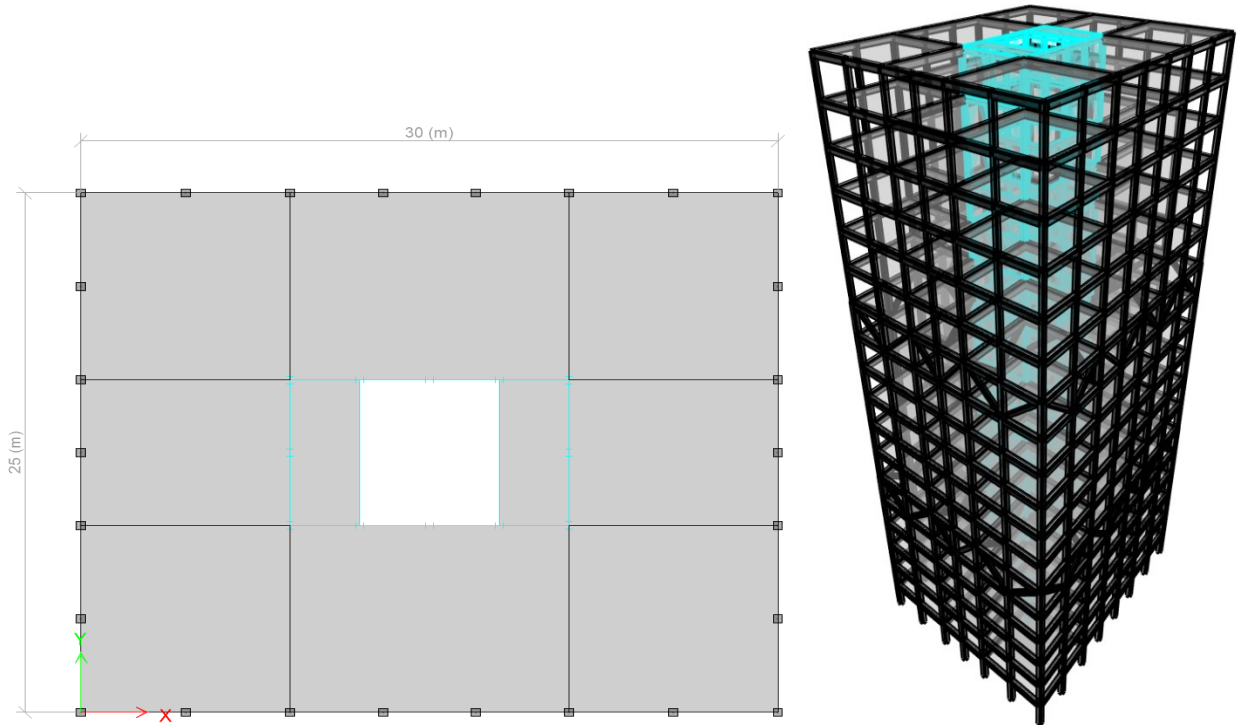


Figure 24 Structural Cross-Section and 3D view of Outrigger Tall timber building.

4.3.2 Numerical Modeling

The numerical modelling of the proposed 18-story hybrid timber building was conducted using ETABS. Timber elements, including GLT braces, beams, and columns, were modelled as frame elements, assuming linear elastic behaviour. In contrast, CLT floor panels were modelled as layered shell elements to accurately calculate structural self-weight and stiffness, as illustrated in Figure 22.

Material properties were defined to account for the orthotropic nature of wood. For Douglas Fir-Larch 16c-E, the modulus of elasticity in the longitudinal direction was set at $E_1=12400$ MPa, while the transverse modulus was $E_2=750$ MPa. For the CLT floor elements, the modulus of elasticity was defined as $E_1=12800$ MPa in the longitudinal direction and $E_2=1280$ MPa in the transverse direction. The density of wood was taken as 4.5 KN/m. In contrast, properties of steel components were defined with a modulus of elasticity $E=200$ GPa and a density of 77 KN/m³. These definitions ensured accurate and consistent representation of all materials in the structural analysis.

The load distribution was implemented following NBCC guidelines. Dead loads of 2.5 KN/m² were applied to represent typical finishes, including tiles, subfloor layers, partitions, ceiling systems, and building services. Live loads were defined as 1.9 KN/m² for residential and office floors. Prefabricated façades were modelled as line loads of 7 KN/m applied along edge beams, while a snow load was applied to the roof to account for environmental conditions.

The LLRS features a steel core integrated with GLT outrigger-belt truss elements at the 6th and 12th floors, as shown in Figure 25, with the core braces, columns, and beams modelled as frame elements. The ETABS model employs advanced techniques and detailed material definitions to accurately capture the structural behaviour of the proposed hybrid timber building, ensuring compliance with NBCC strength and stability requirements.

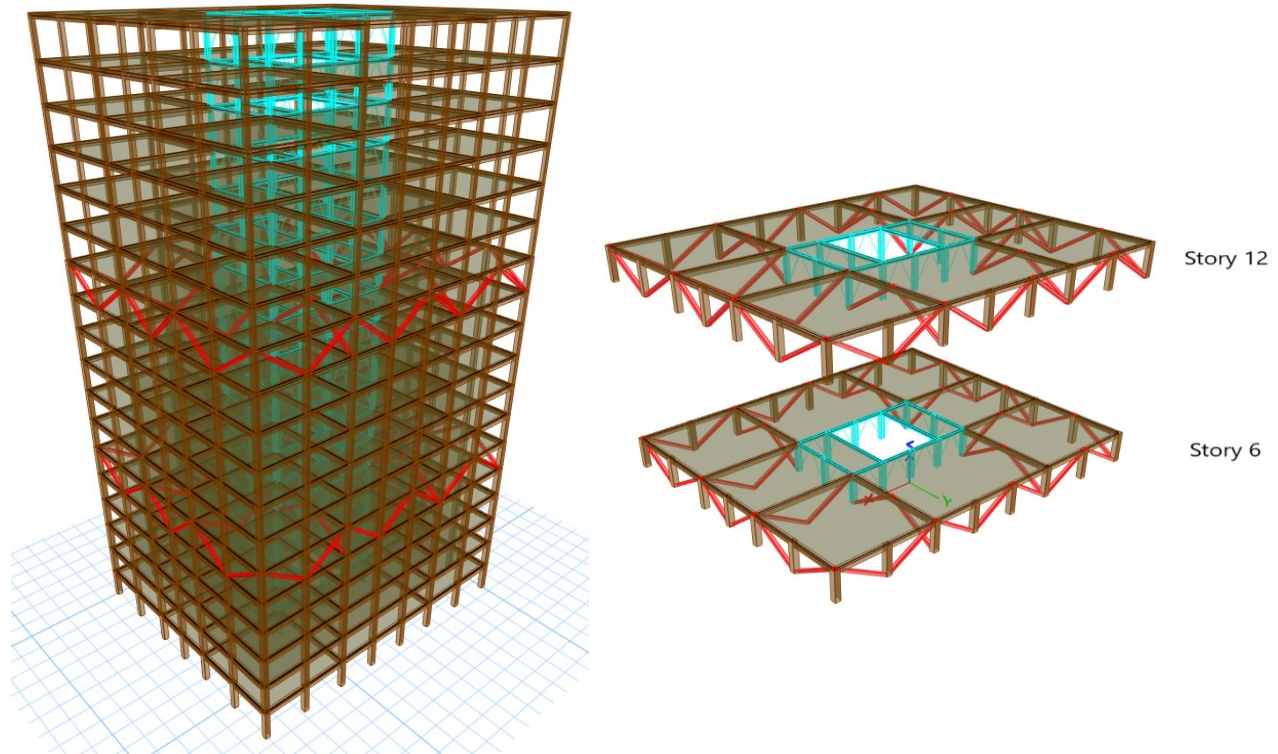


Figure 25 3D Model of Outrigger Tall Timber Building Showing LLRS Placement in ETABS.

4.3.3 Modal Analysis Results

Similar to Bock Commons, the fundamental period (T_a) for shear wall systems is determined. The empirical fundamental period is calculated for the building with a total height of $H=63$ m as 1.12 s, and the upper limit period $T_{lim}=2.24$ s limit. Additionally, the fundamental periods for the first three modes by the ETABS model are presented in Table 4.3.

Table 4.3 Modal Fundamental Periods for The First Three Modes Shape of Outrigger Tall Timber Building.

Mode	Period (s)	Dominant Direction
1	2.12	Translational (Transverse)
2	2.00	Torsional
3	1.71	Translational (Longitudinal)

4.4 Seismic Analysis

In analyzing the seismic behaviour of tall timber buildings, both static and dynamic loads were considered. Static loads were applied to the structure in ETABS based on the design loads specified by the NBCC 2020 and tailored to the Vancouver area using the seismic hazard map. Following the Equivalent Static Load Analysis, dynamic loads were introduced to simulate three different earthquake records through time-history analysis, which was computationally intensive.

The Fast Nonlinear Analysis (FNA) method was employed for the time-history analysis to minimize computational demands. FNA utilizes modal analysis with Ritz vectors to simplify the equilibrium relationships in the elastic structural system. This approach separates the nonlinear components from the elastic ones, significantly reducing computational time. FNA is particularly adequate for systems with limited nonlinear elements, primarily links. For these reasons, FNA was adopted in the analysis presented in the subsequent sections.

4.4.1 Equivalent Static Load Analysis

The equivalent static load analysis (ESLA) is the standard method recommended by building codes for seismic design. This method is relatively straightforward and can be completed manually without finite element software. As a result, it has become widely adopted by designers due to its simplicity and ease of application. The ESLA involves designing the building to resist a force known as the base shear, which is distributed along the height of the structure in an inverted triangular pattern based on the mass of each floor, as illustrated in Figure 26. Canada's fundamental seismic design principles have remained unchanged since the introduction of the first NBCC in 1941. However, significant updates have been made, with the 2005 NBCC edition marking a pivotal shift. This edition introduced ductility and overstrength factors, R_d and R_o , respectively, to replace the force

modification factor (R). These changes led to a new base shear equation in Equation 13, with the upper and lower bounds of the seismic base shear based on the NBCC. For this analysis, R_d and R_o factors were taken as 2.0 and 1.5, respectively, based on findings from the literature review and NBCC guidelines.

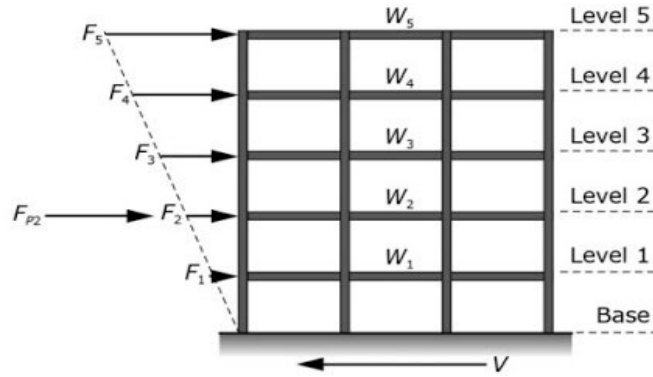


Figure 26 Equivalent Static Load Analysis (ESLA) Force Distribution for a 5-Story Building.

$$\frac{S(2.0)M_v I_e W}{R_d R_o} < \frac{S(T_a)M_v I_e W}{R_d R_o} < \frac{2S(0.2)I_e W}{3R_d R_o} \quad (13)$$

Where $S(T_a)$ is the design spectral response acceleration at the fundamental period T_a ; M_v accounts for the higher mode effects; I_e is the importance factor, and W is the seismic weight of the structure. The loading and climatic information for the site can be seen in Appendix C, Climatic and Seismic Information by NBCC, based on the seismic hazard map.

4.4.2 Response Spectrum Analysis

Response Spectrum Analysis (RSA) is a dynamic method used in seismic design to estimate maximum structural responses under seismic excitation. RSA evaluates peak responses such as displacements, accelerations, and forces using site-specific seismic hazard data from the NBCC. Key parameters include the design spectral response acceleration, importance factors (I_e), site

classifications (Class C or D), and a 5% damping ratio for typical systems. The design spectra accounts for local seismicity, soil conditions, and proximity to the Cascadia Subduction Zone. Seismic hazard values essential for building design under Part 4 of the NBCC can be accessed through the 2020 National Building Code of Canada Seismic Hazard Tool. Additionally, Figure 27 illustrates the response spectrum curves for Vancouver for 2%/50yr, 5%/50yr, and 10%/50yr. These values represent the probabilities of exceeding specific seismic ground motion levels within a 50-year period, with 2%/50yr indicating a rare event, 5%/50yr a moderate event, and 10%/50yr a more frequent event.

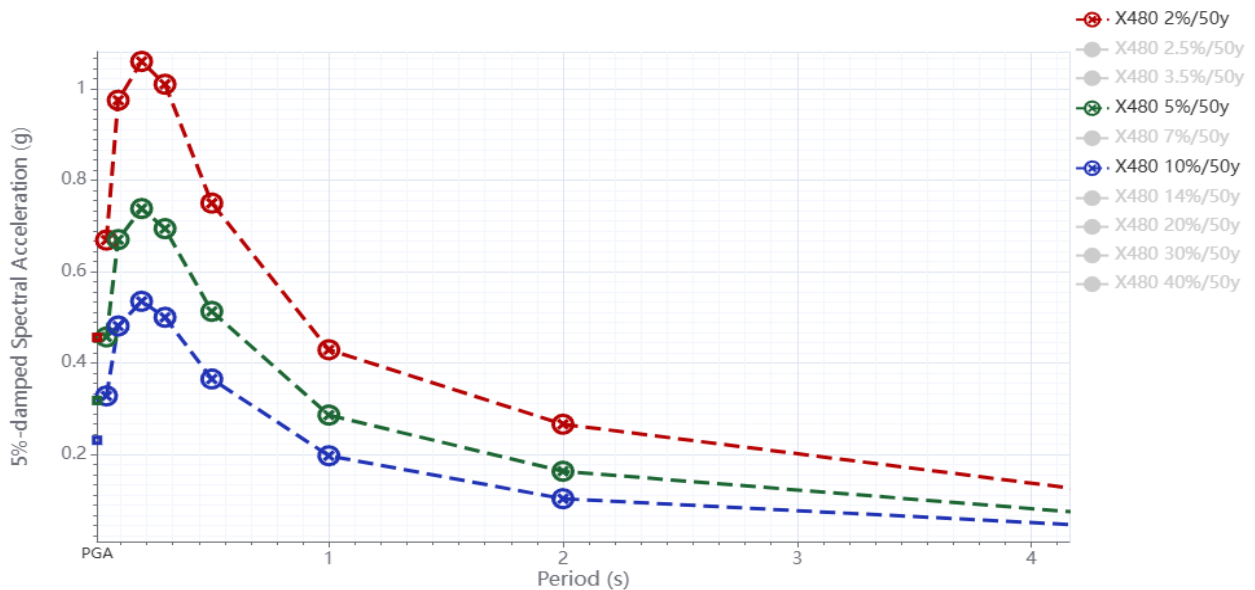


Figure 27 Response Spectrum Curves for Vancouver (Site Class C, $V_{s30}=480$ m/s) [56].

The RSA procedure follows NBCC 2020 provisions, employing Ritz vector analysis to extract modal properties. These modes are combined using the Square Root of the Sum of the Squares (SRSS) or Complete Quadratic Combination (CQC) to assess modal interactions.

This framework highlights RSA's effectiveness in analyzing the dynamic behaviour of tall buildings, particularly in assessing stiffness and damping contributions within the lateral force-resisting system

(LFRS) and ensuring seismic compliance. However, its inability to capture time-dependent structural behaviour emphasizes the need for time history analysis for a more realistic evaluation.

4.4.3 Time History Analysis

Time History Analysis (THA) is a dynamic analysis method that evaluates the seismic performance of structures using actual earthquake ground motion records. It offers a more realistic assessment of building response than static or response spectrum methods. This study's three ground motion records with varying components were sourced from the reliable PEER Ground Motion Database [103].

The analysis involved applying scaled and matched ground motion records to the tall timber building model to assess its dynamic response under seismic loading. Critical parameters, including displacements, accelerations, and internal forces, were evaluated under realistic earthquake conditions. The subsequent sections outline the methodology for selecting, scaling, and matching these records.

4.4.3.1 Selection of Ground Motion Records

Three ground motion records were selected to investigate the building's response to different ground motions. The selected records are the 1994 Northridge earthquake, the 1985 Mexico City Earthquake, and the 2011 Christchurch earthquake. These earthquakes represent a range of magnitudes, durations, and frequency contents, allowing for a comprehensive investigation of the building's response to diverse seismic events. The records were chosen to reflect varying ground motion characteristics that might affect the structure differently, ensuring a robust analysis.

4.4.3.2 Scaling and Matching the Selected Records

The selected ground motion records were scaled and matched to the Vancouver site's Response Spectrum Curve (RSC) using SeismoMatch [104] to reflect site-specific seismic hazards accurately. Two hazard levels were considered: the Maximum Considered Earthquake (MCE), representing a 2% probability of exceedance in 50 years, and the Design Basis Earthquake (DBE), representing a 10% probability of exceedance in 50 years. The DBE was scaled to two-thirds of the MCE. Table 4.4 presents the characteristics of each ground motion before the matching, including their hazard levels, durations, and peak ground accelerations (PGA). The target spectrum, derived from the NBCC provisions for Site Class C, served as the benchmark for the matching process. SeismoMatch adjusted the records to achieve consistency with the RSC, ensuring a precise representation of the seismic hazard. Figure 28 illustrates the scaled, unmatched time-history records of the selected ground motions obtained from the PEER database. Figure 29 presents the response spectrum curves before and after matching to the selected RSC.

Each ground motion record comprises two orthogonal components (X and Y) combined to account for biaxial seismic effects. The X-load case incorporates 100% of the X component with 30% of the Y component, while the Y-load case combines 100% of the Y component with 30% of the X component. This approach ensures a thorough representation of multidirectional seismic demands.

Table 4.4 Scaled Ground Motion Records With Associated Hazard Levels And Key Parameters

Ground Motion	Component Direction	PGA (g)		Duration (s)
		MCE	DBE	
Northridge Earthquake	X	0.75	0.50	50
	Y	0.67	0.45	
Christchurch Earthquake	X	0.60	0.40	35
	Y	0.55	0.37	
Mexico City Earthquake	X	0.25	0.17	60
	Y	0.20	0.13	

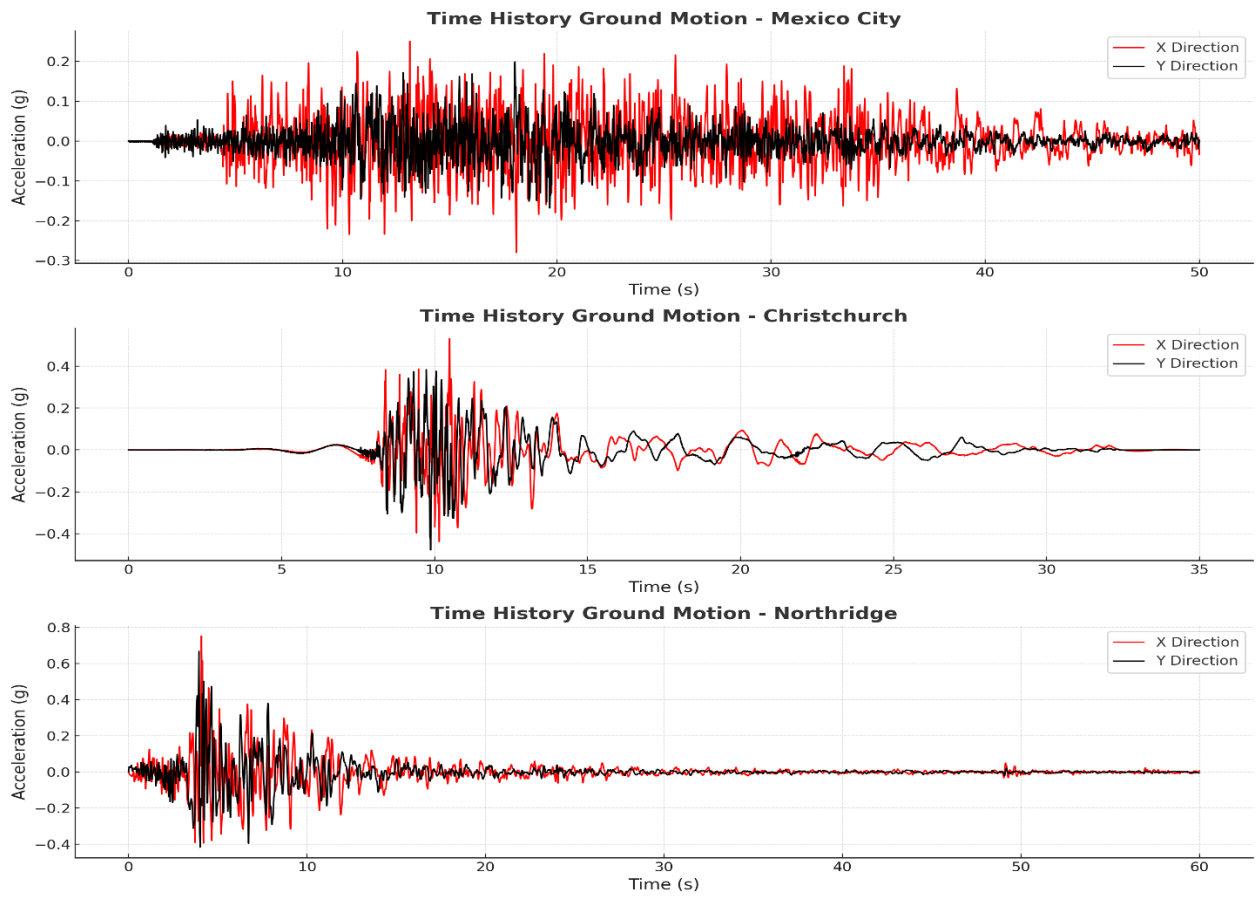


Figure 28 Selected Ground Motion Time-History Records.

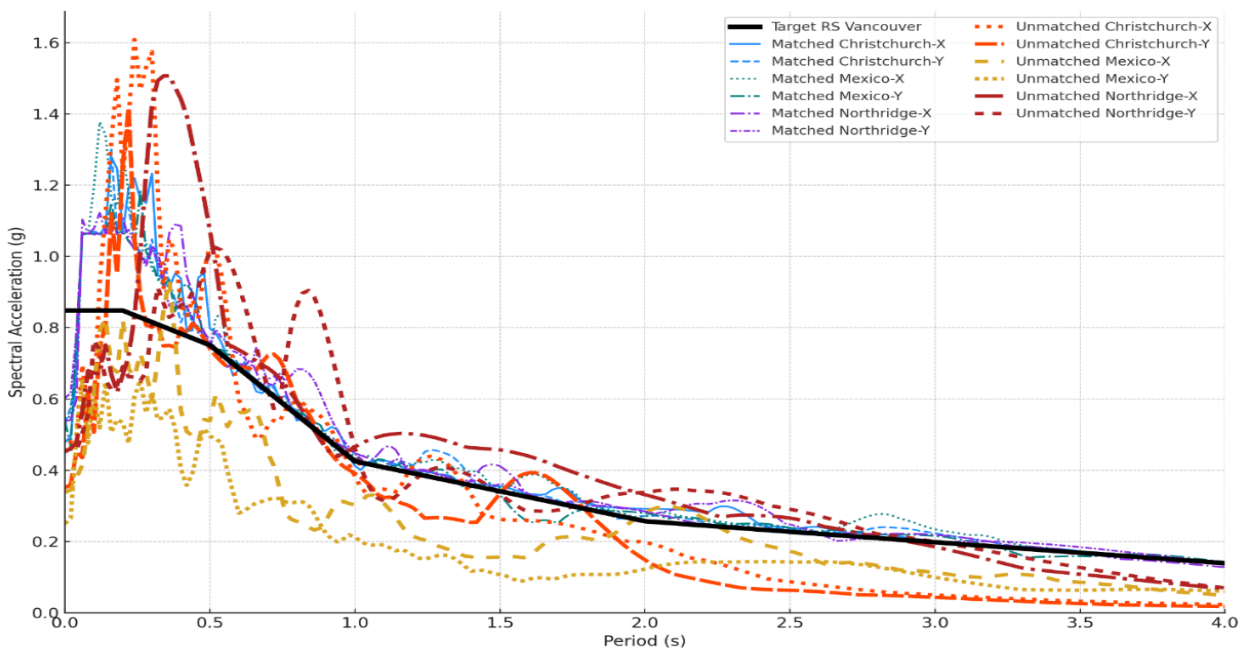


Figure 29 Matched and Unmatched records with Target Spectrum for Vancouver.

4.5 Wind Analysis

This section examines the wind performance of the selected tall timber buildings by the NBCC guidelines, employing static and dynamic wind load analyses. The evaluation emphasizes wind-induced structural responses, occupant comfort, and serviceability criteria specific to tall timber buildings situated in Vancouver. The study incorporates a reference wind pressure of 0.45 kPa, as Appendix C of the NBCC stipulated.

4.5.1 Static Wind Analysis

The static wind load assessment establishes baseline pressures acting on the structures by considering site-specific conditions and terrain characteristics. The NBCC-prescribed equation is used to determine the wind load, as shown below, representing the wind load in Pascals. The parameters include the importance factor ($I_w=1.0$), exposure factor derived from rough terrain ($C_e=1.0$), topographic factor ($C_t=1.0$), gust effect factor ($C_g=2.0$), and external pressure coefficient ($C_p=1.0$). This comprehensive approach ensures accurate static wind pressure estimations tailored to the building's environment.

$$P = I_w q C_e C_t C_g C_p \quad (14)$$

4.5.2 Dynamic Wind Analysis

Dynamic wind analysis is essential for capturing interactions between wind forces and building responses, particularly for tall, slender timber structures susceptible to wind-induced accelerations. Using the Dynamic Procedure and Wind Tunnel Procedure recommended by NBCC for such buildings, the analysis evaluated maximum drift and floor accelerations to ensure compliance with comfort and safety criteria.

The wind tunnel testing was conducted by ASCE 49-12 and NBCC guidelines, utilizing the High-Frequency Force Balance (HFFB) method to assess the dynamic wind tunnel test data. After performing the static analysis, the three base moments M_x , M_y , and M_z were refined to incorporate their fluctuating components, as defined in Equation 15, which form the wind tunnel test data shown in Figure 30 for all selected buildings.

$$M(t) = M_{mean} + M_{fluctuating} \cdot \text{Sin}(\omega t) \quad (15)$$

Here, $\omega = 2\pi f_s$, and $M_{fluctuating} = 0.1M_{mean}$. Where f_s is the Strouhal frequency given by $f_s = \frac{0.2u}{D}$. In this equation, U denotes the wind speed, and D represents the building width perpendicular to the wind direction.

Then, the adjusted base moments were subsequently used to establish three load time functions in ETABS, critical for defining dynamic load cases with duration based on the structure's fundamental period (T_1), ensuring it encompassed multiple vibration cycles to observe the full dynamic effects. To achieve this, a total of 20 cycles of the fundamental period, around 60 s, were considered. However, the load case duration was 100 seconds to capture the free vibration response. The load time functions, represented in Equations 16, 17, and 18, accurately modelled the temporal variations in wind forces and moments.

$$f_{x,i}(t) = P_{x,i} \cdot M_y(t) \quad (16)$$

$$f_{y,i}(t) = P_{y,i} \cdot M_x(t) \quad (17)$$

$$m_{z,i}(t) = P_{z,i} \cdot M_z(t) \quad (18)$$

Where f_i and m_i represent the shear force and torsional moment components, respectively, at level i and P_i denote the point load coefficient corresponding to level i .

In addition to the time load cases, three distinct load patterns were developed in ETABS to calculate the point load coefficients ($P_{X,i}$, $P_{Y,i}$, and $P_{Z,i}$) required for distributing wind loads across the building's stories, consistent with the static analysis.

Finally, by integrating static analysis results with the HFFB procedure into ETABS, the dynamic wind analysis offered a robust evaluation of the building's response to fluctuating wind loads. This comprehensive approach accurately captured wind-induced vibrations, enabling a thorough assessment of the structural performance under dynamic loading conditions.

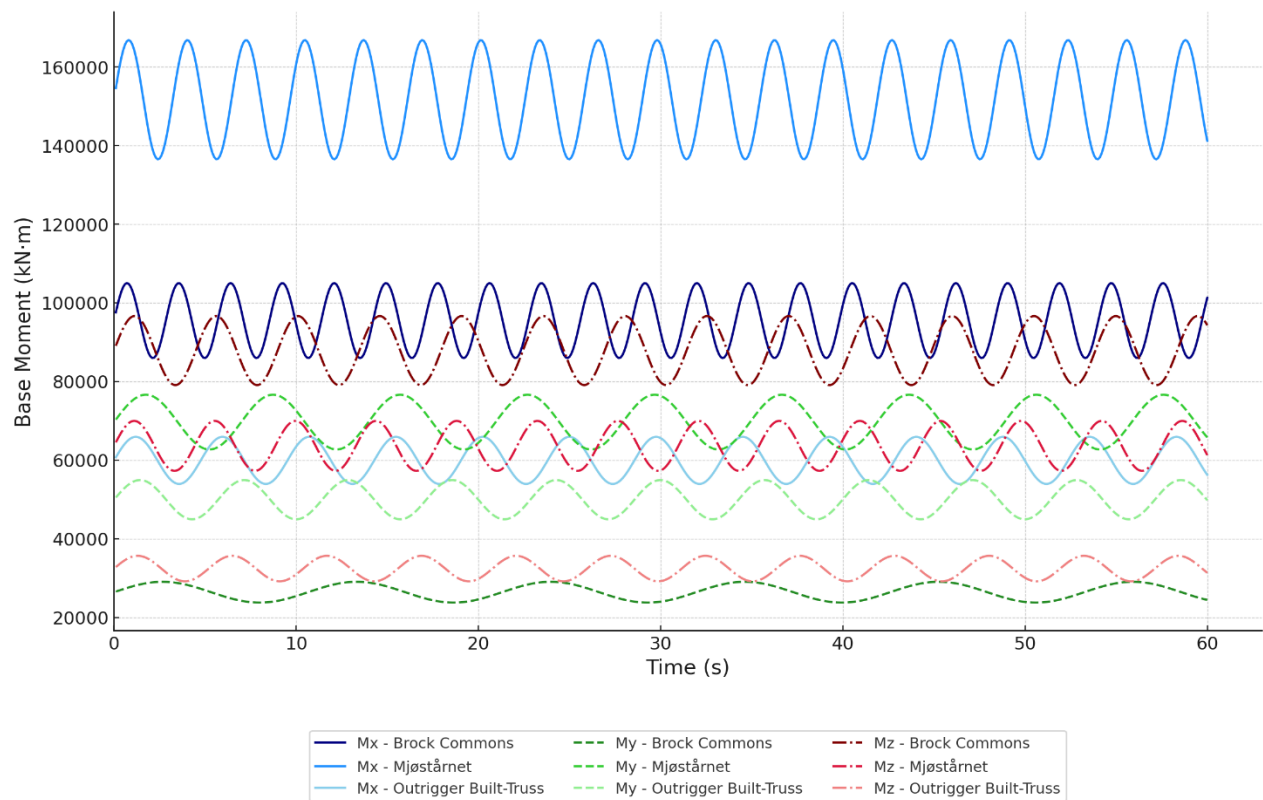


Figure 30 Dynamic Base Moments represent the Wind Tunnel Test Data Across The Buildings.

5 Response of Tall Timber Buildings

This chapter presents the seismic and wind performance analysis of three selected tall timber buildings (Mjøstårnet, Brock Commons, and the Outrigger Building). The evaluations are conducted using results from ETABS modelling, focusing on Equivalent Static Load Analysis, Response Spectrum Analysis, and Time History Analysis for seismic considerations, as well as Static and Dynamic Wind Responses. The findings indicate that the structural responses exceed the permissible limits set by the NBCC, necessitating further performance enhancements, which will be addressed in Chapter 6.

5.1 Seismic Load Cases

The seismic response of the tall timber building was evaluated based on three critical performance parameters: inter-story drift, base shear, and overturning moment. These parameters comprehensively understand the building's behaviour under seismic loading.

Inter-story drift is the relative lateral displacement between consecutive floors during an earthquake, serving as a key indicator of potential damage to structural and non-structural components. According to the NBCC, the maximum allowable drift ratio is 0.025, ensuring structural and non-structural integrity under seismic events. Base shear, which represents the total horizontal force acting at the base, reflects the overall seismic demand on the building and provides essential data for assessing its lateral load resistance. Overturning moment evaluates the rotational forces at the base caused by seismic activity, offering insights into the stability and resilience of the building under extreme loading conditions. These parameters were analyzed using the results from ETABS simulations for all seismic load cases, ensuring a detailed assessment of the structure's seismic performance.

5.1.1 Equivalent Static Load Analysis

The equivalent static analysis was performed in ETABS for three high-rise timber buildings under study, each subjected to six seismic load cases: E_x , E_{x-} , E_{x+} , E_y , E_{y-} , and E_{y+} . These load cases represent static earthquake loads in the X and Y directions, respectively, with additional considerations for centroid shifts (± 0.05 eccentricity) to capture torsional effects as mandated by the NBCC. The seismic input parameters were derived from the seismic hazard map corresponding to the site location of Brock Commons. For all buildings, the ductility-related force modification factor (R_d) and overstrength-related force modification factor (R_o) were set to 2 and 1.5, respectively, ensuring consistent application of NBCC provisions.

The Equivalent Static Analysis results for each building are presented regarding inter-story drift, base shear, and overturning moments, with a comparative discussion highlighting differences in structural behaviour.

5.1.1.1 Inter-Story Drift

Inter-story drifts calculated from linear dynamic analysis (Δ_e) are adjusted using the ductility reduction factor (R_d), the overstrength reduction factor (R_o), and the critical factor (I_e) to determine the realistic inter-story drifts (Δ). This relationship is expressed in Equation 19:

$$\Delta = \Delta_e \frac{R_d R_o}{I_e} \quad (19)$$

Figures 31 and 32 present the maximum drift ratio for the Mjøstårnet, Brock Commons, and Outrigger Building in the X and Y directions, respectively. These results reveal the variations in drift behaviour across the buildings and provide valuable insights into their seismic performance.

The amplified drift ratios account for the realistic dynamic response of the structures, ensuring a thorough evaluation of their compliance with NBCC standards.

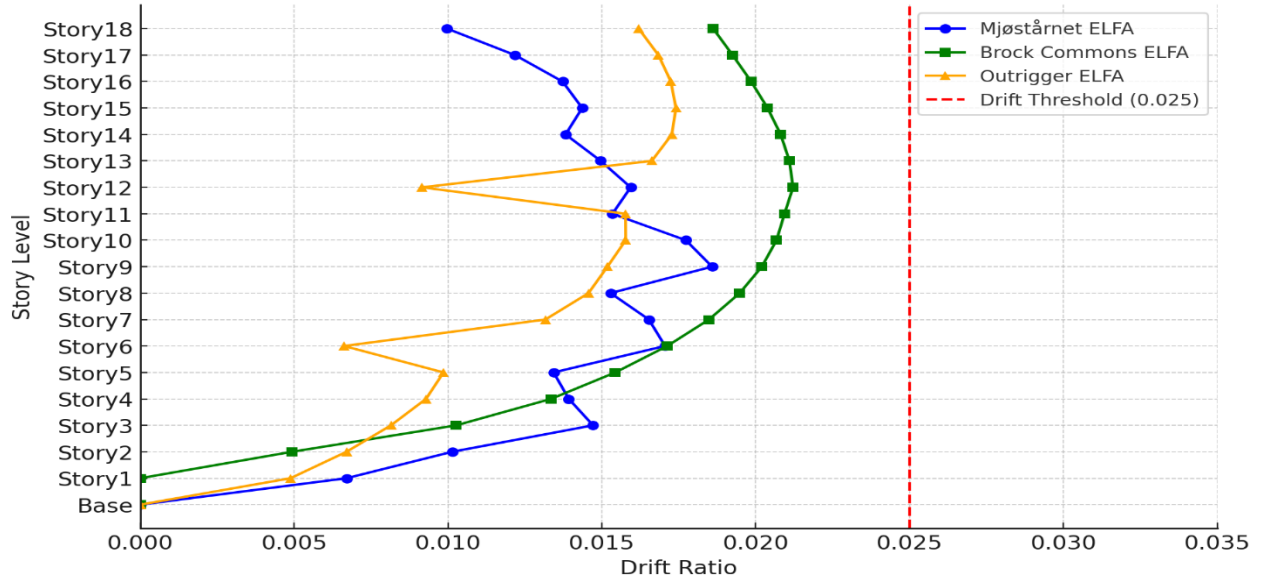


Figure 31 Maximum Drift Ratio in X-Direction for Mjøstårnet, Brock Commons, and Outrigger Building Under Static Seismic Analysis.

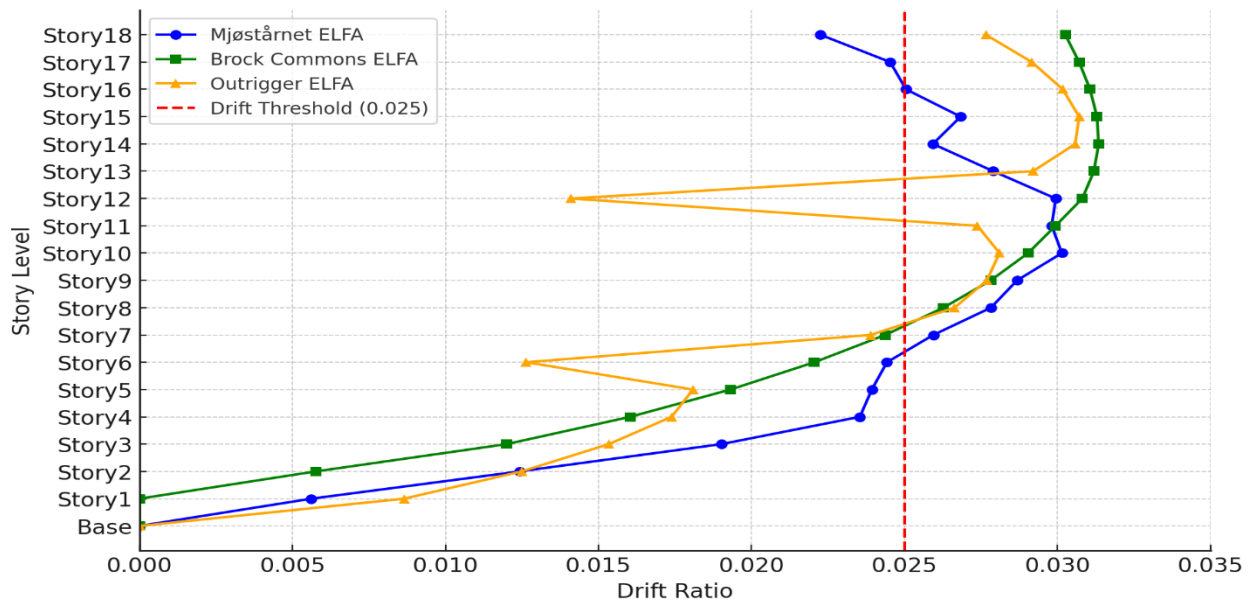


Figure 32 Maximum Drift Ratio in Y-Direction for Mjøstårnet, Brock Commons, and Outrigger Building Under Static Seismic Analysis.

5.1.1.2 Base Shear

The total lateral force acting at the base of a structure is known as the base shear, arising primarily from seismic loads. Its magnitude depends on the structure's weight and stiffness—heavier or stiffer buildings typically experience larger base shears under similar seismic forces.

As shown in Table 5.1, the seismic weight of Mjøstårnet, Brock Commons, and the Outrigger Building is calculated based on 100% dead load plus 25% of the snow and live load. The same table also provides the maximum base shear in the X and Y directions for each building, allowing a direct comparison between the structures' weights and their corresponding lateral force demands.

Table 5.1 Seismic Weight And Maximum Base Shear of Mjøstårnet, Brock Commons, And Outrigger Building.

Building	Seismic Weight (kN)	Maximum Base Shear (kN)	
		X-Direction	Y-Direction
Mjøstårnet	76240	6855	6740
Brock Commons	104030	10880	9660
Outrigger Building	87360	9100	7735

5.1.1.3 Overturning Moment

The magnitude of the overturning moment depends on factors such as the total lateral force, the building's mass distribution, and height. Typically, taller buildings or those subjected to higher lateral forces experience more excellent overturning moments. Figure 33 shows the overturning moments for Mjøstårnet, Brock Commons, and the Outrigger Building in the X and Y directions. This comparison highlights how each building's height and stiffness characteristics influence the

rotational demands it must withstand. Proper structural and foundation design must account for these overturning moments to ensure stability, particularly under extreme loading scenarios.

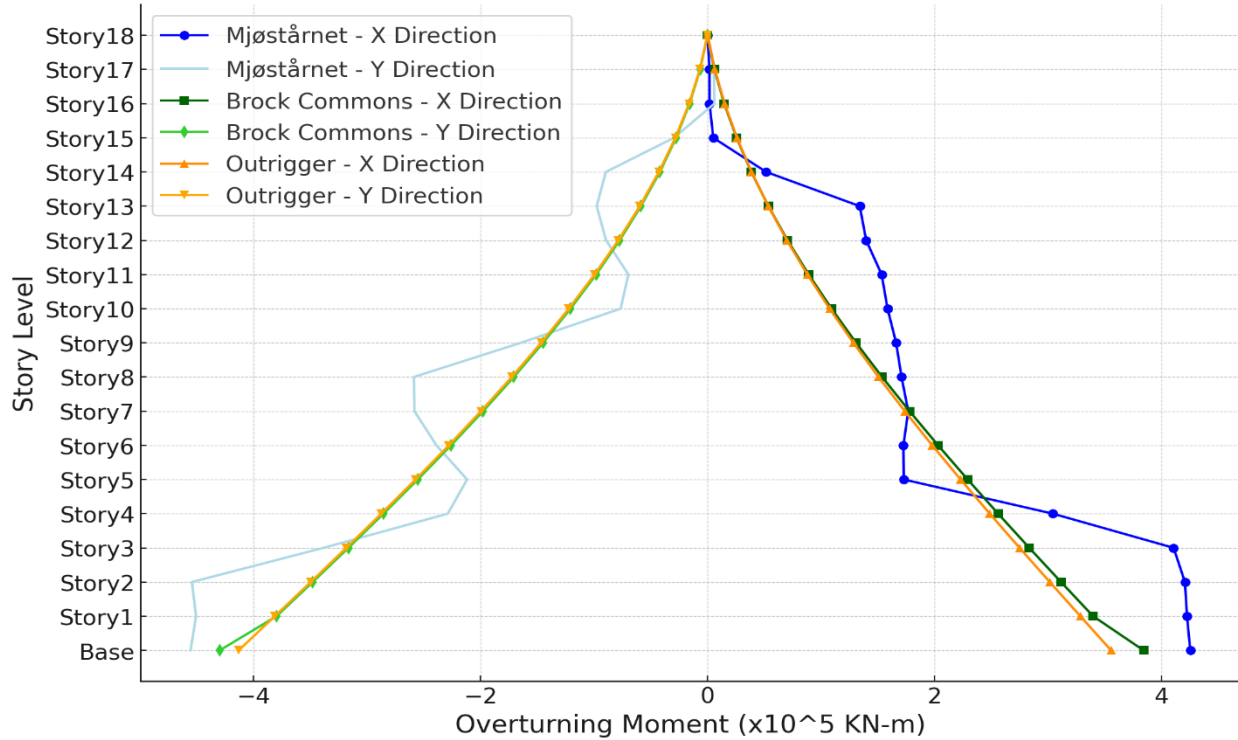


Figure 33 Maximum Overturning Moment for Mjøstårnet, Brock Commons, and Outrigger Building Under Static Seismic Analysis.

5.1.2 Response Spectrum Analysis

Response spectrum analysis (RSA) considers multiple vibration modes under seismic loads by applying a site-specific response spectrum and combining modal results (e.g., SRSS or CQC). For Mjøstårnet, Brock Commons, and the Outrigger Building, RSA was performed in ETABS using the same parameters and seismic coefficients ($R_d = 2$, $R_o = 1.5$) as the Equivalent Static Analysis, with design spectra from NBCC for the Brock Commons site.

5.1.2.1 Inter-Story Drift

Under response spectrum analysis (RSA), each significant vibration mode of the structure is excited by a site-specific response spectrum that reflects the local seismic hazard. The individual modal responses—encompassing displacements, velocities, and accelerations—are combined through standard methods (e.g., SRSS or CQC) to determine the overall structural response. This process provides a more refined evaluation of inter-story drift compared to Equivalent Static Analysis since RSA accounts for the unique contribution of each mode.

Figures 34 and 35 illustrate the maximum adjusted drift ratios, calculated like the Equivalent Static Load Analysis using Equation 19, for the X and Y directions, respectively, in Mjøstårnet, Brock Commons, and the Outrigger Building. A comparison of these results with those from the Equivalent Static Analysis highlights the impact of multi-modal interactions.

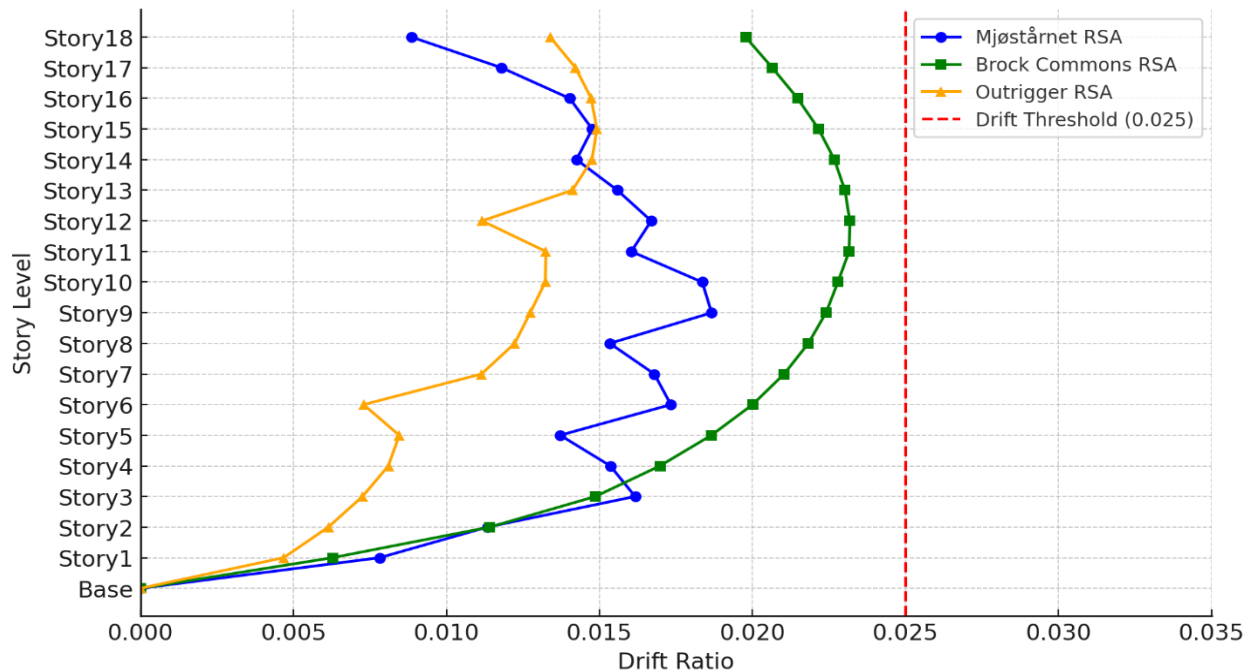


Figure 34 Maximum Drift Ratio in X-Direction for Mjøstårnet, Brock Commons, and Outrigger Building Under RSA.

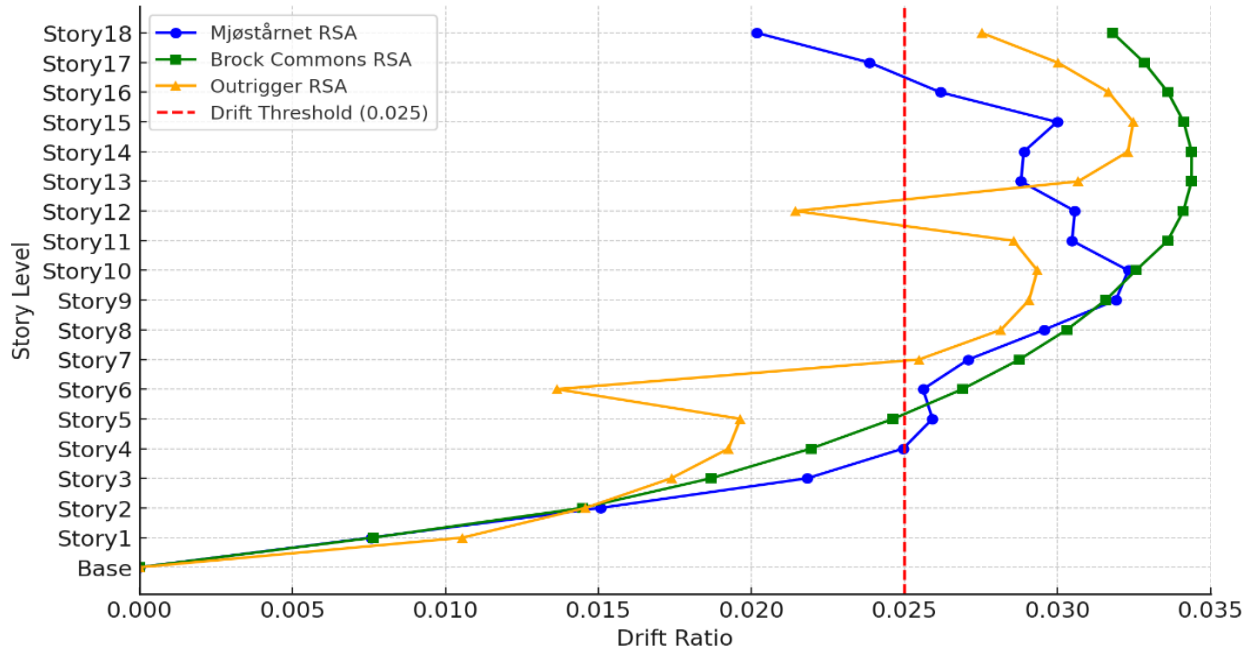


Figure 35 Maximum Drift Ratio in Y-Direction for Mjøstårnet, Brock Commons, and Outrigger Building Under RSA.

5.1.2.2 Base Shear

In response spectrum analysis (RSA), base shear is determined by combining the modal contributions in each principal direction using standard techniques (e.g., SRSS or CQC). To account for ductility (R_d), overstrength (R_o) reduction factors, and the important factor (I_e), the resulting base shear values were adjusted based on the R_d and R_o factors, following Equation (20). This adjustment provides a more realistic representation of the seismic demand than the raw modal outputs (V_{RSA}), ensuring consistency with code provisions.

$$V = V_{RSA} \frac{I_e}{R_d R_o} \tag{20}$$

For Mjøstårnet, Brock Commons, and the Outrigger Building, the RSA-derived base shear captures the influence of each structure’s height, mass distribution, and stiffness. By comparing these values

to those from the Equivalent Static Analysis, the impact of multi-modal effects—and the associated reductions due to R_d and R_o —becomes more apparent, offering a more comprehensive view of each building’s seismic force demands.

As shown in Table 5.2, the maximum base shear values in the X and Y directions are presented for Mjøstårnet, Brock Commons, and the Outrigger Building. By comparing these RSA-derived values with those from the Equivalent Static Analysis, the role of multi-modal interactions and code adjustments (through R_d and R_o) in shaping the final design forces becomes evident.

Table 5.2 Maximum Base Shear of Mjøstårnet, Brock Commons, And Outrigger Building Under RSA.

Building	Maximum Base Shear (KN)	
	X-Direction	Y-Direction
Mjøstårnet	7735	6735
Brock Commons	9625	11620
Outrigger Building	11575	9870

5.1.2.3 Overturning Moment

Like base shear, the overturning moment under response spectrum analysis (RSA) is derived by combining the modal contributions in each principal direction using methods such as SRSS or CQC. This approach accounts for multiple vibration modes that may not be fully captured in the equivalent static analysis, providing a more accurate picture of the structure’s dynamic behaviour. By applying the same R_d and R_o factors used for base shear (as specified in Equation 20), the RSA-derived overturning moments are adjusted to reflect realistic ductility and overstrength effects. Taller or more rigid buildings like Mjøstårnet typically exhibit higher overturning moments, underlining the importance of proper structural detailing and foundation design. Comparing these RSA results with their equivalent static counterparts offers a more comprehensive understanding of each building’s rotational demands under seismic loading. Figure 36 illustrates the Maximum Overturning Moment

for Mjøstårnet, Brock Commons, and the Outrigger Building under RSA, visually comparing the rotational demands on these structures and highlighting the differences in their seismic performance.

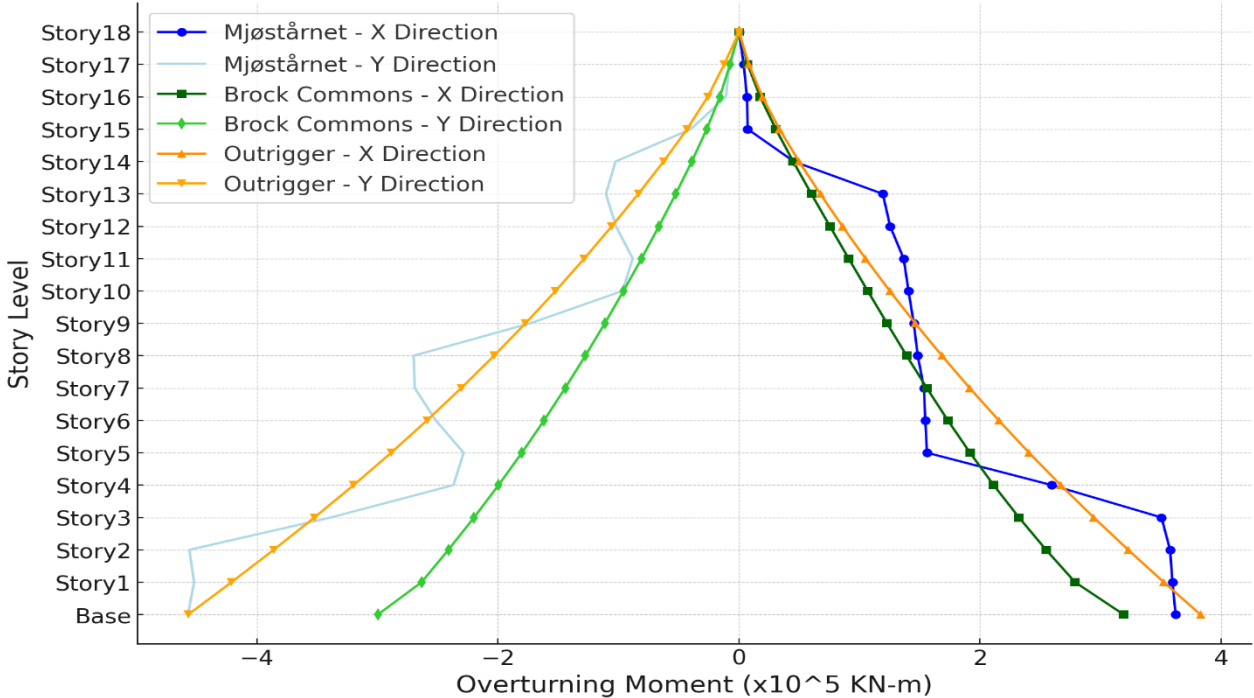


Figure 36 Maximum Overturning Moment for Mjøstårnet, Brock Commons, and Outrigger Building Under RSA.

5.1.3 Time History Analysis

Based on the preliminary results from the linear static and dynamic analyses, it is evident that the drift ratio in the transverse direction (Y-axis) exceeds the allowable limit of 0.025 as prescribed by the NBCC. Extensive history analyses were conducted to address this observation and provide a more comprehensive understanding of the structural response.

The analyses evaluated drift ratios in the X and Y directions using three ground motion records scaled and matched with a target response spectrum for Vancouver's seismic conditions. The focus was on the design-based earthquake (DBE) hazard level, emphasizing life safety as a key

performance objective. Each time, the history load case lasted 100 seconds to examine both loaded and free vibration scenarios.

The results are shown in Figures 38–42. Figures 37 and 38 present the maximum drift ratios in the X and Y directions for Mjøstårnet, Brock Commons, and the Outrigger Building under the Christchurch earthquake. Figures 39 and 40 show the results for the Mexico City earthquake, while Figures 41 and 42 illustrate the Northridge earthquake. These figures provide a detailed comparison of structural performance under varying seismic excitations.

Under the Christchurch earthquake, Brock Commons exceeds the drift limit in the X direction, while Mjøstårnet and the Outrigger Building perform acceptably. In the Y direction, all buildings exceed the limit, indicating lower stiffness in this direction. For the Mexico City earthquake, all buildings meet the X-direction drift limit. However, Mjøstårnet and the Outrigger Building exceed the limit in the Y direction, reflecting vulnerabilities under prolonged shaking. Under the Northridge earthquake, all buildings exceeded the Y-direction drift limit. Mjøstårnet and Brock Commons slightly exceed the limit in the X direction, while the Outrigger Building performs acceptably.

Brock Commons consistently exhibits higher drift ratios across all records due to its torsional first mode, while the Outrigger Building performs better due to its enhanced stiffness and lateral resistance. These results highlight the need for modern structural control strategies to improve structural performance.

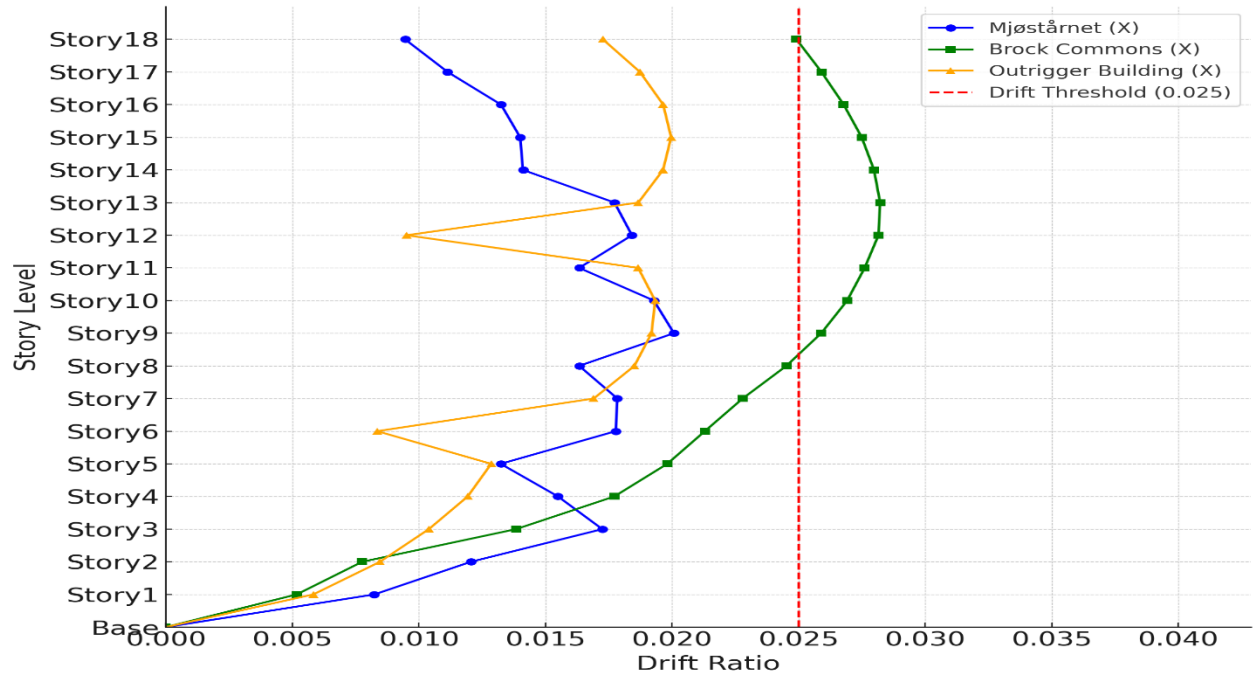


Figure 37 Maximum Drift Ratio in X-Direction for Mjøstårnet, Brock Commons, and Outrigger Building Under Christchurch Earthquake.

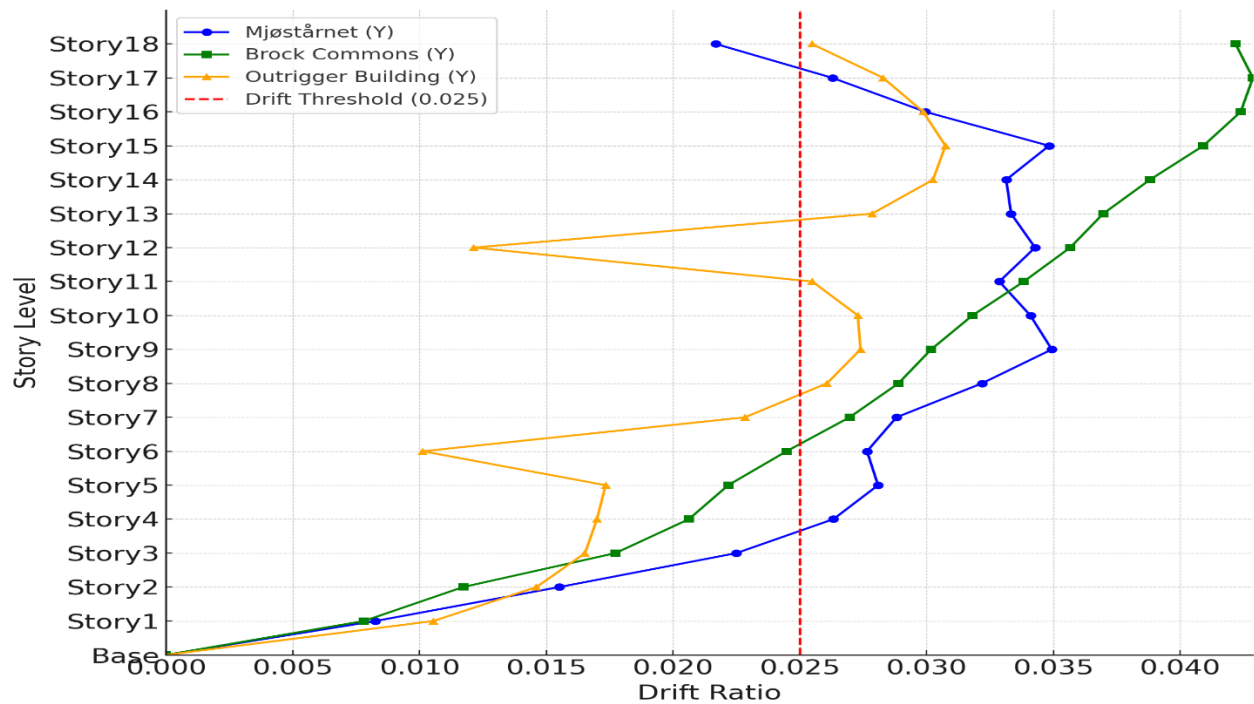


Figure 38 Maximum Drift Ratio in Y-Direction for Mjøstårnet, Brock Commons, and Outrigger Building Under Christchurch Earthquake.

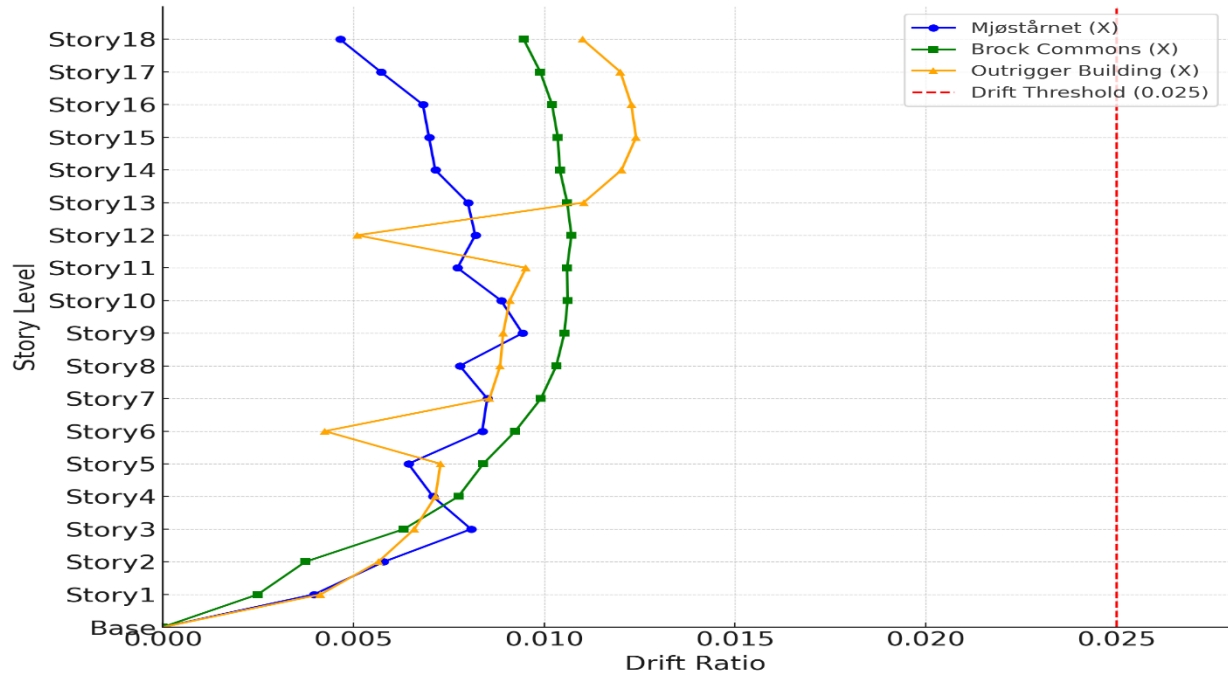


Figure 39 Maximum Drift Ratio in X-Direction for Mjøstårnet, Brock Commons, and Outrigger Building Under Mexico City Earthquake.

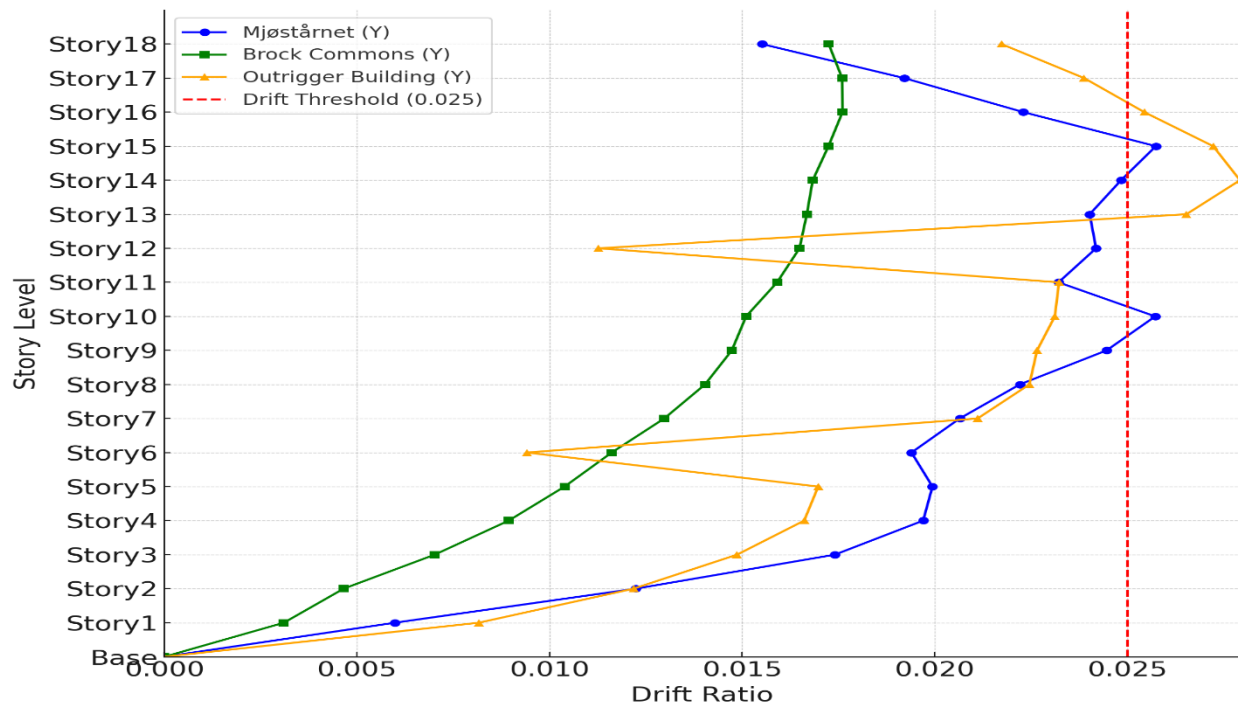


Figure 40 Maximum Drift Ratio in Y-Direction for Mjøstårnet, Brock Commons, and Outrigger Building Under Mexico City Earthquake.

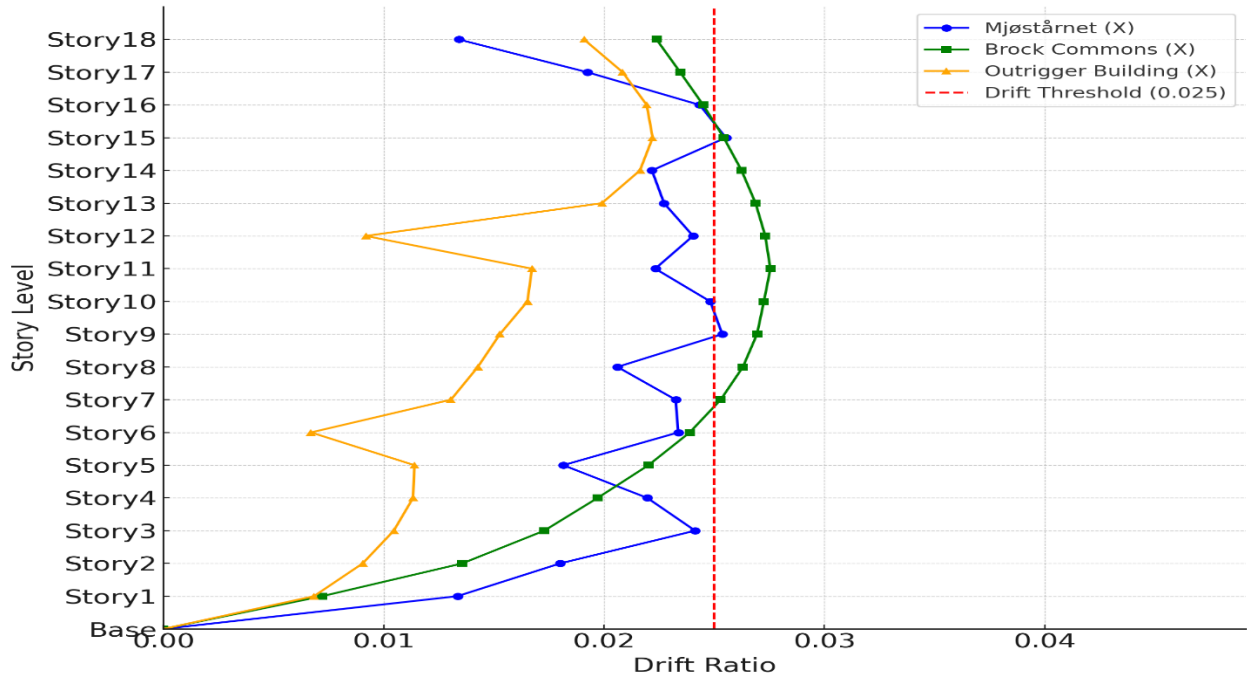


Figure 41 Maximum Drift Ratio in X-Direction for Mjøstårnet, Brock Commons, and Outrigger Building Under Northridge Earthquake.

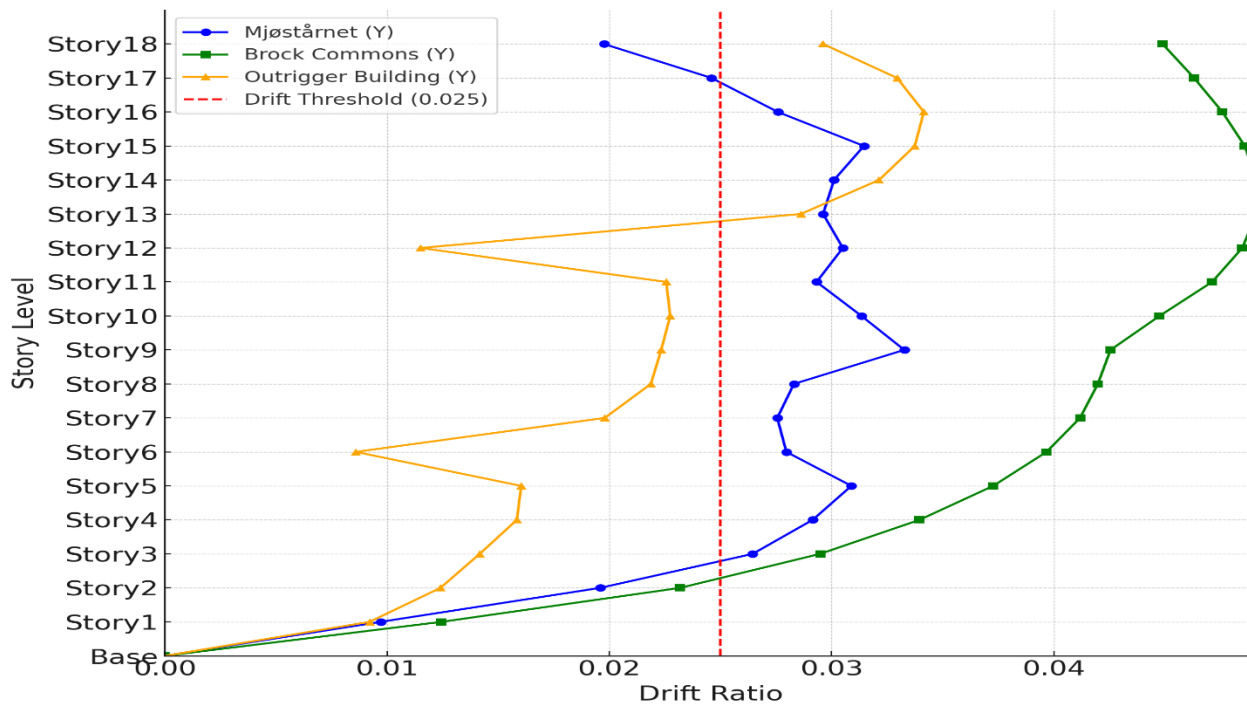


Figure 42 Maximum Drift Ratio in Y-Direction for Mjøstårnet, Brock Commons, and Outrigger Building Under Northridge Earthquake.

5.2 Wind Responses

This section presents the wind responses due to static and dynamic wind loads defined in the previous chapter. It evaluates the structural responses of the analyzed buildings under these loads, focusing on inter-story drift and inter-story accelerations.

5.2.1 Inter-Story Drift

The inter-story drift is a critical parameter for assessing the lateral displacement of structures subjected to wind loads. Excessive inter-story drift may lead to occupant discomfort and damage to non-structural elements. For this study, inter-story drift was calculated for the analyzed buildings using wind loads determined from the target wind hazard spectrum specific to the location.

Figures 43 and 44 illustrate the maximum drift ratios in the X and Y directions for Mjøstårnet, Brock Commons, and the Outrigger Building under static wind loads. Similarly, Figures 45 and 46 present the maximum drift ratios in the X and Y directions for the buildings under dynamic wind loads. The maximum lateral displacements of the selected buildings, shown in Figures 47 and 48, align closely with the actual recorded data for Mjøstårnet [12], confirming the accuracy of the analysis.

Both static and dynamic wind analyses indicate that the buildings exceed the drift limit in the transverse direction (Y direction). It is crucial to highlight that dynamic wind analysis for tall timber buildings must account for gust effects, wind-induced vibrations, and higher mode shapes, which are not fully captured in static analysis. The static analysis relies on calculating total wind loads and distributing them along the building height based on story height and stiffness. In contrast, dynamic analysis provides a more comprehensive understanding, as seen in the differing drift profiles of the Outrigger Building.

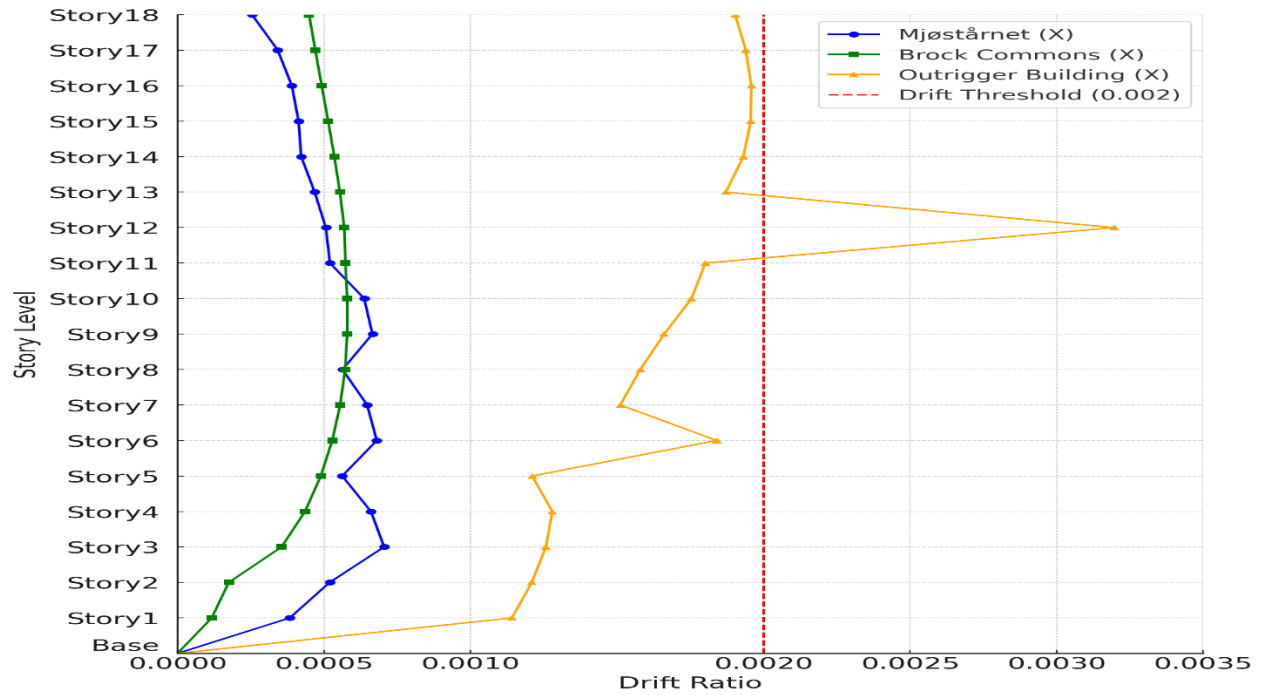


Figure 43 Maximum Drift Ratio in X-Direction for Mjøstårnet, Brock Commons, and Outrigger Building Under Static Wind Analysis.

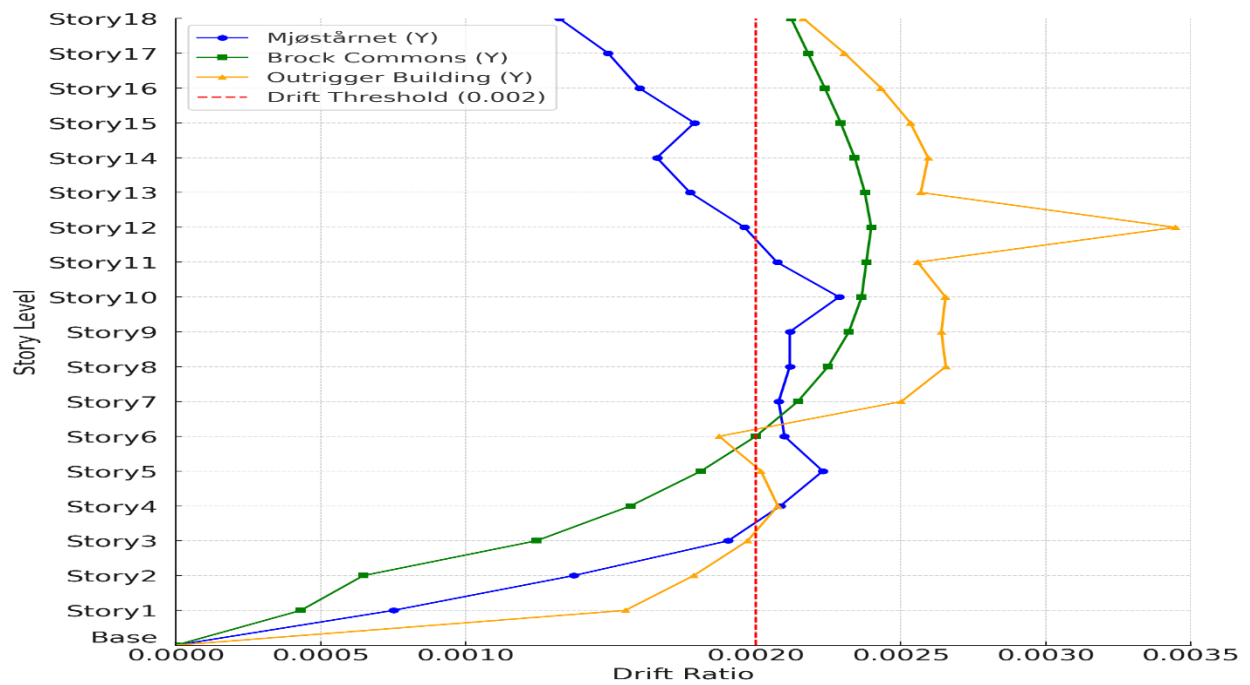


Figure 44 Maximum Drift Ratio in Y-Direction for Mjøstårnet, Brock Commons, and Outrigger Building Under Static Wind Analysis.

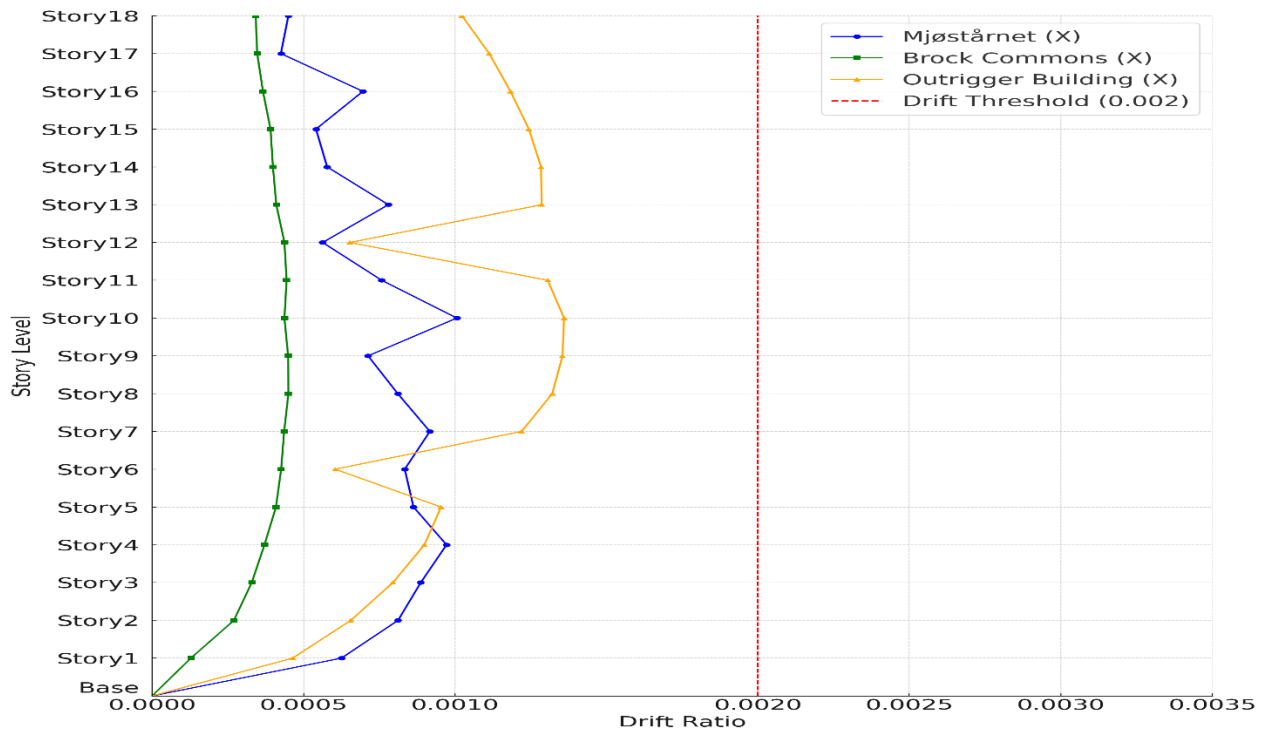


Figure 45 Maximum Drift Ratio in X-Direction for Mjøstårnet, Brock Commons, and Outrigger Building Under Dynamic Wind Analysis.

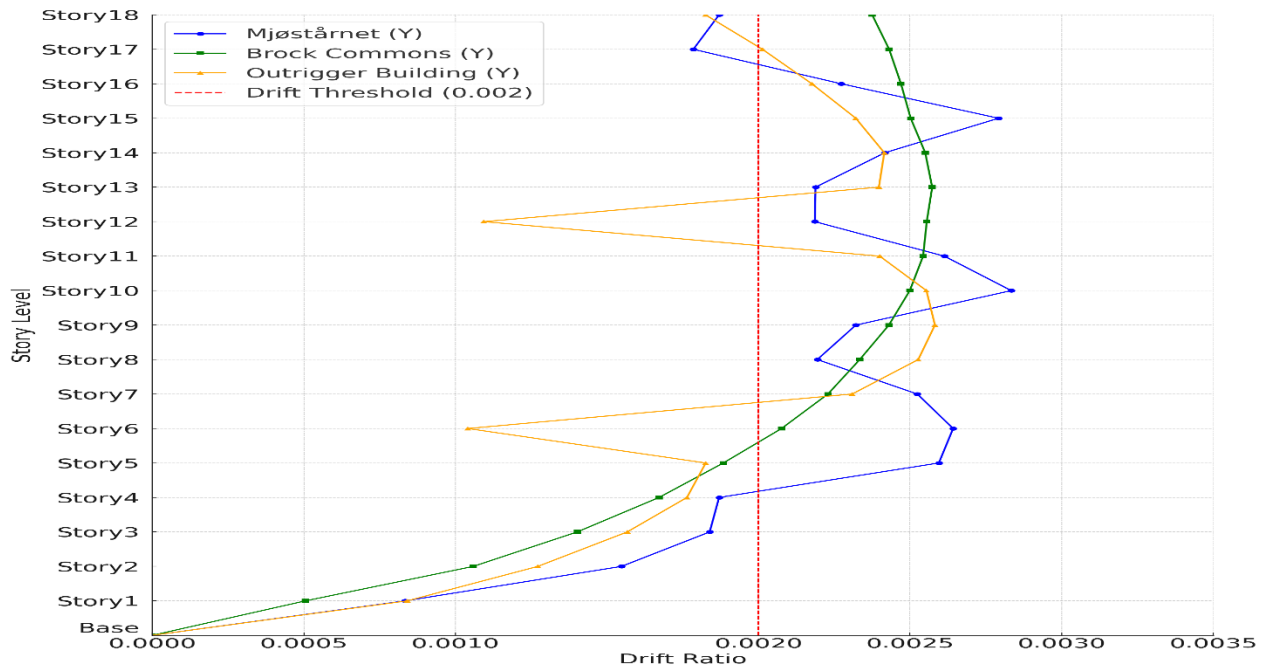


Figure 46 Maximum Drift Ratio in Y-Direction for Mjøstårnet, Brock Commons, and Outrigger Building Under Dynamic Wind Analysis.

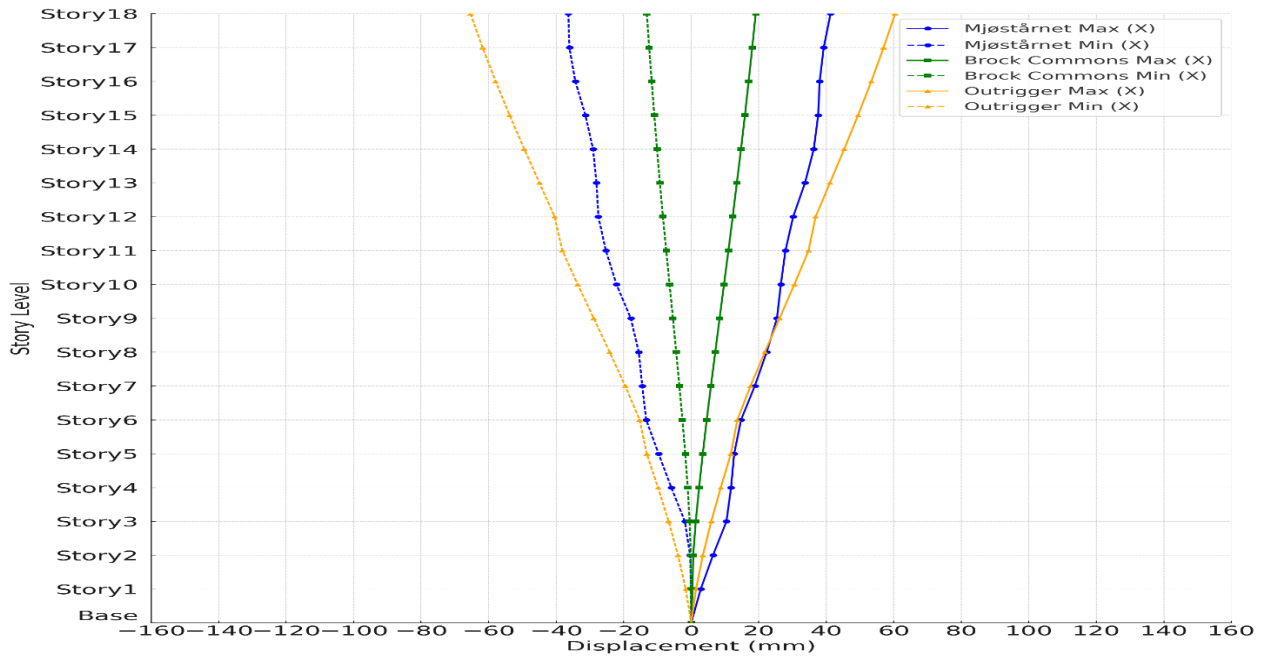


Figure 47 Maximum Lateral Displacement in X-Direction for Mjøstårnet, Brock Commons, and Outrigger Building Under Dynamic Wind Analysis.

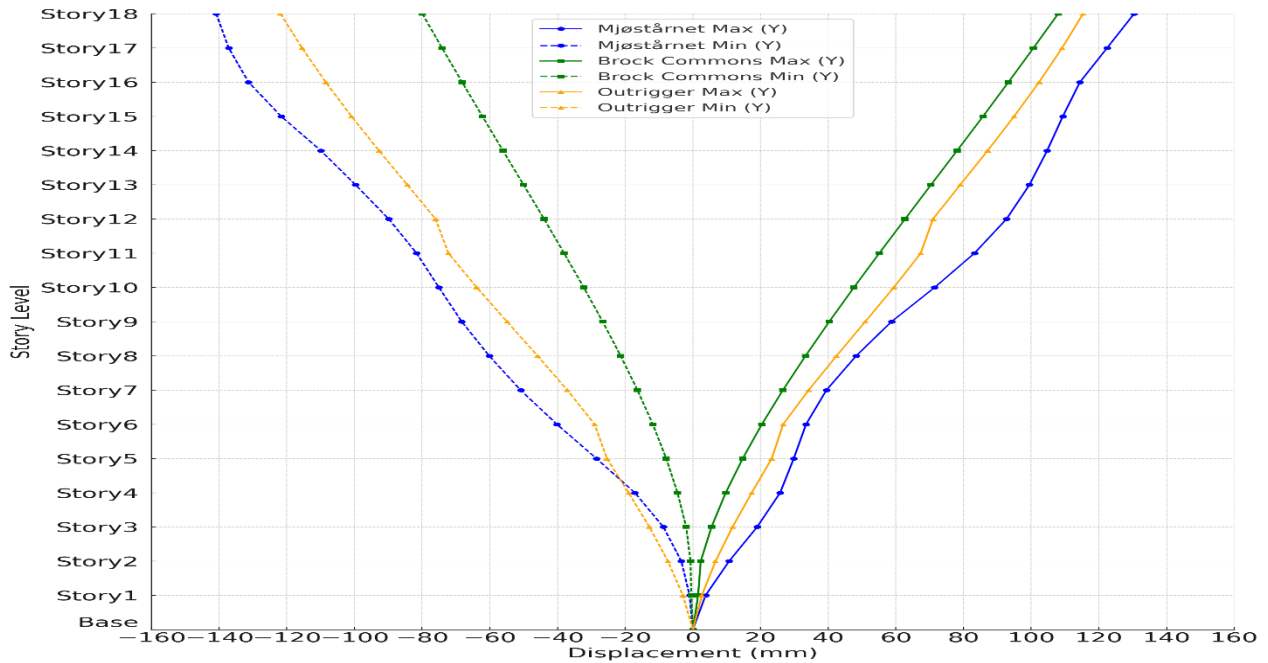


Figure 48 Maximum Lateral Displacement in Y-Direction for Mjøstårnet, Brock Commons, and Outrigger Building Under Dynamic Wind Analysis.

5.2.2 Inter-Story Accelerations

Inter-story accelerations are critical for evaluating the comfort of occupants and the performance of sensitive equipment. High accelerations can lead to discomfort and operational challenges in tall timber buildings. For the studied structures, inter-story accelerations were computed using dynamic wind load simulations, considering the natural frequencies and damping characteristics of each building. Additionally, the inter-story accelerations were compared against the limit of 20 milli-g, where g represents the ground acceleration, to evaluate compliance and ensure occupant comfort.

This study focuses on the maximum accelerations observed at Story 18 for each building, providing key insights into their performance at the critical upper levels. Figures 49-51 show the maximum story acceleration for Mjøstårnet, Brock Commons, and Outrigger Building in both X and Y directions. Finally, all buildings exceeded the acceleration limit by 3 times, underscoring the need for structural control systems to mitigate wind-induced responses.

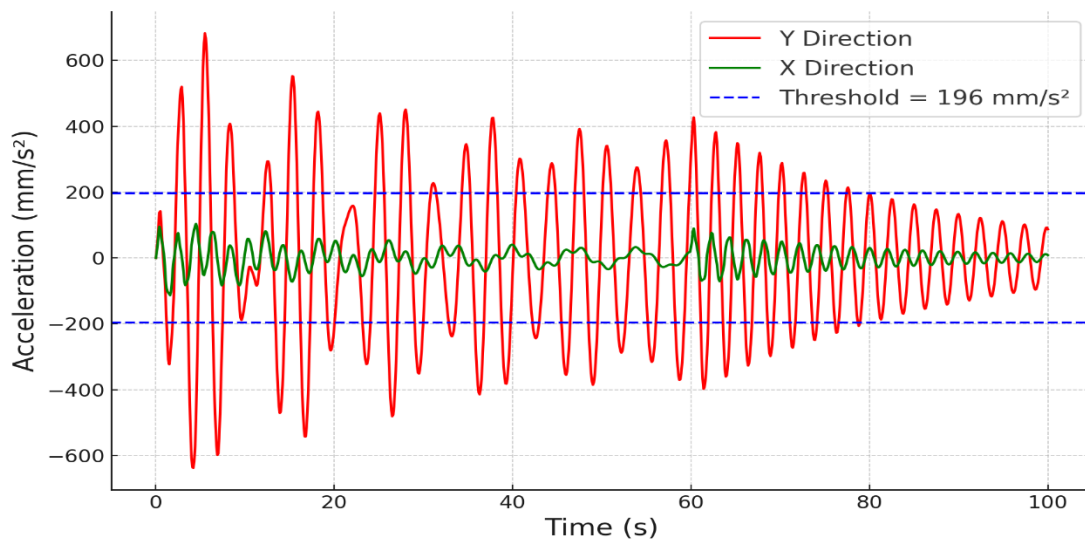


Figure 49 Story Acceleration Response in X And Y-Direction for Mjøstårnet Building Under Dynamic Wind Analysis.

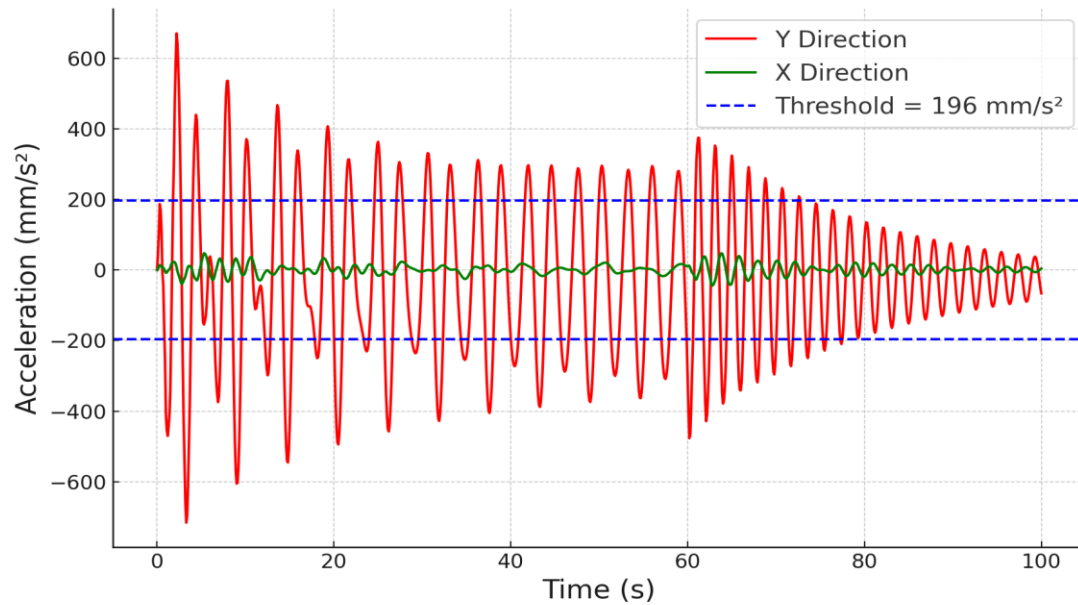


Figure 50 Story Acceleration Response in X And Y-Direction for Brock Commons Building Under Dynamic Wind Analysis.

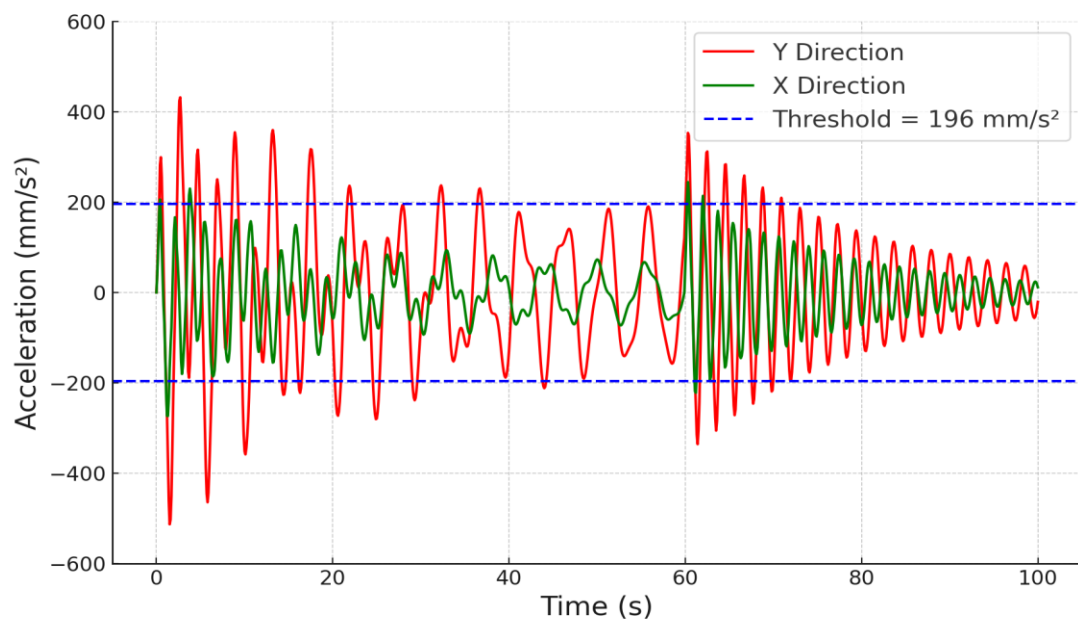


Figure 51 Story Acceleration Response in X And Y-Direction for Outrigger Building Under Dynamic Wind Analysis.

6 Fluid Viscous Dampers in Tall Wood Building

6.1 Installing FVDs

Fluid Viscous Dampers (FVDs) can be implemented in tall timber buildings in various configurations to enhance structural performance. They are typically connected to brace elements, such as timber brace elements or mega brace elements, as shown in Figure 52, to ensure sufficient relative displacement along the damper axis to activate them. FVDs may also be integrated within shear walls or strategically positioned at high relative displacements to maximize energy dissipation.

The placement of FVDs is often symmetric about the building's center of mass to prevent torsional motion and maintain structural balance. The flexibility in their configuration and placement makes FVDs adaptable to various design constraints and project-specific requirements, ensuring optimal performance under seismic and wind events.



Figure 52 Fluid Viscous Dampers in Diagonal Mega-Brace Configurations (Source: Taylor Devices).

6.2 Design and Modeling of FVDs

According to NBCC, designing structures with FVDs require detailed modelling of their non-linear force-deformation characteristics and conducting three-dimensional non-linear dynamic analysis. Damping contributions are restricted to ensure realistic results, and ground motion histories must align with the structure's response spectrum. This ensures that FVDs are effectively integrated, enhancing the structural resilience of buildings under dynamic loading conditions.

The FVDs were modelled as link elements with properties based on the Maxwell model of viscoelasticity, which represents the damper as a combination of a dashpot (C, α) and a linear spring (K_d), as shown in Figure 53. Extender braces, which connect dampers across stories, were included in the analysis, with their stiffness calculated as springs in series with the damper's stiffness using Equation 21. The stiffness of the extender braces was further evaluated using Equation 22, which accounts for material properties (E), cross-sectional area (A), and length (L). These calculations accurately represented the combined stiffness (K_d^*) of the damper system and its connecting components.

$$K_d^* = \frac{1}{K_d} + \frac{1}{K_b} \quad (21)$$

$$K_b = \frac{AE}{L} \quad (22)$$

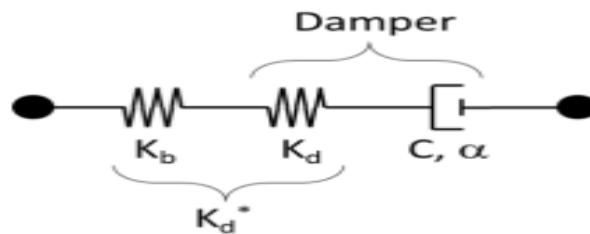


Figure 53 Model for Damper in Series with an Extender Brace.

The process began by identifying the controlling performance objective, such as the drift ratio (QE) and the target performance objective or the component capacity (QER), to determine the dashpot parameters. Based on these criteria, the required viscous damping (β_v) necessary to meet the target performance objective was calculated using Equation 23. Where (β_i) is the inherent damping of the building.

$$\beta_v = -\beta_i + \frac{1}{100} e^{\left(5.6-4 \frac{Q_{ER}}{Q_E}\right)} \quad (23)$$

Linear damper properties were determined using Equation 24, given in the FVDs design manual by Taylor Devices.

$$C_{ji} = \frac{4 K_i T \beta_v}{\pi n_{di} \cos^2 \theta_{ji}} \quad (24)$$

Where (K_i) is the floor stiffness, which can be estimated by dividing story shear by story drift, (T) is the fundamental period of Building in the direction of the dampers, (n_{di}) is the number of dampers in that direction, and (θ_{ij}) is the angel of the j^{th} damper on the i^{th} floor measured from horizontal.

Subsequently, the non-linear damper properties (C_{ji_N}) were determined based on equivalent energy dissipation, as outlined in Equation 25.

$$C_{ji_N} = C_{ji} \frac{\pi}{3.675} \left(\frac{2 \pi d_{ji}}{B_1} \right)^{(1-\alpha)} \quad (25)$$

Where (d_{ji}) is the damper displacement of the j^{th} damper on the i^{th} floor, which can be estimated as the desired drift ratio (0.025) times the story height (H) multiplied by $\cos(\theta_{ij})$, (α) is the damping exponent, and (B_1) is the damping coefficient, as depicted in equation 26.

$$B = \frac{4}{[5.6 - \ln 100 \beta_1]} \quad (26)$$

Finally, the maximum load effects on the dampers were calculated using Equation 27.

$$F_{ji} = 1.15 C_{ji_N} \cdot \left(\frac{5.4 \pi d_{ji}}{T} \right)^{\alpha} \quad (27)$$

Table 6.1 summarizes the maximum drift ratios recorded for Brock Commons, Mjøstårnet, and the proposed Outrigger Building, alongside the target drift ratio of 0.025 set for design-based earthquake performance. The table also presents the additional viscous damping required to meet the target performance objectives.

Table 6.1 *Drift Ratios And Required Viscous Damping for Tall Timber Buildings.*

Building	Maximum Drift Ratio (%)	Required Viscous Damping (%)
Brock Commons	4.9	33.6
Mjøstårnet	3.5	14.0
Outrigger	3.4	12.8

Brock Commons requires significantly more damping than Mjøstårnet and the Outrigger Building due to its torsional first mode shape, caused by an offset between the building's center of rigidity and center of mass. This condition amplifies the drift ratio, necessitating a higher damping ratio and a non-uniform damper configuration to minimize eccentricity. To address this, 46 Fluid Viscous Dampers (FVDs) were installed in Brock Commons, with 8 of these dampers strategically placed alongside a mega brace element at the building edge, in front of the core along the X direction, as shown in Figure 54. This configuration effectively mitigated the torsional effect, shifted it to higher mode shapes, and reduced the additional required viscous damping to 18.3%. In contrast, both Mjøstårnet and the Outrigger Building employed uniform damper configurations.

In Mjøstårnet, 30 FVDs were connected to the brace truss system and uniformly distributed around the building, as shown in Figure 55. Similarly, in the Outrigger Building, 32 FVDs were installed directly on the outrigger elements at stories 6 and 12, as depicted in Figure 56.

The literature review suggests that the optimal damper velocity exponent ranges between 0.3 and 0.5 for seismic applications and between 0.5 and 1.0 for wind applications. To ensure adequate performance under both seismic and wind loading conditions, the exponent was chosen as 0.5, striking a balance between the requirements of both scenarios.

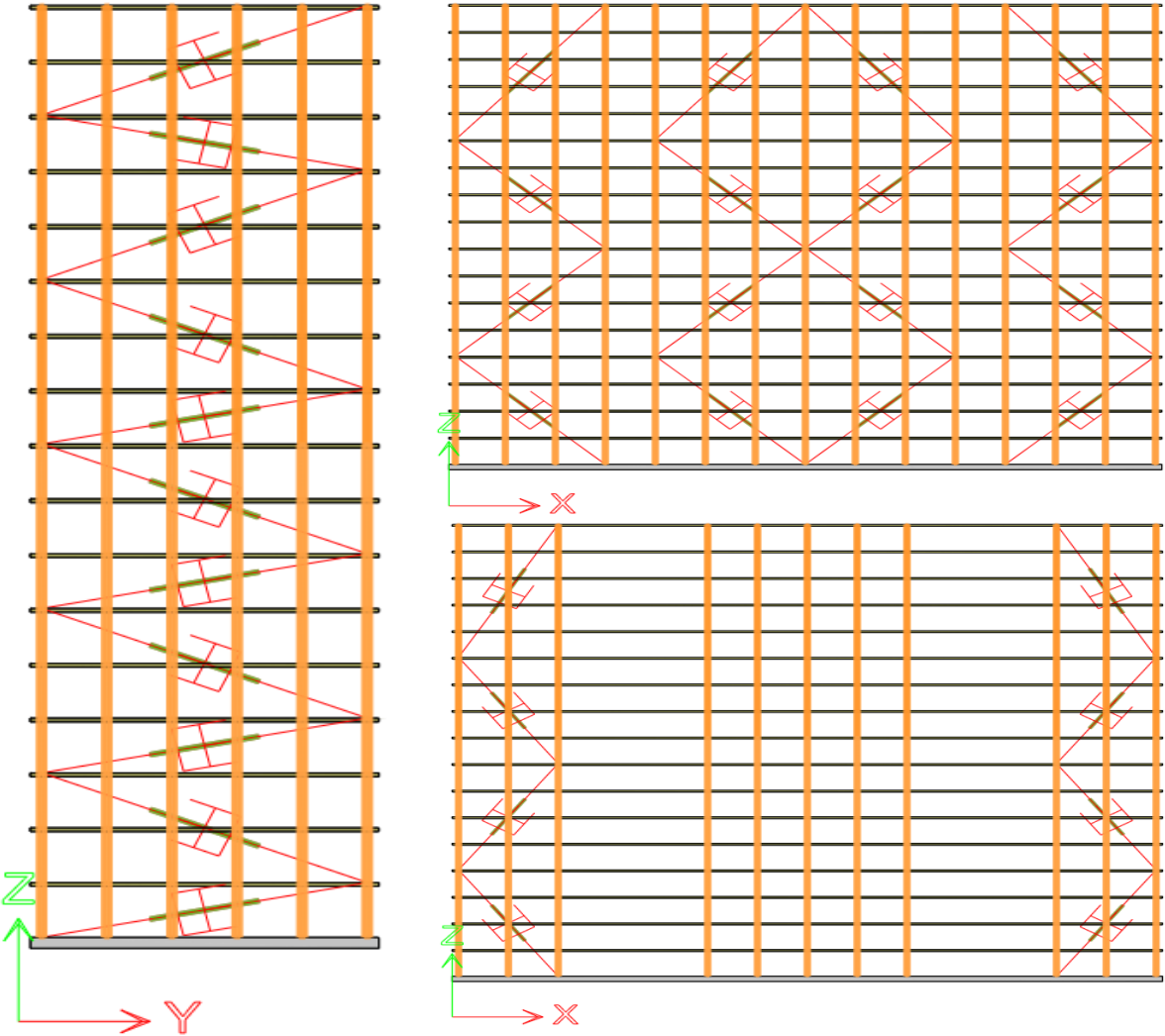


Figure 54 Fluid Viscous Damper Configuration for Brock Commons Tall Timber Building.

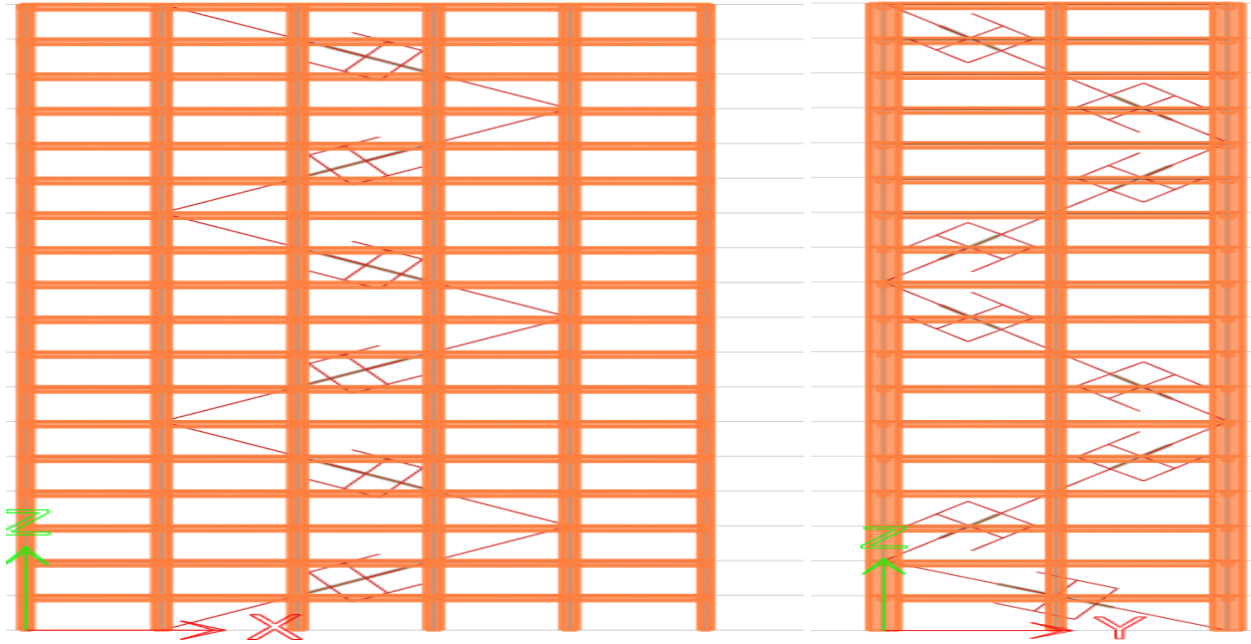


Figure 55 Fluid Viscous Damper Configuration for Mjøstårnet Tall Timber Building.

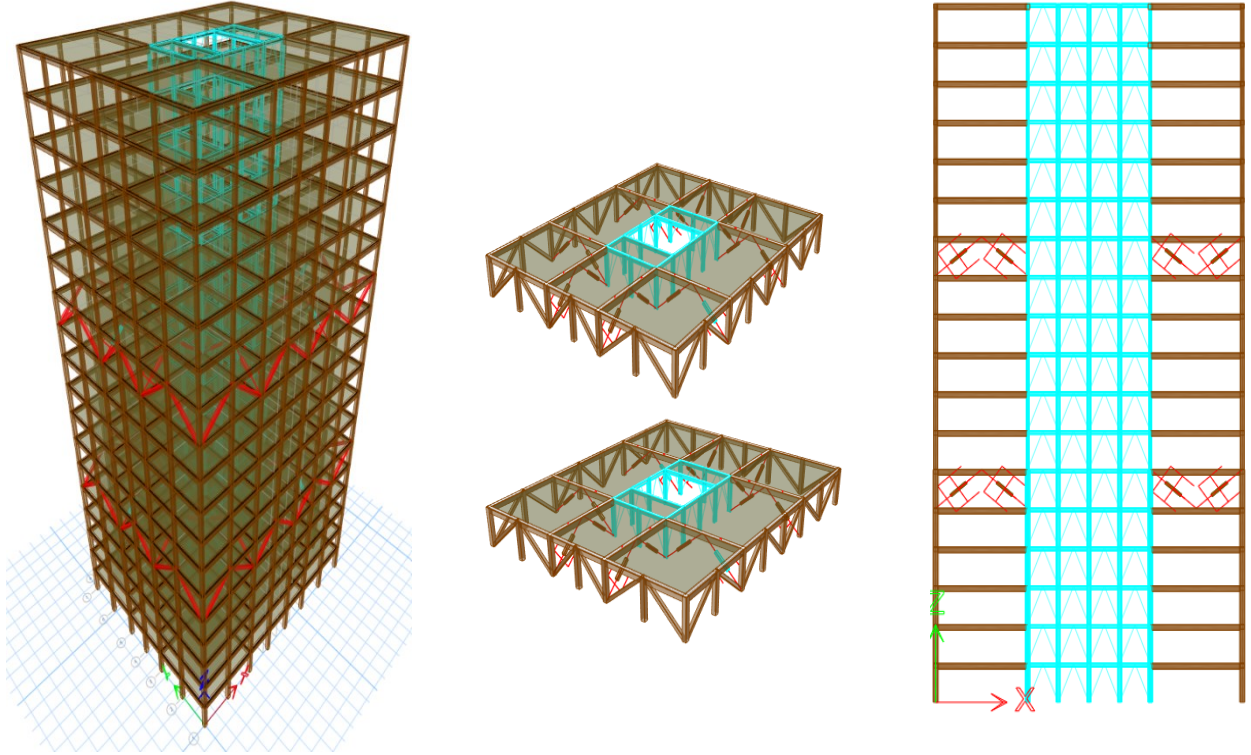


Figure 56 Fluid Viscous Damper Configuration for Outrigger Tall Timber Building.

Moreover, the findings show that the linear damping coefficient is consistent across upper levels but increases at the first level due to column base fixity and lower story drifts. While a single damping constant is typically sufficient, varying damper sizes may be necessary for significant story drift differences. For efficiency, this study utilized a single damper size with uniform parameters sourced from Taylor Devices, as presented in Table 6.2, which outlines the properties of the damper.

Table 6.2 Fluid Viscous Damper Properties and Parameters.

Building	Number of Dampers in Y Direction	C_j (KN-sec/m)	C_{jN} (KN-(sec/m)^{0.5})	FVD Stiffness (KN/mm)	Maximum Viscous Force (KN)
Brock Commons	22	11100	4755	840	4000
Mjøstårnet	18	4100	2378	500	1500
Outrigger	16	7200	3132	525	2000

6.3 Effectiveness of FVDs in Tall Timber Buildings

6.3.1 Modal Analysis

FVDs do not contribute additional stiffness to the system, ensuring that the natural period of the building remains unchanged. For more flexible buildings, this retrofit approach preserves the building period outside the constant amplitude plateau, effectively limiting the seismic forces acting on the structure.

Table 6.3 presents the fundamental periods of Brock Commons, Mjøstårnet, and the Outrigger Building both before and after the installation of the dampers. The table also includes the mass participation ratios and the mode shape directions for each building. While the periods of Mjøstårnet and the Outrigger Building remain consistent, a decrease is observed for Brock Commons. This reduction is attributed to adding brace elements required to accommodate the dampers and mitigate the torsional effect.

Table 6.3 *Fundamental Periods, Mass Participation Ratios, and Mode Shape Directions Before and After Installing FVDs.*

Building	Conventional Building		Building with FVDs	
	Period (s)	Mass Participation	Period (s)	Mass Participation
Brock Commons	2.13	51%-RZ	1.78	61%-UY
Mjøstårnet	2.47	76%-UY	2.49	76%UY
Outrigger	2.12	68%-UY	2.15	68%-UY

6.3.2 Seismic Responses

Implementing fluid viscous dampers (FVDs) in tall timber buildings, including Brock Commons, Mjøstårnet, and the Outrigger Building, demonstrated varying seismic performance outcomes. The hysteretic behaviour of the dampers was analyzed to evaluate their effectiveness in dissipating seismic energy. In Brock Commons, the hysteretic loops of the FVDs aligned well with expectations. These loops, characterized by the enclosed area, represent the additional energy dissipated through damping, indicating that the designed damping coefficients and placement of dampers successfully achieved the intended seismic performance, as demonstrated in Figure 57. Similarly, in the Outrigger Building, the hysteretic loops showed effective energy dissipation, as shown in Figure 58.

In contrast, the hysteretic loops observed in Mjøstårnet exhibited a lower area than initially anticipated, suggesting that the original damping coefficients were insufficient to meet the seismic performance targets. Iterative adjustments were made by progressively increasing the damping coefficient of the FVDs. After several iterations, the damping coefficient was increased to 6500 kN.(m/s)^{0.5}, which successfully enhanced the dampers' performance, as evidenced by Figure 59. This

adjustment enabled the structure to achieve the seismic targets, including a maximum inter-storey drift ratio of less than 0.025.

The improved damping system effectively reduced seismic responses, particularly story drift and displacements. Figures 60–63 illustrate this, with Figure 63 showing time-history displacements in the X and Y directions for a corner joint at story 18 of the Mjøstårnet, Outrigger, and Brock Commons buildings under various earthquakes. The data highlights the dampers' role in minimizing peak movements and controlling oscillations, improving overall seismic resilience.

Similarly, the damping system significantly reduced base shear across all seismic events, as detailed in Figures 64–66. These figures specifically present the base shear responses for all buildings under the Christchurch earthquake, illustrating the system's effectiveness in reducing seismic demand and enhancing compliance with structural design criteria.

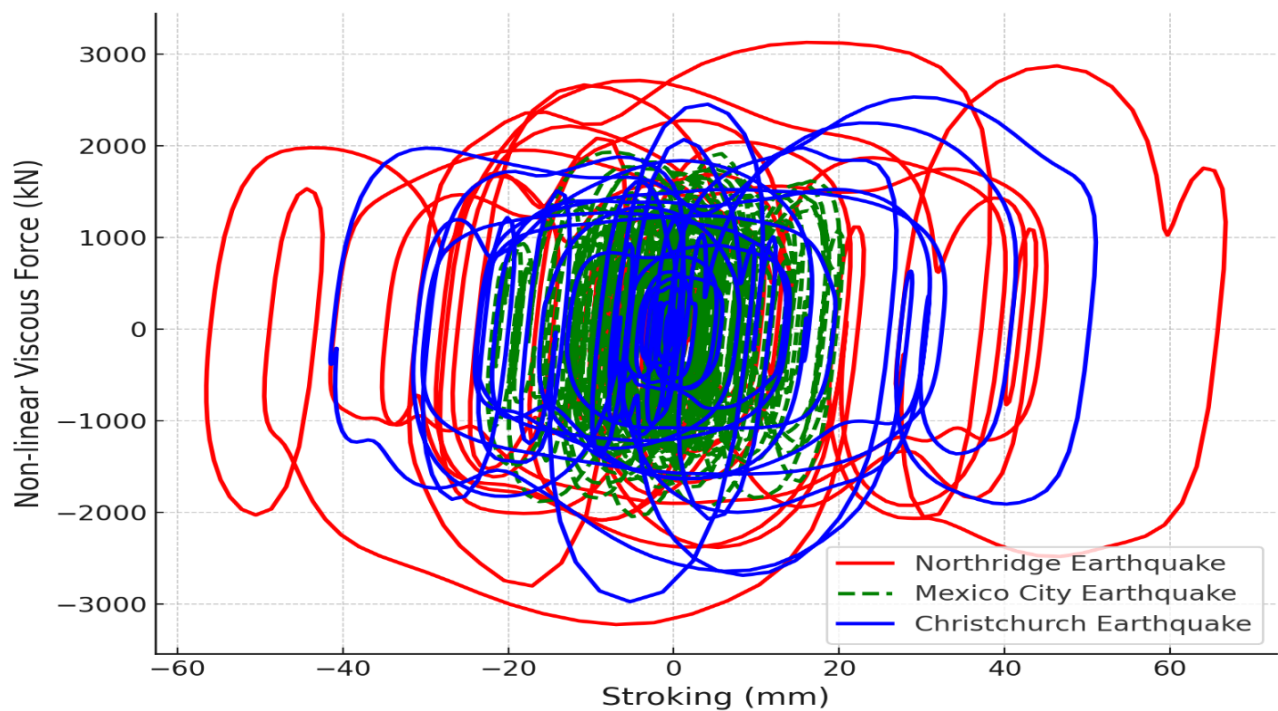


Figure 57 Hysteretic Loop of a Damper in Brock Commons Building under Seismic Events.

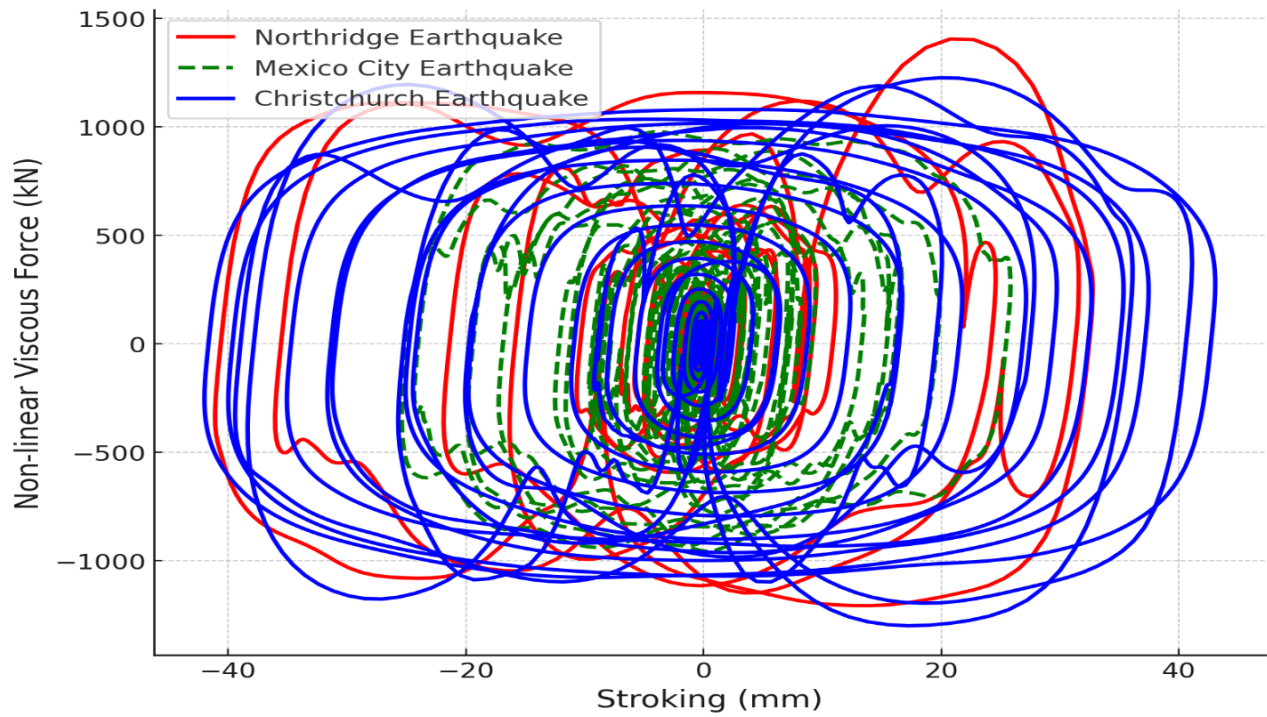


Figure 58 Hysteretic Loop of a Damper in Outrigger Building under Seismic Events.

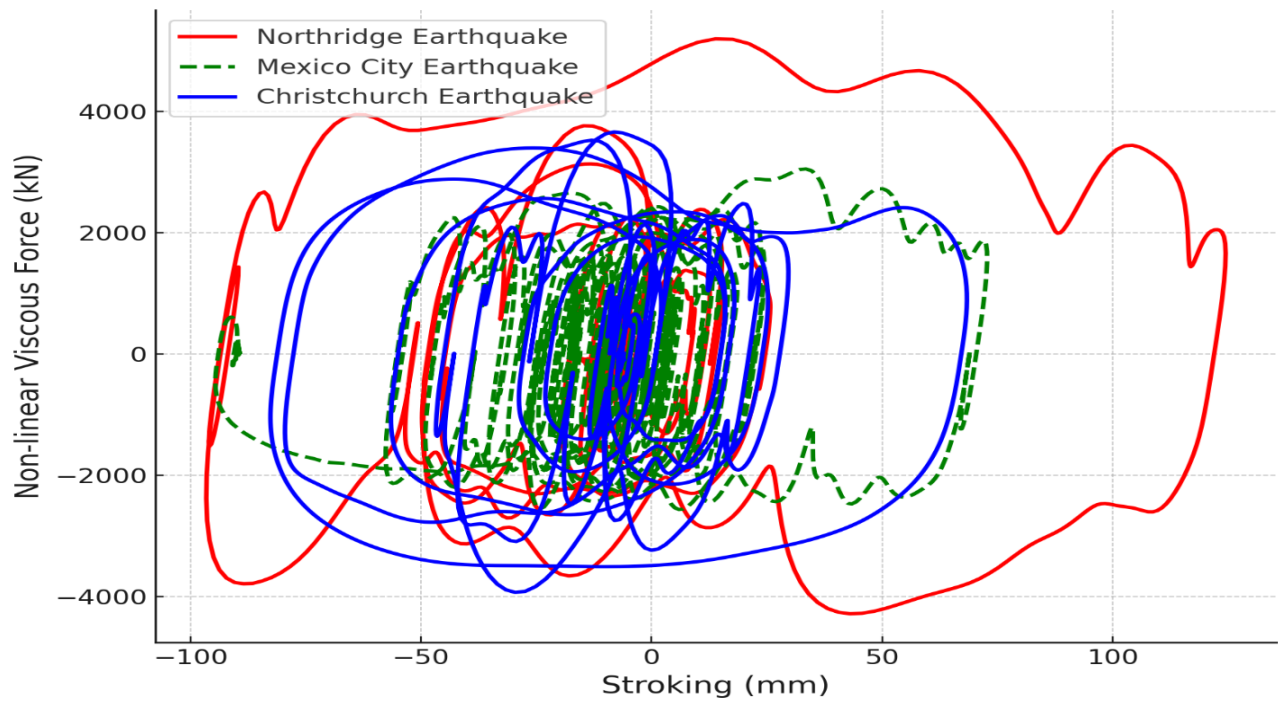


Figure 59 Hysteretic Loop of a Damper in Mjøstårnet Building under Seismic Events.

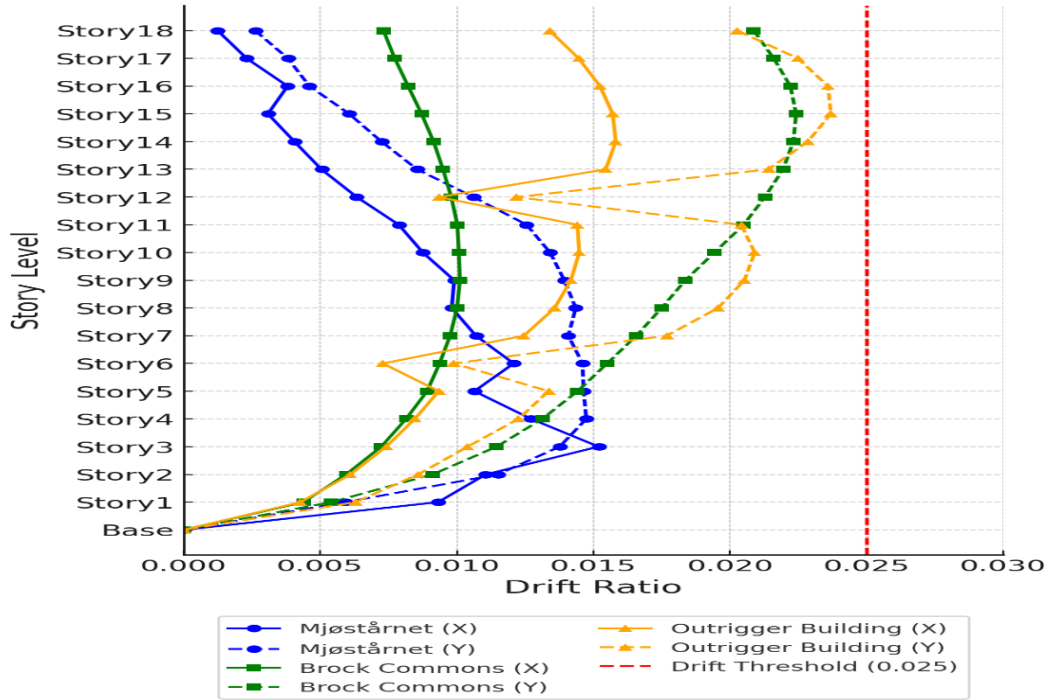


Figure 60 Maximum Drift Ratio for Mjøstårnet, Brock Commons, and Outrigger Buildings with FVDs Under Christchurch Earthquake.

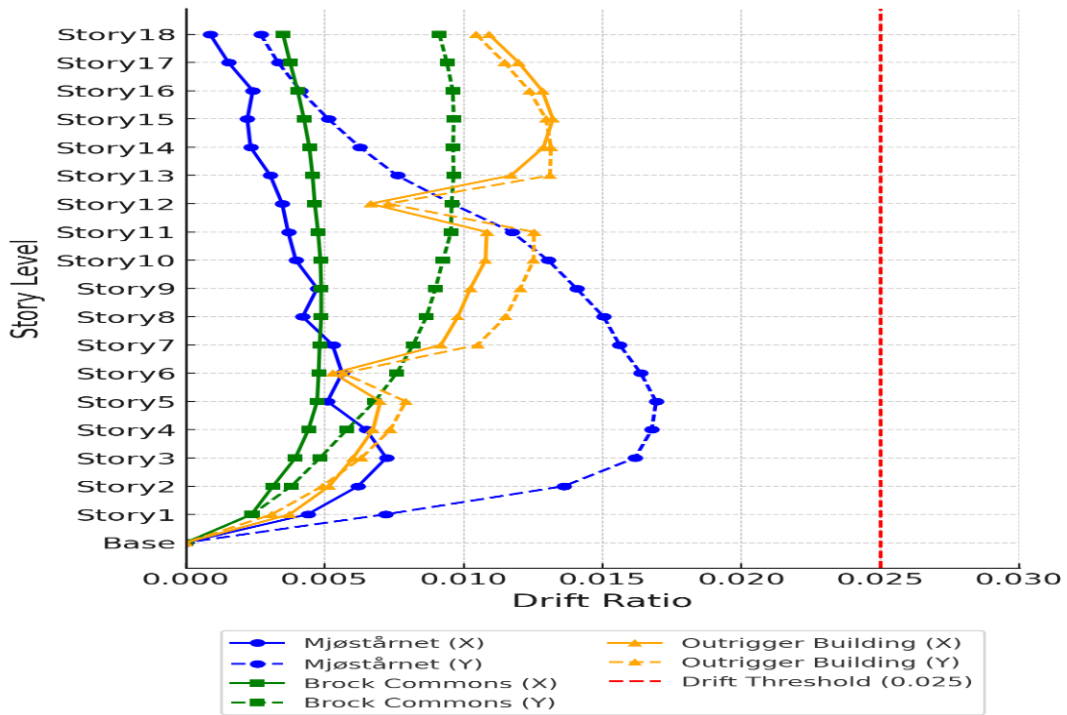


Figure 61 Maximum Drift Ratio for Mjøstårnet, Brock Commons, and Outrigger Buildings with FVDs Under Mexico City Earthquake.

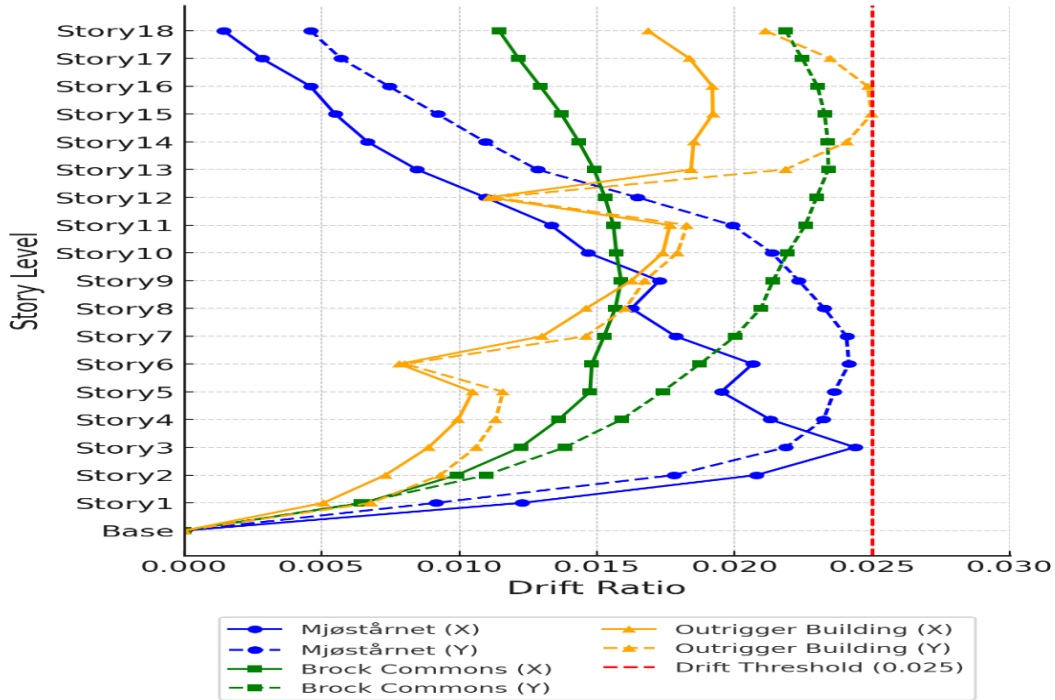


Figure 62 Maximum Drift Ratio for Mjøstårnet, Brock Commons, and Outrigger Buildings with FVDs Under Northridge Earthquake.

The drift profiles in both X and Y directions showed a clear reduction in disparity, highlighting the effectiveness of FVDs in distributing and dissipating seismic energy. In the Mjøstårnet building, FVDs successfully redirected damage from the weak to the strong axis, enhancing overall stability and underscoring the importance of precise damper calibration.

To further investigate how damage transfers between directions with time, time history displacement responses were analyzed, as shown in Figure 63. In this figure, the Mjøstårnet building was subjected to the Mexico City earthquake, the Outrigger building was analyzed under the Northridge earthquake, and the Brock Commons building experienced the Christchurch earthquake. These distinct ground motion records were selected to reflect a variety of seismic characteristics—such as long-duration shaking, near-fault effects, and high-frequency content—providing a comprehensive assessment of the damping system's performance across diverse seismic scenarios.

The results revealed that the fluid viscous dampers (FVDs) not only minimized peak displacements but also contributed to a more balanced and controlled seismic response across both axes over the duration of the events. Furthermore, the Outrigger Building highlighted a potential limitation of the system: while the FVDs effectively reduced drift at targeted levels, they also transferred seismic demand to adjacent stories that were not equipped with dampers, emphasizing the importance of strategic placement in damper design.

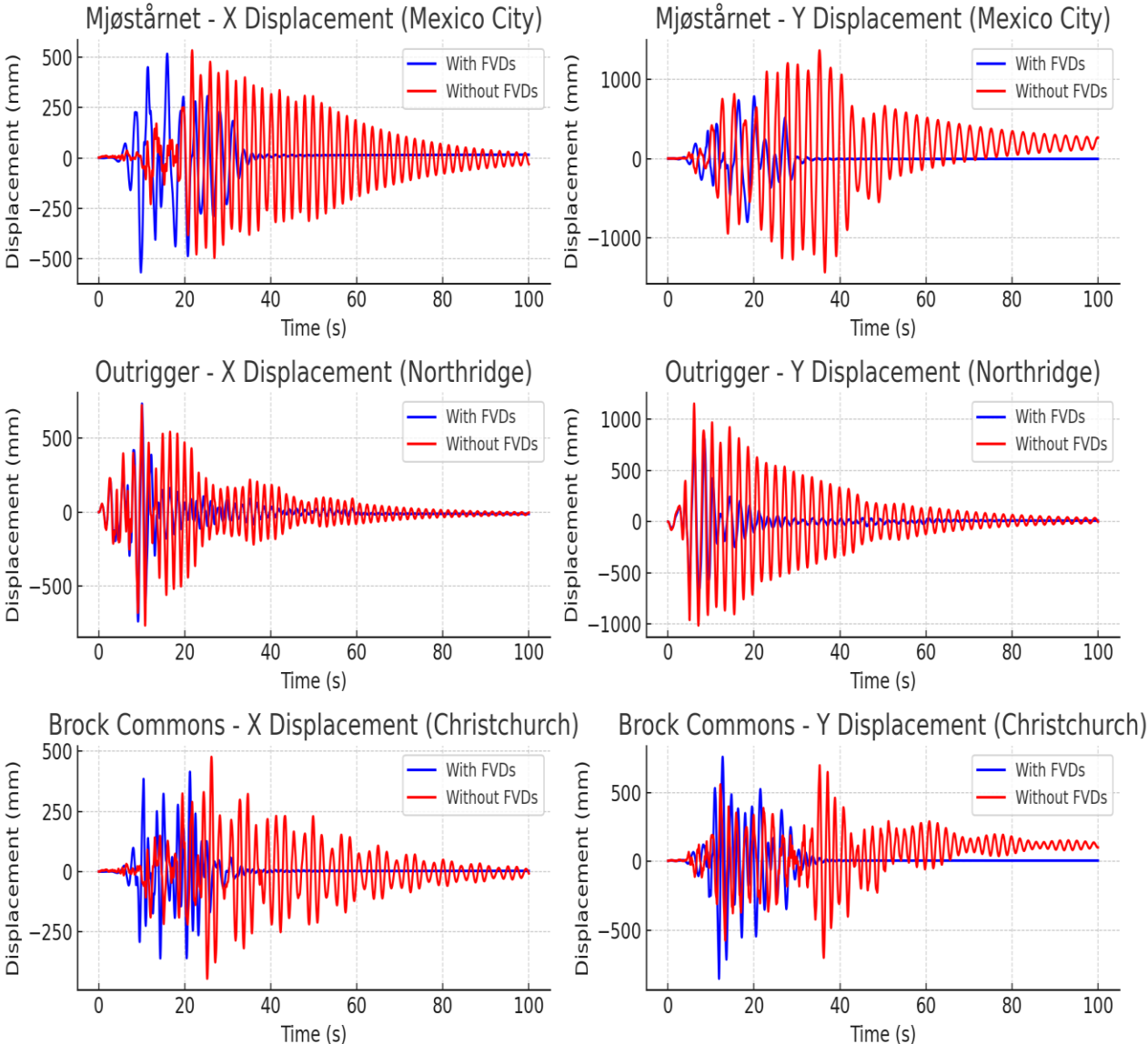


Figure 63 Time History Displacement Responses at Story 18 (With and Without Dampers).

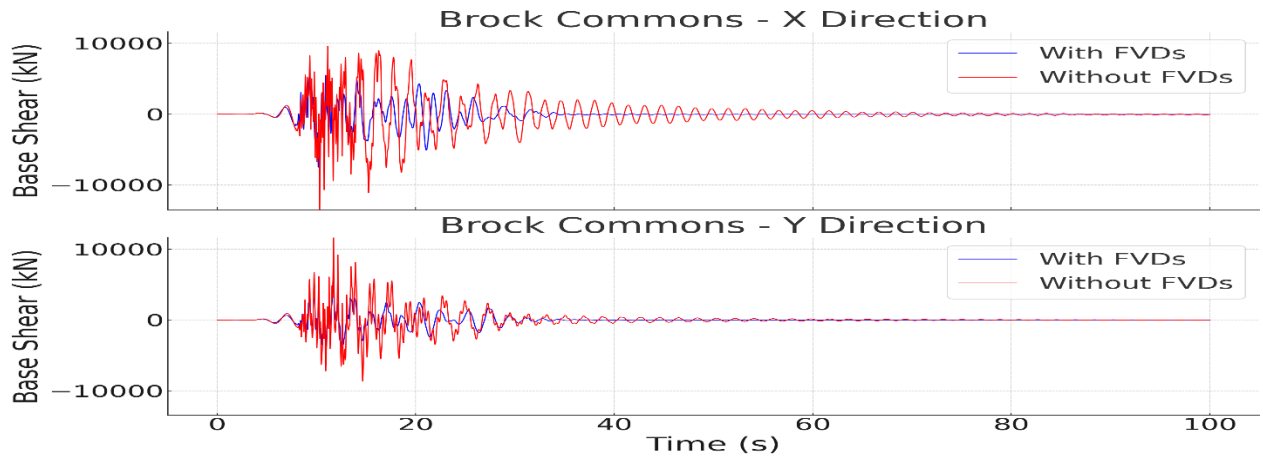


Figure 64 Time History Base Shear Response for Brock Commons Under Christchurch Earthquake.

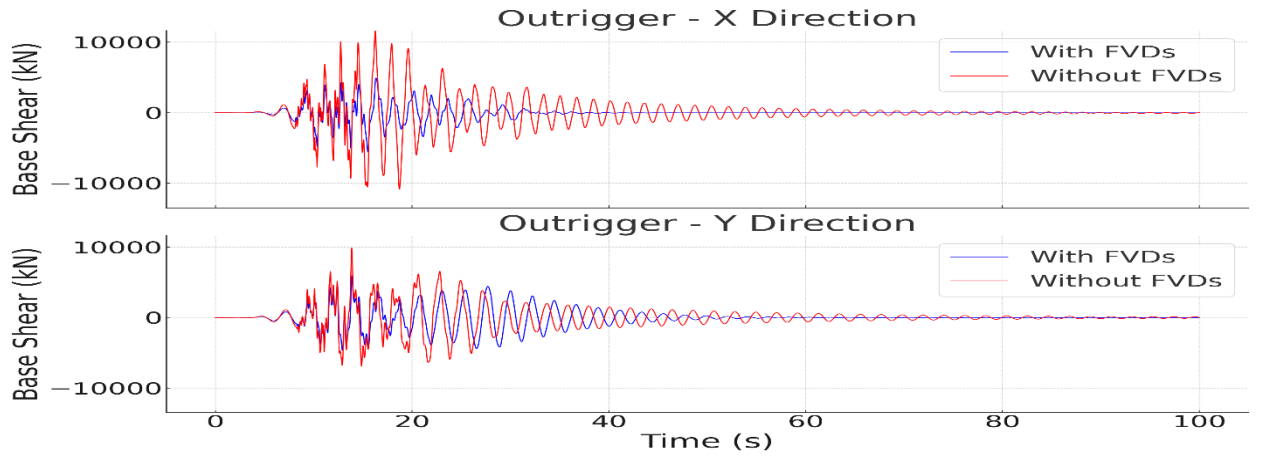


Figure 65 Time History Base Shear Response for the Proposed Outrigger Under Christchurch Earthquake.

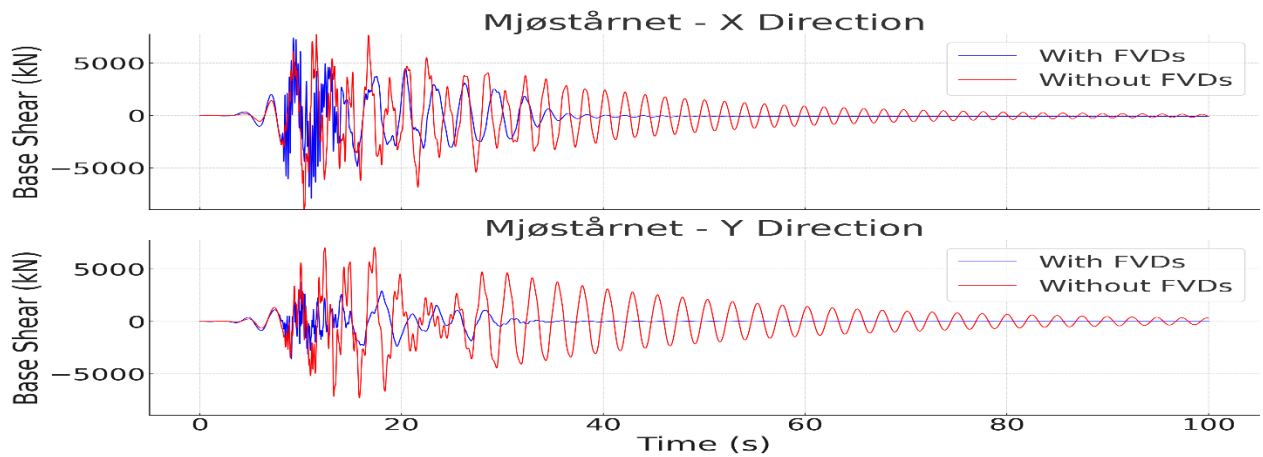


Figure 66 Time History Base Shear Response for Mjøstårnet Under Christchurch Earthquake.

Table 6.4 presents a detailed comparison of the maximum overturning moment responses recorded during the Northridge earthquake, both with and without FVDs. The results clearly highlight the dampers' effectiveness in reducing rotational demands on the structure, thereby improving overall stability and minimizing the risk of structural distress or failure during strong ground motions.

Table 6.4 Maximum Overturning Moments Response With and Without FVDs for Tall Timber Buildings Under Northridge Earthquake in (KN.m x10⁵).

Building	Conventional Building		Building with FVDs	
	M _X	M _Y	M _X	M _Y
Brock Commons	3.44	2.73	2.27	2.52
Outrigger	4.50	4.77	3.60	4.31
Mjøstårnet	3.05	4.26	1.38	1.89

The cumulative energy plots shown in Figures 67, 68, and 69 illustrate the total energy input and dissipation behavior of the three building models—Brock Commons, Outrigger, and the Mjøstårnet building—under seismic loading, based on nonlinear time history analysis using ETABS. These plots provide insight into how each structure dissipates energy through inherent damping, viscous damping, and nonlinear inelastic mechanisms.

The additional viscous damping ratios were estimated by examining the proportion of nonlinear viscous damping relative to the total global damping and scaling it with the assumed inherent damping value. This approach provided approximate values of 12.5% for Brock Commons, 11% for Outrigger, and 10% for the Mjøstårnet building. These results closely match the target damping levels defined during the damper design phase, offering strong confidence that the installed dampers functioned effectively under seismic excitation.

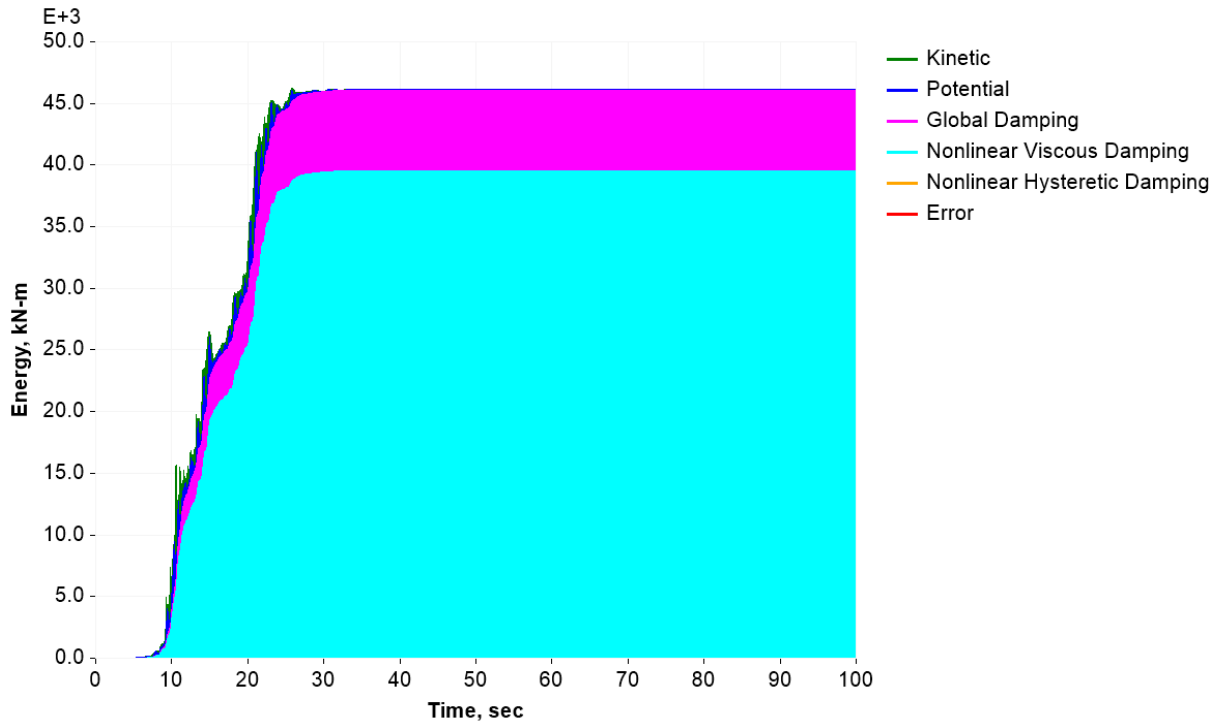


Figure 67 Cumulative Energy Plot for Brock Commons Building Under Christchurch Earthquake.

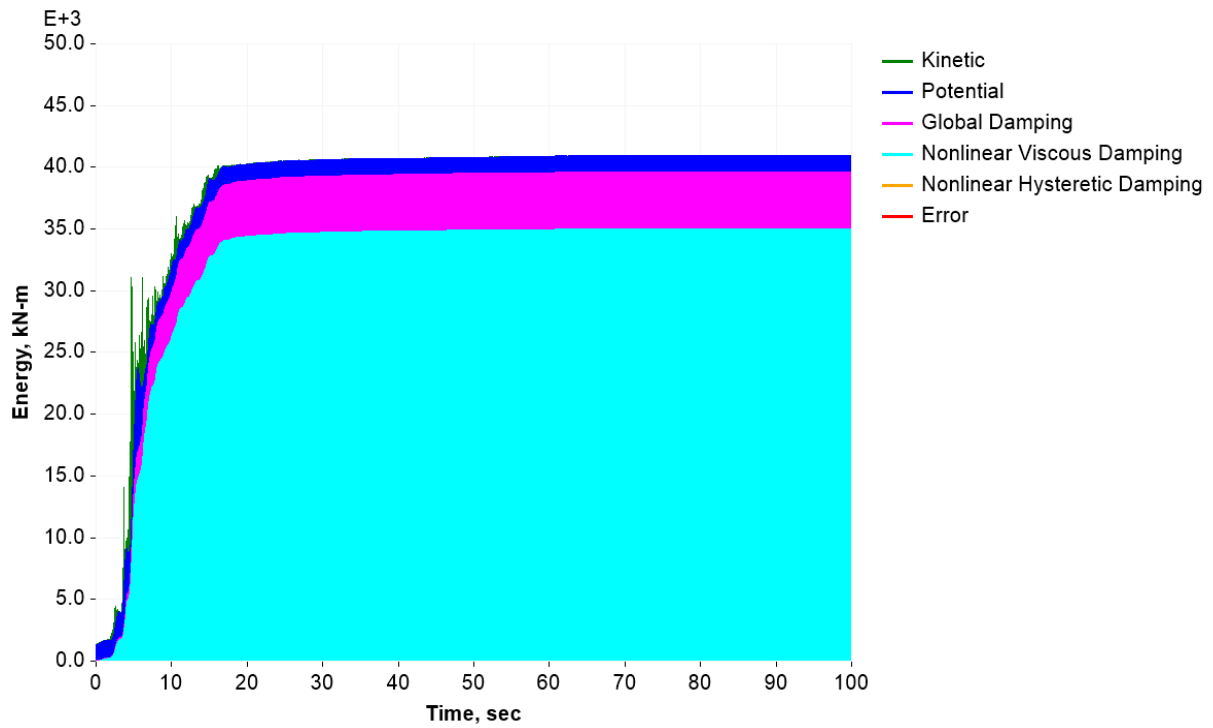


Figure 68 Cumulative Energy Plot for Outrigger Building Under Christchurch Earthquake.

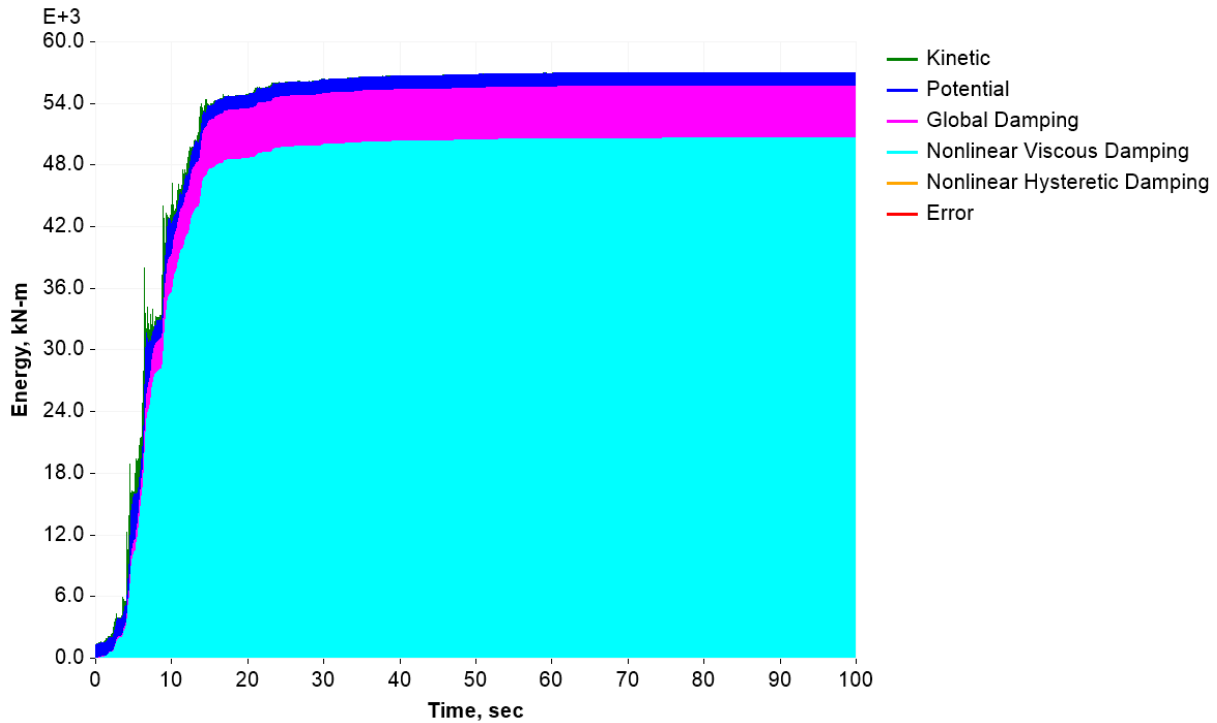


Figure 69 Cumulative Energy Plot for Mjøstårnet Building Under Christchurch Earthquake.

In conclusion, the cumulative energy plots served as an effective validation tool for evaluating the damping performance of the three building models under seismic loading. By comparing the energy dissipation behavior with the predefined damping targets, it was confirmed that the supplemental dampers successfully contributed the intended level of additional damping, reducing seismic demands on key structural components. This verification not only supports the accuracy of the nonlinear modeling approach but also reinforces the effectiveness of the damper design in enhancing overall seismic resilience, damage control, and energy management. Additionally, the plots demonstrated the value of integrating energy-based assessments into advanced performance-based design strategies.

6.3.3 Wind Responses

Fluid viscous dampers (FVDs) were implemented in Mjøstårnet, Brock Commons, and the Outrigger Building to address seismic and wind-induced responses. While seismic applications emphasize the prevention of structural damage under extreme loading, wind design targets occupant comfort by controlling drift ratios and story accelerations. The FVDs in these tall timber structures were carefully calibrated to meet specific acceleration and drift criteria under wind events by taking the damper exponent as 0.5, with wind application considered at a later stage in the seismic design process. The dampers' effectiveness is demonstrated in the hysteretic loops recorded during wind loading (Figures 70, 71, and 72). These loops show how much energy is absorbed and dissipated by the FVDs, thereby restricting lateral and vibrational responses. The alignment of the recorded loops with design expectations confirms that the selected damping coefficients were appropriate.

Maximum drift ratios under wind events for Mjøstårnet, Brock Commons, and the Outrigger Building (Figure 73) remained within acceptable limits, underscoring the importance of added damping in tall timber buildings, which inherently have lower damping than steel or concrete structures. Similarly, occupant comfort was evaluated through story acceleration responses in the X and Y directions (Figures 74–76), all remaining below-specified thresholds. This highlights how precise FVD calibration ensures structural safety and reduced motion for building occupants.

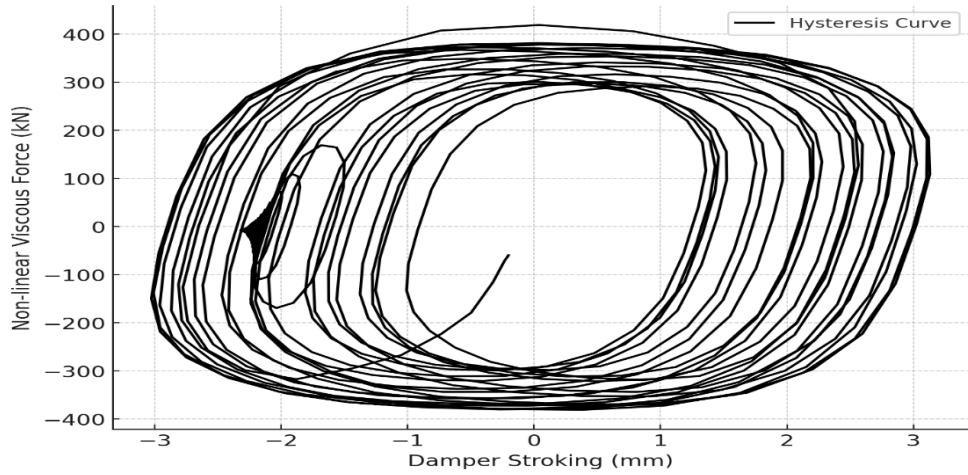


Figure 70 Hysteretic Loop of a Damper in Brock Commons Building under Wind Events.

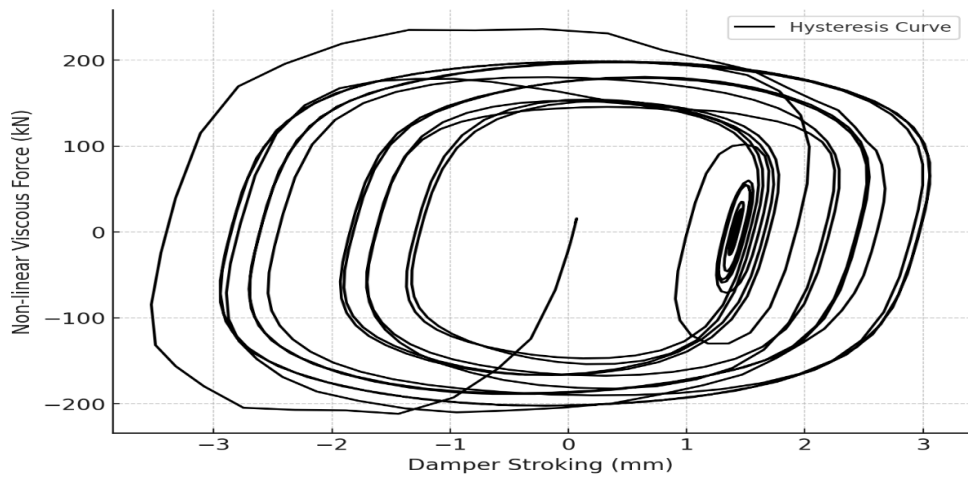


Figure 71 Hysteretic Loop of a Damper in Outrigger Building under Wind Events.

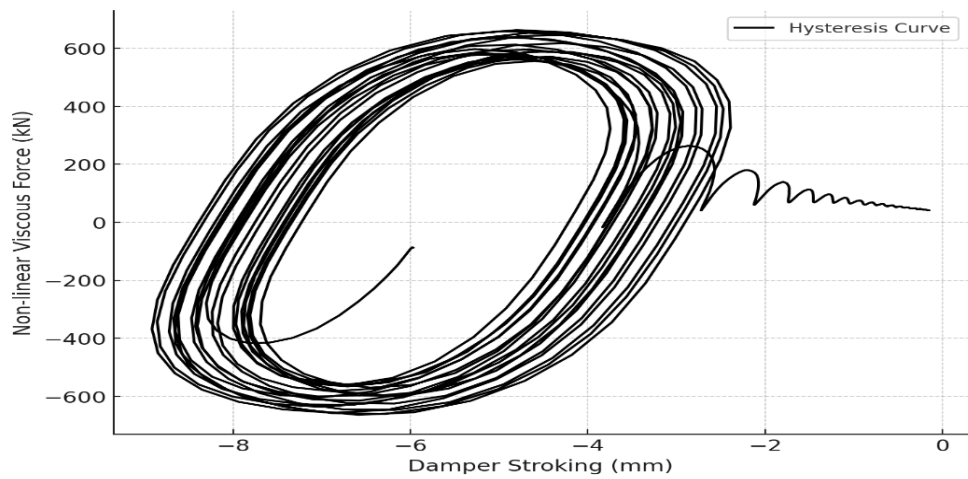


Figure 72 Hysteretic Loop of a Damper in Mjøstårnet Building under Wind Events.

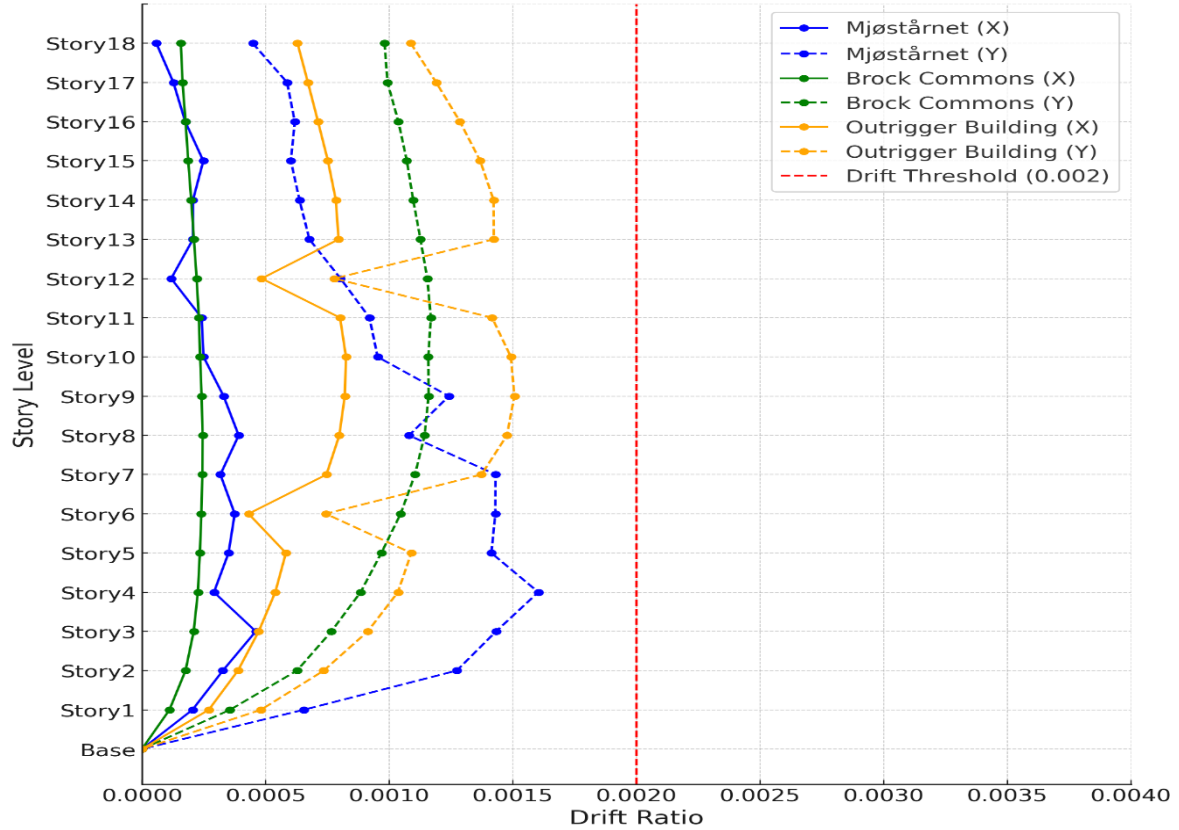


Figure 73 Maximum Drift Ratio for Mjøstårnet, Brock Commons, and Outrigger Building With FVDs Under Dynamic Wind Analysis.

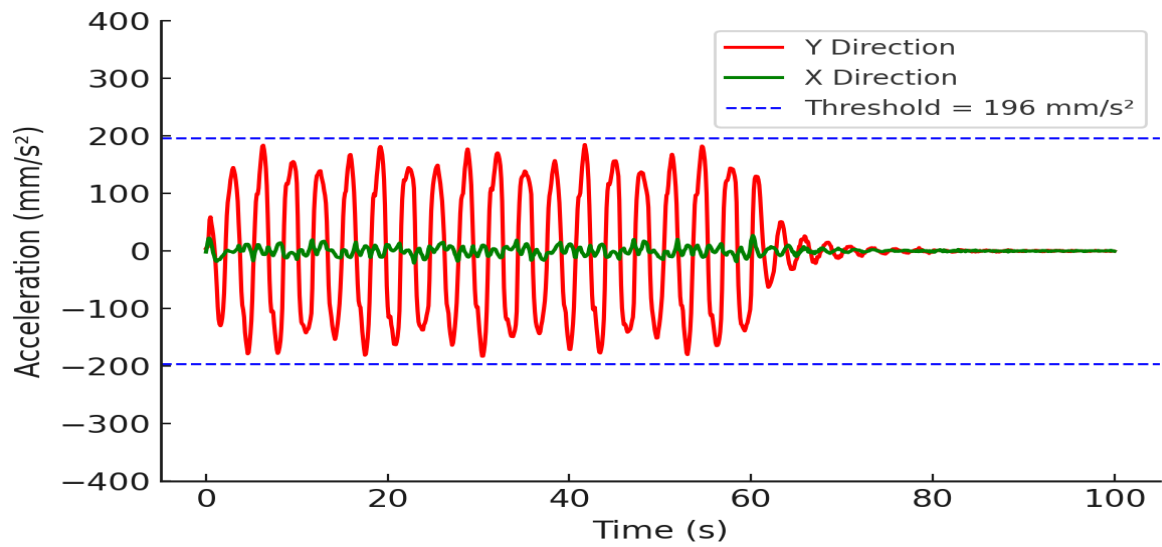


Figure 74 Story Acceleration Response for Mjøstårnet Building With FVDs Under Dynamic Wind Analysis.

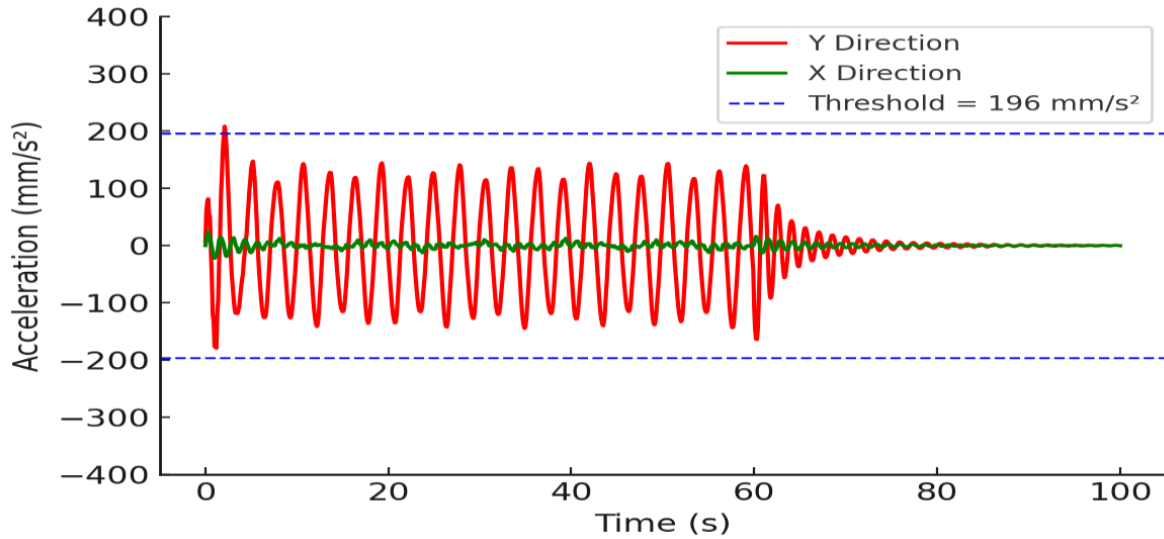


Figure 75 Story Acceleration Response for Brock Commons Building With FVDs Under Dynamic Wind Analysis.

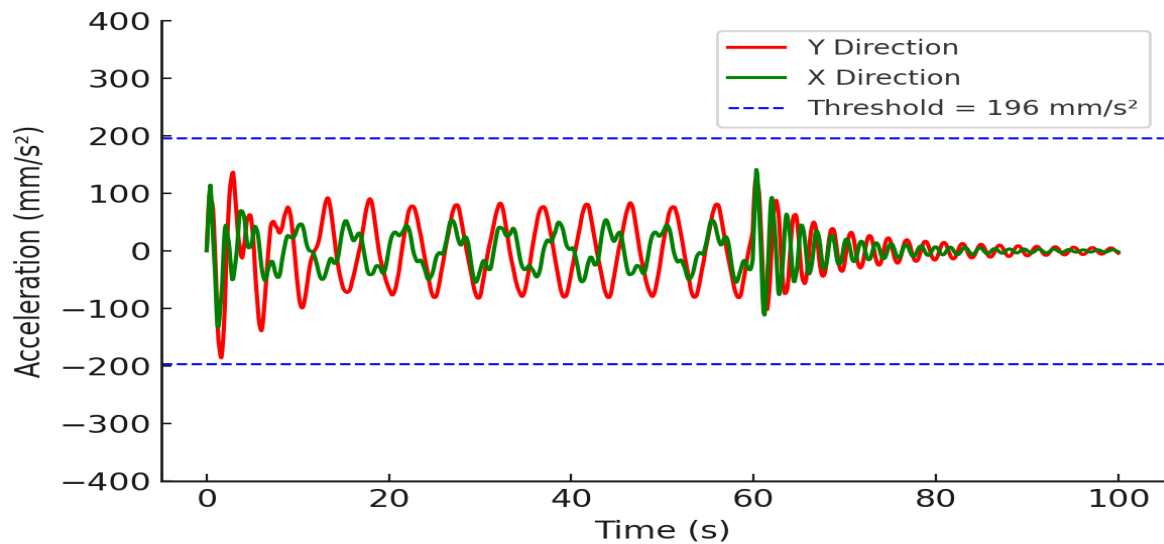


Figure 76 Story Acceleration Response for Outrigger Building With FVDs Under Dynamic Wind Analysis.

In conclusion, FVDs effectively curtail drift ratios and story accelerations under wind conditions in these tall timber buildings, confirming their adaptability for controlling wind responses. By dissipating a substantial portion of wind-induced energy, FVDs enhance occupant comfort and affirm the viability of tall timber construction in areas subject to significant wind loads.

6.4 Practical Considerations

6.4.1 Connections

FVDs in a mega-brace system generate velocity-dependent, nonlinear damping forces that can be decomposed into two components, one horizontal and one vertical as shown in Figure 77. The horizontal force counters the structure's inertial forces, effectively reducing shear demands on primary vertical elements such as columns and walls. Meanwhile, the vertical force acts as an additional gravity load on those same elements.

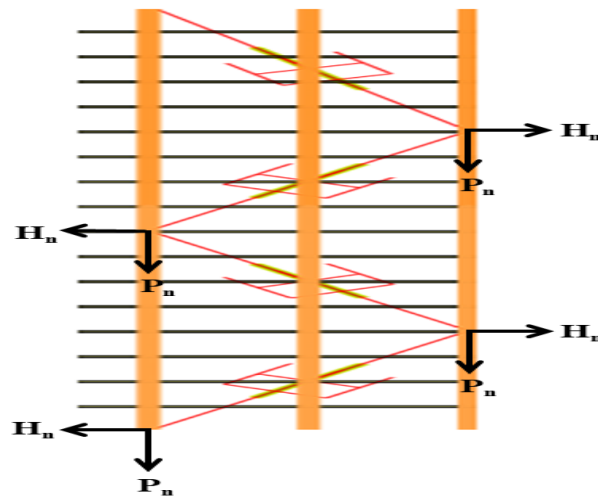


Figure 77 Damper Frame and Its Nonlinear Damping Force Path Mechanism.

When comparing a structure with FVDs to one without, it is clear that the dampers significantly reduce lateral drift and enhance energy dissipation. However, as shown in Figures 78, 79, and 80, these benefits also redistribute internal forces, notably increasing axial loads in lower-floor columns where the dampers are attached. This underscores the importance of re-checking demand/capacity ratios for columns, walls, and foundations to ensure that any newly introduced forces remain within allowable limits. Ultimately, the proper design of the damper frame and its connections is vital. It ensures that the building capitalizes on the substantial damping benefits provided by FVDs without overburdening the critical load-carrying elements.

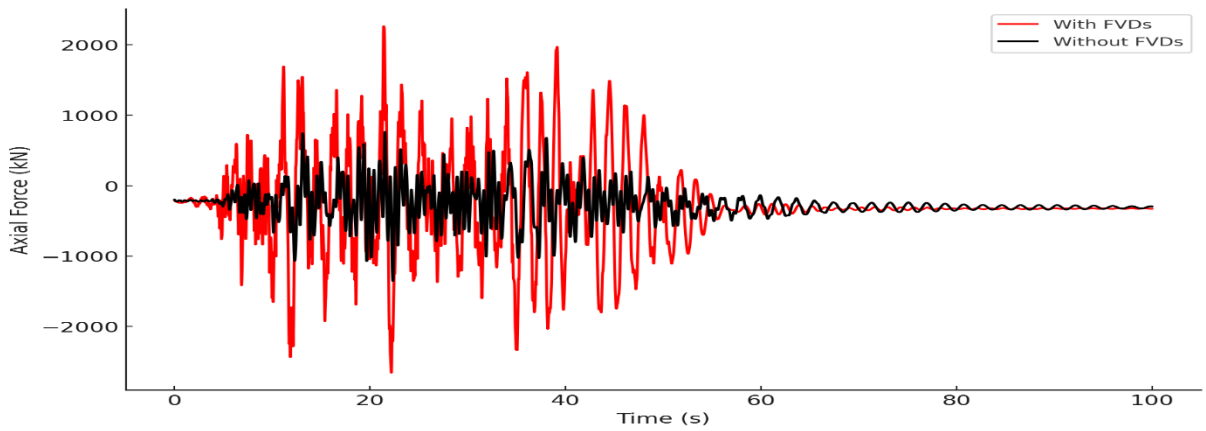


Figure 78 Effect of FVDs on Column Axial Forces for Brock Commons Building under Mexico City Earthquake.

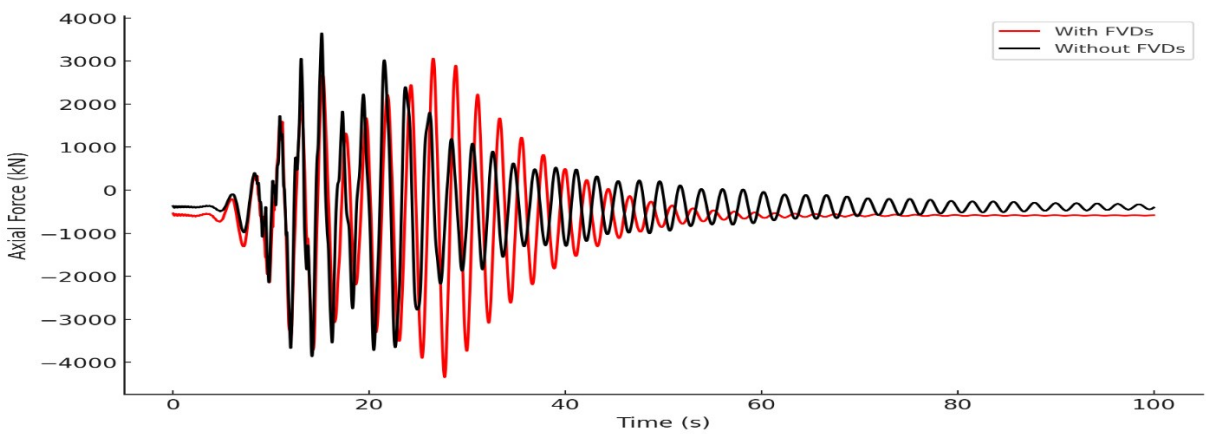


Figure 79 Effect of FVDs on Column Axial Forces for Outrigger Building under Christchurch Earthquake.

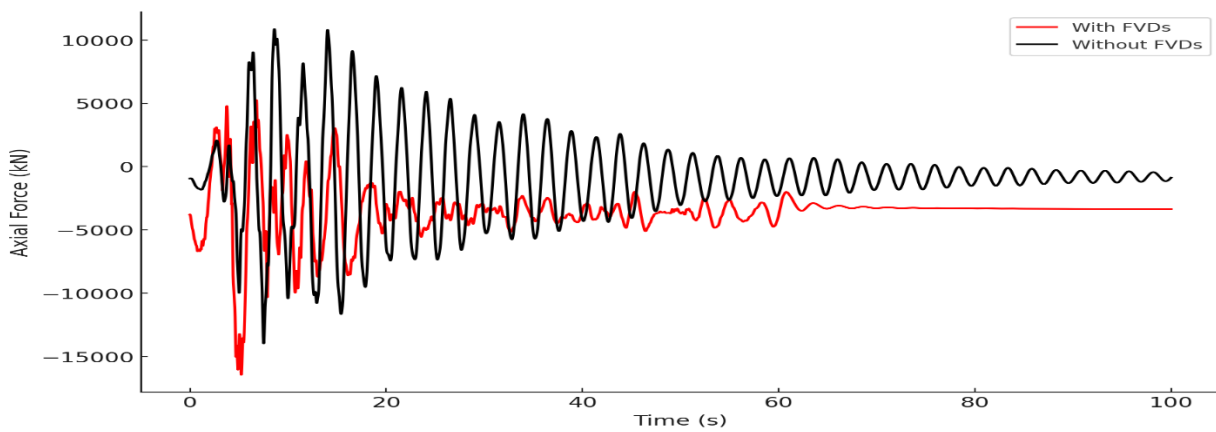


Figure 80 Effect of FVDs on Column Axial Forces for Mjøstårnet Building under Northridge Earthquake.

6.4.2 Availability and Cost

The financial investment required for tall timber buildings and associated damping systems can vary widely based on project scope, regional market conditions, and performance objectives. For instance, Brock Commons Tallwood House at the University of British Columbia, an 18-story student residence, was developed with a total approved project budget of \$51.5 million [105]. Similarly, Mjøstårnet in Brumunddal, Norway—also standing 18 stories tall—incurred a total cost of 450 million NOK, or around CAD 56.7 million, as documented by Moelven and HENT.

This study showed that Mjøstårnet required 30 FVDs, Brock Commons required 46 FVDs, and the Outrigger Building required 32 FVDs to achieve the target performance—an average of roughly 36 dampers. Additionally, this research found that distributing stiffness contributions by designing different sizes and parameters for dampers across the building height could optimize overall structural behaviour. However, each building in this study was designed with a single damper configuration for simplicity. In practice, specific stories could utilize smaller dampers without compromising performance. Accordingly, an average damper price was selected to compare the overall project budgets.

Industry data and case studies suggest that smaller-capacity dampers (for moderate loads) typically range from \$10,000 to \$30,000 (CAD) per unit, while larger-capacity units designed for high-seismic or tall-building applications can exceed \$50,000 (CAD) per unit. In aggregate, damper systems often represent about 1% to 3% of the overall structural costs, though this percentage may rise if numerous dampers or complex framing modifications are required. Worldwide availability of fluid viscous dampers has also grown as specialized manufacturers expand their product offerings, making it increasingly feasible to integrate high-performance damping into modern tall timber construction.

6.5 Sustainability

Fluid Viscous Dampers (FVDs) provide significant sustainability benefits for tall timber buildings, particularly in seismic regions. FVDs help minimize structural damage, extend building lifespans, and reduce material usage by eliminating the need for larger timber sections to resist lateral loads, aligning with sustainability goals by cutting environmental impact. Additionally, FVDs mitigate the need for frequent repairs or demolition, conserving resources and reducing waste. Studies, such as FEMA P-58, recommend an optimal damping level of 25%-45% to address residual drifts that could lead to costly demolitions [106], further enhancing economic and environmental sustainability.

One of the primary sustainability advantages of using FVDs arises from their ability to drastically reduce the embodied energy and carbon emissions associated with conventional lateral load-resisting systems. Table 6.5 presents a comparative analysis of embodied energy and carbon emissions for concrete cores, steel cores, and FVDs, clearly illustrating the significant environmental benefits of FVDs when achieving identical target lateral performance in an 18-story tall timber building.

Table 6.5 Embodied Energy of Structural Systems.

System	Volume (m³)	Mass (tons)	Embodied Energy (MJ)	Carbon Emissions (kg CO₂)
Concrete Core	900	2160	2,376,000	280,800
Steel Core	50	392.5	13,737,500	726,125
FVDs	5.5*	15.5	416,250	30,188

*Estimated average volume based on dampers configuration and numbers.

These data highlight the remarkable efficiency of FVDs in reducing embodied energy and carbon emissions compared to traditional lateral load-resisting systems. Specifically, concrete cores require

approximately 5.7 times more energy and emit roughly 9.3 times more CO₂ compared to FVDs. Steel cores, by comparison, demand about 33 times more energy and produce approximately 24.1 times more CO₂ emissions than FVDs. Furthermore, timber as a renewable material, particularly benefits from FVDs by preserving its structural integrity and leveraging its carbon sequestration properties.

Moreover, the integration of FVDs contributes to broader sustainability objectives through reduced lifecycle environmental impacts. By significantly limiting structural damage, these systems not only reduce embodied energy and emissions during construction but also throughout the building's operational phase. This ensures lower environmental impacts related to ongoing maintenance, repairs, and replacements over the lifespan of the structure. Additionally, since FVDs do not require external energy to function, their operation remains energy-neutral, further reinforcing their sustainability profile.

The durability and reliability of FVDs further enhance their sustainability credentials. Due to their robust construction and minimal maintenance requirements, FVDs provide long-term sustainability benefits by ensuring consistent performance without significant intervention. This reduces the overall ecological footprint associated with building operations and maintenance, aligning closely with modern sustainability targets and resilience objectives.

In conclusion, FVDs serve as a sustainable solution for improving the lateral performance of tall timber buildings, conserving energy, reducing CO₂ emissions, minimizing waste, and enhancing resilience to seismic and wind challenges. Their adoption aligns well with contemporary environmental priorities, contributing meaningfully to sustainable urban development and resilient infrastructure.

7 Conclusion

This thesis undertook a comprehensive approach to investigating the dynamic performance of tall timber buildings by first conducting a thorough literature review that illuminated past challenges and recent developments related to seismic and wind engineering in high-rise timber structures. Through this review, a knowledge base was established regarding the unique material properties of wood and its behavior when subjected to the high lateral forces generated by earthquakes and strong winds. A particular focus was placed on the modelling advancements that have allowed engineers to more accurately predict and assess these structures' responses under dynamic loading conditions. Upon this foundation, numerical models were developed and verified for three representative tall timber buildings: Mjøstårnet, Brock Commons, and a proposed outrigger-based configuration. Each model's structural characteristics and assumptions were meticulously examined to ensure the reliability of subsequent analyses. Verification against known benchmarks helped confirm that the chosen modelling techniques could capture the salient features of real-world timber structures, including their inherent flexibility and relatively lower damping capacity compared to traditional steel or concrete systems.

The analysis phase was instrumental in understanding how these tall timber buildings respond to various loading scenarios. Static and dynamic wind analyses as well as static and dynamic seismic assessments were performed using ground motion records from Northridge, Christchurch, and Mexico City. This comprehensive approach provided a multi-faceted view of each building's performance, allowing for robust evaluations of serviceability, comfort criteria, and structural safety. The results confirmed that modern tall timber buildings offer promising sustainability and material advantages. However, their susceptibility to excessive lateral drifts and accelerations can pose significant challenges in seismic-prone regions or areas subject to intense wind events.

To address these concerns, this thesis explored the strategic use of Fluid Viscous Dampers (FVDs) to mitigate large-amplitude oscillations. FVDs are passive, frequency-independent devices that do not require external power, and they do not contribute additional stiffness to the structural system—therefore, no tuning to a particular frequency is necessary, and the building’s fundamental period remains unchanged. Instead, FVDs rely on velocity-dependent mechanisms to dissipate seismic and wind-induced energy, converting it into heat.

In a typical tall timber building, the inherent damping ratio is often only about 1.5% of critical, but by distributing FVDs over a building’s height, a substantially larger effective damping can be achieved. Consequently, the hysteretic energy is redirected away from the main structural elements, protecting them from localized inelastic deformations and allowing most members to remain elastic. These devices also exhibit reliable, stable performance without regular maintenance and are thus well-suited for long-term deployment in high-rise timber buildings.

The study demonstrated that the integration of FVDs reduces key structural response parameters—particularly drift ratios, story accelerations, base shear, and overturning moments—under strong seismic and wind excitations. This approach offers a modest cost increase of approximately 1–3% of the total project budget, an investment that can avert extensive post-event repairs or demolition if the damage threshold exceeds 40% of the original building cost. Moreover, FVDs can enable more economical designs for shear walls, columns, and foundations by lowering the overall structural demands. As a result, smaller concrete foundations may suffice, reducing reliance on non-sustainable materials and further enhancing the environmental credentials of tall timber construction. Nevertheless, the introduction of FVDs must be accompanied by practical design considerations, particularly in how they redistribute internal forces. Concentrating dampers in lower stories can significantly increase axial loads on columns; thus, demand/capacity ratios for these elements must

be carefully rechecked to ensure the newly introduced forces remain within acceptable limits.

Beyond these structural and cost-related advantages, FVDs also reduce the carbon emissions associated with post-event repairs and facilitate rapid functional recovery by minimizing damage to primary structural components. This resilience supports sustainable urban development by reducing downtime for residents and businesses, thereby enabling continued economic activity even in regions characterized by high seismic or wind risk.

By demonstrating how an 18-story mass-timber structure, equipped with carefully planned damping measures, can meet both comfort and safety standards, this thesis underscores the growing feasibility of tall timber construction as an eco-friendly alternative to conventional steel and concrete high-rises. Overall, this thesis achieved the following:

- Increased the state-of-the-art knowledge on understanding the behavior of tall timber buildings.
- Established the effectiveness of using the NBCC code for the dynamic performance assessment of tall timber buildings.
- Evaluated FVD performance per Taylor Devices guidelines to recommend an optimized response mitigation system for tall timber buildings.

These achievements underline the feasibility of designing and constructing safe, comfortable, and sustainable tall timber buildings in regions susceptible to seismic and wind hazards.

Future Work Recommendations

To further refine the design and analysis of tall timber buildings, the following avenues for future research are proposed:

- Incorporate detailed modelling of timber connections in nonlinear analyses to more accurately capture their energy dissipation capacity and overall deformability under seismic and wind forces.
- Employ an energy-based approach for damper placement rather than relying solely on stiffness-based methods, potentially offering more targeted mitigation of high-demand zones and improved cost-effectiveness.
- Explore the use of viscoelastic dampers, which can reduce structural response amplitudes while providing self-centering capabilities to facilitate quicker post-event recovery.
- Explore comprehensive life-cycle assessment (LCA) analyses to quantify long-term sustainability impacts of FVDs comparisons with other damping systems.

By pursuing these avenues, future research can further enhance the safety, resilience, and sustainability of tall timber buildings, solidifying their role as a viable alternative to conventional high-rise construction methods.

8 References

- [1] R. Verhaegh, M. Vola, and J. de Jong, “Haut - A 21-storey Tall Timber Residential Building,” *International Journal of High-Rise Buildings*, vol. 9, no. 3, pp. 213–220, 2020, doi: 10.21022/IJHRB.2020.9.3.213.
- [2] E. Poirier *et al.*, “Design process innovation on brock commons tallwood house,” *Construction Innovation*, vol. 22, no. 1, pp. 23–40, Jan. 2022, doi: 10.1108/CI-11-2019-0116.
- [3] R. M. Foster, T. P. S. Reynolds, and M. H. Ramage, “Proposal for Defining a Tall Timber Building,” *Journal of Structural Engineering*, vol. 142, no. 12, Dec. 2016, doi: 10.1061/(asce)st.1943-541x.0001615.
- [4] S. Krötsch and L. Müller, “1. The development of multistorey timber construction,” in *Manual of Multistorey Timber Construction*, DETAIL, 2018, pp. 10–13. doi: 10.11129/9783955533953-002.
- [5] B. T. Teweldebrhan and S. Tesfamariam, “Performance-based design of tall-coupled cross-laminated timber wall building,” *Earthq Eng Struct Dyn*, vol. 51, no. 7, pp. 1677–1696, Jun. 2022, doi: 10.1002/eqe.3633.
- [6] S. Tesfamariam, “Performance-Based Design of Tall Timber Buildings Under Earthquake and Wind Multi-Hazard Loads: Past, Present, and Future,” *Front Built Environ*, vol. 8, Mar. 2022, doi: 10.3389/fbuil.2022.848698.
- [7] W. H. Baiz and E. Hoskara, “Developing a measurement scale for sustainable high-rise building in city of Erbil,” *Journal of Asian Architecture and Building Engineering*, vol. 21, no. 3, pp. 717–734, May 2022, doi: 10.1080/13467581.2021.1900855.
- [8] Daniel Safarik, Jacob Elbrecht, and William Miranda, “CTBUH - State of Tall Timber 2022,” *CTBUH Journal*, 2022.
- [9] Z. Chen and Y.-H. Chui, “Lateral Load-Resisting System Using Mass Timber Panel for High-Rise Buildings,” *Front Built Environ*, vol. 3, Jul. 2017, doi: 10.3389/fbuil.2017.00040.
- [10] S. Staub-French *et al.*, “Construction process innovation on Brock Commons Tallwood House,” *Construction Innovation*, vol. 22, no. 1, pp. 1–22, Jan. 2022, doi: 10.1108/CI-11-2019-0117.
- [11] A. Fernandez, J. Komp, and J. Peronto, “Ascent - Challenges and Advances of Tall Mass Timber Construction,” *International Journal of High-Rise Buildings*, vol. 9, no. 3, pp. 235–244, 2020, doi: 10.21022/IJHRB.2020.9.3.235.
- [12] R. Abrahamsen, “Mjøstårnet-Construction of an 81 m tall timber building,” 2017.
- [13] K. V. Sharma, V. Parmar, L. Gautam, S. Choudhary, and J. Gohil, “Modelling efficiency of fluid viscous dampers positioning for increasing tall buildings’ Resilience to earthquakes induced structural vibrations,” *Soil Dynamics and Earthquake Engineering*, vol. 173, p. 108108, Oct. 2023, doi: 10.1016/j.soildyn.2023.108108.

- [14] H. E. Ilgin, “High-Rise Residential Timber Buildings: Emerging Architectural and Structural Design Trends,” *Buildings*, vol. 14, no. 1, Jan. 2024, doi: 10.3390/buildings14010025.
- [15] T. Reynolds, W. Chang, and R. Harris, “Dynamic Response of Tall Timber Buildings to Wind Load,” 2011.
- [16] A. Bukauskas *et al.*, “Whole timber construction: A state of the art review,” *Constr Build Mater*, vol. 213, pp. 748–769, Jul. 2019, doi: 10.1016/j.conbuildmat.2019.03.043.
- [17] F. Arriaga, X. Wang, G. Íñiguez-González, D. F. Llana, M. Esteban, and P. Niemz, “Mechanical Properties of Wood: A Review,” *Forests*, vol. 14, no. 6, p. 1202, Jun. 2023, doi: 10.3390/f14061202.
- [18] F. Dubois, J. Dopeux, O. Pop, and M. Metrope, “Long-term creep behavior of timber columns: Experimental and numerical protocols,” *Eng Struct*, vol. 275, p. 115283, Jan. 2023, doi: 10.1016/j.engstruct.2022.115283.
- [19] B. Zhang, C. Othmani, and F. Takali, “Comparison and parametric study of characteristics of eleven types of anisotropic woods based on the behaviour of Lamb wave propagation,” *Acta Mech*, 2024, doi: 10.1007/s00707-024-04141-4.
- [20] DF Haasbroek and L. Pretorius, “Orthotropic failure criterion for timber,” *R&D JOURNAL*, vol. 10, Jan. 1994.
- [21] G.-G. Wang, X. Zhang, Z.-Z. Gao, Y.-L. Wang, C. Yu, and Z. Wang, “Dynamic testing and analysis of Poisson’s ratio constants of timber,” in *Mechanics and Architectural Design*, WORLD SCIENTIFIC, Feb. 2017, pp. 9–18. doi: 10.1142/9789813149021_0002.
- [22] Z. Gao, X. Zhang, Y. Wang, R. Yang, G. Wang, and Z. Wang, “Measurement of the Poisson’s ratio of materials based on the bending mode of the cantilever plate,” *Bioresources*, vol. 11, no. 3, pp. 5703–5721, 2016, doi: 10.15376/biores.11.3.5703-5721.
- [23] A. Olsson and B. Källsner, “Shear modulus of structural timber evaluated by means of dynamic excitation and FE analysis,” *Materials and Structures/Materiaux et Constructions*, vol. 48, no. 4, pp. 977–985, 2015, doi: 10.1617/s11527-013-0208-0.
- [24] J. P. Cabral, B. Kafle, M. Subhani, J. Reiner, and M. Ashraf, “Densification of timber: a review on the process, material properties, and application,” Dec. 01, 2022, *Springer*. doi: 10.1186/s10086-022-02028-3.
- [25] V. Ermakov and E. Stepanova, “Moisture content and its influence on glued timber structures,” *IOP Conf Ser Mater Sci Eng*, vol. 869, no. 5, p. 052015, Jun. 2020, doi: 10.1088/1757-899X/869/5/052015.
- [26] E. Sharapov, C. Brischke, H. Miltitz, and E. Smirnova, “Prediction of modulus of elasticity in static bending and density of wood at different moisture contents and feed rates by drilling resistance measurements,” *European Journal of Wood and Wood Products*, vol. 77, no. 5, pp. 833–842, Sep. 2019, doi: 10.1007/s00107-019-01439.
- [27] O. V. Startsev, A. Makhonkov, V. Erofeev, and S. Gudojnikov, “Impact of moisture content on dynamic mechanical properties and transition temperatures of wood,” *Wood Mater Sci Eng*, vol. 12, no. 1, pp. 55–62, Jan. 2017, doi: 10.1080/17480272.2015.1020566.

- [28] D. Sandberg, A. Kutnar, and G. Mantanis, “Wood modification technologies - a review,” *IForest*, vol. 10, no. 6, pp. 895–908, Dec. 2017, doi: 10.3832/ifor2380-010.
- [29] M. Premrov and V. Žegarac Leskovar, “Innovative Structural Systems for Timber Buildings: A Comprehensive Review of Contemporary Solutions,” Jul. 01, 2023, *Multidisciplinary Digital Publishing Institute (MDPI)*. doi: 10.3390/buildings13071820.
- [30] J. Mohammadi and L. Ling, “Can Wood Become an Alternative Material for Tall Building Construction?,” *Practice Periodical on Structural Design and Construction*, vol. 22, no. 4, Nov. 2017, doi: 10.1061/(asce)sc.1943-5576.0000334.
- [31] R. Gupta and T. Siller, “Stress distribution in structural composite lumber under torsion,” *For Prod J*, vol. 55(2), pp. 51–56, 2005.
- [32] F. Lam and B. A. Craig, “Shear strength in structural composite lumber,” *Journal of Materials in Civil Engineering*, 2000.
- [33] J. Cover, “Mass timber: The new sustainable choice for tall buildings,” *International Journal of High-Rise Buildings*, vol. 9, no. 1, pp. 87–93, Mar. 2020, doi: 10.21022/IJHRB.2020.9.1.87.
- [34] V. De Araujo *et al.*, “Is Cross-Laminated Timber (CLT) a Wood Panel, a Building, or a Construction System? A Systematic Review on Its Functions, Characteristics, Performances, and Applications,” 2023, doi: 10.3390/10.3390/f14020264.
- [35] R. Brandner, G. Flatscher, A. Ringhofer, G. Schickhofer, and A. Thiel, “Cross laminated timber (CLT): overview and development,” *European Journal of Wood and Wood Products*, vol. 74, no. 3, pp. 331–351, May 2016, doi: 10.1007/s00107-015-0999-5.
- [36] B. D’Amico, F. Pomponi, and J. Hart, “Global potential for material substitution in building construction: The case of cross laminated timber,” *J Clean Prod*, vol. 279, Jan. 2021, doi: 10.1016/j.jclepro.2020.123487.
- [37] A. Younis and A. Dodoo, “Cross-laminated timber for building construction: A life-cycle-assessment overview,” Jul. 15, 2022, *Elsevier Ltd*. doi: 10.1016/j.jobe.2022.104482.
- [38] Z. Li and K. D. Tsavdaridis, “Design for Seismic Resilient Cross Laminated Timber (CLT) Structures: A Review of Research, Novel Connections, Challenges and Opportunities,” *Buildings*, vol. 13, no. 2, p. 505, Feb. 2023, doi: 10.3390/buildings13020505.
- [39] P. Wei, B. J. Wang, H. Li, L. Wang, S. Peng, and L. Zhang, “A comparative study of compression behaviors of cross-laminated timber and glued-laminated timber columns,” *Constr Build Mater*, vol. 222, pp. 86–95, Oct. 2019, doi: 10.1016/j.conbuildmat.2019.06.139.
- [40] L. Tupénaitė *et al.*, “MULTIPLE CRITERIA ASSESSMENT OF HIGH-RISE TIMBER BUILDINGS,” *Engineering Structures and Technologies*, vol. 11, no. 3, pp. 87–94, Feb. 2020, doi: 10.3846/est.2019.11952.
- [41] J. Zhou, C. Li, L. Ke, J. He, and Z. Wang, “Experimental Study on Loading Capacity of Glued-Laminated Timber Arches Subjected to Vertical Concentrated Loads,” *Advances in Civil Engineering*, vol. 2020, no. 1, Jan. 2020, doi: 10.1155/2020/7987414.

- [42] R. Fahrni, M. Klippel, A. Just, A. Ollino, and A. Frangi, “Fire tests on glued-laminated timber beams with specific local material properties,” *Fire Saf J*, vol. 107, pp. 161–169, Jul. 2019, doi: 10.1016/j.firesaf.2017.11.003.
- [43] T. Wang, Y. Wang, R. Crocetti, L. Franco, M. Schweigler, and M. Wälinder, “An innovative timber-steel hybrid beam consisting of glulam mechanically reinforced by means of steel rod: Analytical and preliminary numerical investigations,” *Journal of Building Engineering*, vol. 43, p. 102549, Nov. 2021, doi: 10.1016/j.job.2021.102549.
- [44] M. F. Sepahvand, J. Akbari, and K. Kusunoki, “Plastic design of moment resisting frames using mechanism control,” *J Constr Steel Res*, vol. 153, pp. 275–285, Feb. 2019, doi: 10.1016/j.jcsr.2018.10.015.
- [45] S. Tulebekova, K. A. Malo, A. Rønquist, and P. Nåvik, “Modeling stiffness of connections and non-structural elements for dynamic response of taller glulam timber frame buildings,” *Eng Struct*, vol. 261, Jun. 2022, doi: 10.1016/j.engstruct.2022.114209.
- [46] P. Desai, V. Katti, and A. V. Katti, “Bracings as Lateral Load Resisting Structural System,” *International Research Journal of Engineering and Technology*, 2017, [Online]. Available: www.irjet.net
- [47] D. D. Ahiwale, D. P. N. Kontoni, and P. L. Darekar, “Seismic performance assessment of reinforced concrete frames with different bracing systems,” *Innovative Infrastructure Solutions*, vol. 8, no. 3, Mar. 2023, doi: 10.1007/s41062-023-01071-3.
- [48] C. F. Gilbert and J. Erochko, “Development and testing of hybrid timber-steel braced frames,” *Eng Struct*, vol. 198, p. 109495, Nov. 2019, doi: 10.1016/j.engstruct.2019.109495.
- [49] E. S. Firoozabad, K. Rama, M. Rao, and B. Bagheri, “Effect of Shear Wall Configuration on Seismic Performance of Building,” 2012.
- [50] T. A. Ozkul, A. Kurtbeyoglu, M. Borekci, B. Zengin, and A. Kocak, “Effect of shear wall on seismic performance of RC frame buildings,” *Eng Fail Anal*, vol. 100, pp. 60–75, Jun. 2019, doi: 10.1016/j.engfailanal.2019.02.032.
- [51] D. A. N. V. Kumar, “Seismic Performance of a Reinforced Concrete Multi-Storey Building Having Circular Shear Wall and Square Shear Wall at Core of the Building,” *International Journal of Civil Engineering and Technology (IJCIET)*, vol. 8, no. 3, pp. 928–941, 2017.
- [52] K. S. Ahmed, M. Kawsher, R. Ahmed, R. Sabrin, S. Z. Sarothi, and A. Farzana, “A Displacement Based Design Approach For Seismic Assessment of Flat Slab Structure With Core Shear Wall,” in *Proceedings of the 7th World Congress on Civil, Structural, and Environmental Engineering*, Avestia Publishing, Apr. 2022. doi: 10.11159/icsect22.125.
- [53] T. Y. Yang, S. Lepine-Lacroix, J. A. R. Guerrero, J. B. W. McFadden, and M. A. Q. Al-Janabi, “Seismic performance evaluation of innovative balloon type CLT rocking shear walls,” *Resilient Cities and Structures*, vol. 1, no. 1, pp. 44–52, Mar. 2022, doi: 10.1016/j.rcns.2022.03.004.

- [54] O. A. Hegeir and H. Stamatopoulos, “Feasibility of outrigger structural system for tall timber buildings: A numerical study,” *International Wood Products Journal*, vol. 15, no. 1, pp. 20–38, Mar. 2024, doi: 10.1177/20426445231216013.
- [55] M. A. Bezabeh, G. T. Bitsuamlak, M. Popovski, and S. Tesfamariam, “Dynamic Response of Tall Mass-Timber Buildings to Wind Excitation,” *Journal of Structural Engineering*, vol. 146, no. 10, Oct. 2020, doi: 10.1061/(asce)st.1943-541x.0002746.
- [56] NBC 2020, “2020 National Building Code of Canada Seismic Hazard Tool,” 2020.
- [57] D Boggs and CP Petersen, “Acceleration indexes for human comfort in tall buildings—Peak or RMS,” *CTBUH*, 1997.
- [58] R. B. Denoon and K. T. Strobel, “Practical Considerations in the Assessment of Building Motion Acceptability,” 2012.
- [59] C. P. D. Amoussou, H. Lei, Y. Halabi, and W. Alhaddad, “Performance-based seismic design methodology for tall buildings with outrigger and ladder systems,” *Structures*, vol. 34, pp. 2288–2307, Dec. 2021, doi: 10.1016/j.istruc.2021.08.078.
- [60] M. Kolaj, J. Adams, and S. Halchuk, “The 6th generation seismic hazard model of Canada,” The 17th World Conference on Earthquake Engineering, 2020, pp. 1–12.
- [61] A. K. Chopra, “DYNAMICS OF STRUCTURES Theory and Applications to Earthquake Engineering Fifth Edition in SI Units.”
- [62] X. Jiao, Y. Zhao, and W. Ma, “Nonlinear dynamic characteristics of a micro-vibration fluid viscous damper,” *Nonlinear Dyn*, vol. 92, no. 3, pp. 1167–1184, May 2018, doi: 10.1007/s11071-018-4116-2.
- [63] D. P. Taylor, “BUILDINGS: DESIGN FOR DAMPING,” 1999.
- [64] S. C. Auclair, C. Dagenais, and G. Bitsuamlak, “LONG-TERM MONITORING OF TALL MASS TIMBER BUILDINGS - EVALUATION OF DYNAMICS PROPERTIES,” in *13th World Conference on Timber Engineering, WCTE 2023*, World Conference on Timber Engineering (WCTE), 2023, pp. 2922–2929. doi: 10.52202/069179-0382.
- [65] T. Kijewski-Correa and J. D. Pirnia, “Dynamic behavior of tall buildings under wind: insights from full-scale monitoring,” *The Structural Design of Tall and Special Buildings*, vol. 16, no. 4, pp. 471–486, Dec. 2007, doi: 10.1002/tal.415.
- [66] Z. Chen and M. Popovski, “Seismic Response of Braced Heavy Timber Frames with Riveted Connections,” *Journal of Performance of Constructed Facilities*, vol. 35, no. 5, Oct. 2021, doi: 10.1061/(ASCE)CF.1943-5509.0001618.
- [67] C. Molina Hutt, I. Almufti, M. Willford, and G. Deierlein, “Seismic Loss and Downtime Assessment of Existing Tall Steel-Framed Buildings and Strategies for Increased Resilience,” *Journal of Structural Engineering*, vol. 142, no. 8, Aug. 2016, doi: 10.1061/(ASCE)ST.1943-541X.0001314.
- [68] S. Mahin, J. W. Lai, S. Wang, and M. Schoettler, “Evaluating and improving the seismic performance of older tall buildings,” in *Proceedings of the Second International Conference on Performance-based*

- and Life-cycle Structural Engineering (PLSE 2015)*, School of Civil Engineering, The University of Queensland, Jan. 2015, pp. 25–37. doi: 10.14264/uql.2016.1098.
- [69] Y. H. Chai and Y. Chen, “Reexamination of the Vibrational Period of Coupled Shear Walls by Differential Transformation,” *Journal of Structural Engineering*, vol. 135, no. 11, pp. 1330–1339, Nov. 2009, doi: 10.1061/(ASCE)ST.1943-541X.0000059.
- [70] P. R. Mukherjee and A. Coull, “Free vibrations of coupled shear walls,” *Earthq Eng Struct Dyn*, vol. 1, no. 4, pp. 377–386, Jan. 1972, doi: 10.1002/eqe.4290010408.
- [71] O. Lavan, “On the efficiency of viscous dampers in reducing various seismic responses of wall structures,” *Earthq Eng Struct Dyn*, vol. 41, no. 12, pp. 1673–1692, Oct. 2012, doi: 10.1002/eqe.1197.
- [72] Y. Liu, J. Wu, and M. Donà, “Effectiveness of fluid-viscous dampers for improved seismic performance of inter-storey isolated buildings,” *Eng Struct*, vol. 169, pp. 276–292, Aug. 2018, doi: 10.1016/j.engstruct.2018.05.031.
- [73] S. Moradpour and M. Dehestani, “Optimal DDBD procedure for designing steel structures with nonlinear fluid viscous dampers,” *Structures*, vol. 22, pp. 154–174, Dec. 2019, doi: 10.1016/j.istruc.2019.08.005.
- [74] R. Greco, J. Avakian, and G. C. Marano, “A comparative study on parameter identification of fluid viscous dampers with different models,” *Archive of Applied Mechanics*, vol. 84, no. 8, pp. 1117–1134, Aug. 2014, doi: 10.1007/s00419-014-0869-3.
- [75] S. Tesfamariam, K. Skandalos, K. Goda, M. A. Bezabeh, G. Bitsuamlak, and M. Popovski, “Quantifying the Ductility-Related Force Modification Factor for 10-Story Timber–RC Hybrid Building Using FEMA P695 Procedure and Considering the 2015 NBC Seismic Hazard,” *Journal of Structural Engineering*, vol. 147, no. 5, May 2021, doi: 10.1061/(ASCE)ST.1943-541X.0003007.
- [76] B. F. Spencer and S. Nagarajaiah, “State of the Art of Structural Control,” *Journal of Structural Engineering*, vol. 129, no. 7, pp. 845–856, Jul. 2003, doi: 10.1061/(ASCE)0733-9445(2003)129:7(845).
- [77] R. Smith, R. Merello, and M. Willford, “Intrinsic and supplementary damping in tall buildings,” *Proceedings of the Institution of Civil Engineers - Structures and Buildings*, vol. 163, no. 2, pp. 111–118, Apr. 2010, doi: 10.1680/stbu.2010.163.2.111.
- [78] A. Ghobarah, “Performance-based design in earthquake engineering: state of development,” *Eng Struct*, vol. 23, no. 8, pp. 878–884, Aug. 2001, doi: 10.1016/S0141-0296(01)00036-0.
- [79] Federal Emergency Management Agency (FEMA274), “NEHRP Commentary on the Guidelines for the Seismic Rehabilitation of Buildings,” Federal Emergency Management Agency, Washington, D.C., 1997.
- [80] C. Christopoulos, R. Tremblay, H.-J. Kim, and M. Lacerte, “Self-Centering Energy Dissipative Bracing System for the Seismic Resistance of Structures: Development and Validation,” *Journal of Structural Engineering*, vol. 134, no. 1, pp. 96–107, Jan. 2008, doi: 10.1061/(ASCE)0733-9445(2008)134:1(96).

- [81] A. V. Bhaskararao and R. S. Jangid, "Seismic analysis of structures connected with friction dampers," *Eng Struct*, vol. 28, no. 5, pp. 690–703, Apr. 2006, doi: 10.1016/j.engstruct.2005.09.020.
- [82] F. Y. Cheng, *Smart structures: innovative systems for seismic response control*. CRC Press, 2008. doi: 10.1201/9781420008173.
- [83] T. T. Soong and B. F. Spencer, "Supplemental energy dissipation: state-of-the-art and state-of-the-practice," 2002. [Online]. Available: www.elsevier.com/locate/engstruct
- [84] N. E. Canney, K. B. Eriksen, and A. T. Tiapon, "A review of the state of practice for fluid viscous damper applications in North America and New Zealand," NZSEE 2023 Annual Conference, 2023.
- [85] S. Wang and S. A. Mahin, "High-performance computer-aided optimization of viscous dampers for improving the seismic performance of a tall building," *Soil Dynamics and Earthquake Engineering*, vol. 113, pp. 454–461, Oct. 2018, doi: 10.1016/j.soildyn.2018.06.008.
- [86] M. Di Paola and G. Navarra, "Stochastic seismic analysis of mdof structures with nonlinear viscous dampers," *Struct Control Health Monit*, vol. 16, no. 3, pp. 303–318, Apr. 2009, doi: 10.1002/stc.254.
- [87] D. I. Narkhede and R. Sinha, "Behavior of nonlinear fluid viscous dampers for control of shock vibrations," *J Sound Vib*, vol. 333, no. 1, pp. 80–98, Jan. 2014, doi: 10.1016/j.jsv.2013.08.041.
- [88] M. Martinez-Rodrigo and M. L. Romero, "An optimum retrofit strategy for moment resisting frames with nonlinear viscous dampers for seismic applications," *Eng Struct*, vol. 25, no. 7, pp. 913–925, Jun. 2003, doi: 10.1016/S0141-0296(03)00025-7.
- [89] M. C. Constantinou, T. T. Soong, and G. F. Dargush, "Passive Energy Dissipation Systems for Structural Design and Retrofit Monograph Series," 1998.
- [90] S. Sorace and G. Terenzi, "Seismic Protection of Frame Structures by Fluid Viscous Damped Braces," *Journal of Structural Engineering*, vol. 134, no. 1, pp. 45–55, Jan. 2008, doi: 10.1061/(ASCE)0733-9445(2008)134:1(45).
- [91] D. De Domenico and G. Ricciardi, "Improved stochastic linearization technique for structures with nonlinear viscous dampers," *Soil Dynamics and Earthquake Engineering*, vol. 113, pp. 415–419, Oct. 2018, doi: 10.1016/j.soildyn.2018.06.015.
- [92] D. De Domenico and G. Ricciardi, "Earthquake protection of structures with nonlinear viscous dampers optimized through an energy-based stochastic approach," *Eng Struct*, vol. 179, pp. 523–539, Jan. 2019, doi: 10.1016/j.engstruct.2018.09.076.
- [93] S. Wang, "Enhancing Seismic Performance of Tall Buildings by Optimal Design of Supplemental Energy-Dissipation Devices."
- [94] X. He, Y. Yang, X. Xiao, and Y. Deng, "Research on Fluid Viscous Damper Parameters of Cable-Stayed Bridge in Northwest China," *Shock and Vibration*, vol. 2017, 2017, doi: 10.1155/2017/4532325.

- [95] M. Martinez-Paneda and A. Y. Elghazouli, “Optimal application of fluid viscous dampers in tall buildings incorporating integrated damping systems,” *Structural Design of Tall and Special Buildings*, vol. 30, no. 17, Dec. 2021, doi: 10.1002/tal.1892.
- [96] M. Dicleli and A. Mehta, “Seismic performance of chevron braced steel frames with and without viscous fluid dampers as a function of ground motion and damper characteristics,” *J Constr Steel Res*, vol. 63, no. 8, pp. 1102–1115, Aug. 2007, doi: 10.1016/j.jcsr.2006.09.005.
- [97] A. Occhiuzzi, “Additional viscous dampers for civil structures: Analysis of design methods based on effective evaluation of modal damping ratios,” *Eng Struct*, vol. 31, no. 5, pp. 1093–1101, May 2009, doi: 10.1016/j.engstruct.2009.01.006.
- [98] C. Christopoulos; A. Filiatrault, *Principles of Passive Supplemental Damping and Seismic Isolation*. Pavia, Italy: IUSS Press, 1835.
- [99] P. Gangwani and A. Suthar, “Comparative Study on Seismic Analysis of Irregular Tall Buildings with Varied Location of Fluid Viscous Damper,” *International Research Journal of Engineering and Technology*, 2021, [Online]. Available: www.irjet.net
- [100] M. Moudgil, “FEASIBILITY STUDY OF USING CROSS-LAMINATED TIMBER CORE FOR THE UBC TALL WOOD BUILDING,” 2014.
- [101] T. Connolly, C. Loss, A. Iqbal, and T. Tannert, “Feasibility study of mass-timber cores for the UBC tall wood building,” *Buildings*, vol. 8, no. 8, Aug. 2018, doi: 10.3390/buildings8080098.
- [102] K.-L. Chang and C.-C. Chen, “Outrigger System Study for Tall Building Structure with Central Core and Square Floor Plate,” in *CTBUH, Proceedings of the CTBUH 2004 Seoul Conference*, 2004, pp. 853–866.
- [103] Pacific Earthquake Engineering Research Center, “PEER Ground Motion Database,” ngawest2.berkeley.edu.
- [104] R. Pinho. Stelios Antoniou, “Seismo Match,” 2024.
- [105] P. Fast, B. Gafner, R. Jackson, and J. Li, “CASE STUDY: AN 18 STOREY TALL MASS TIMBER HYBRID STUDENT RESIDENCE AT THE UNIVERSITY OF BRITISH COLUMBIA, VANCOUVER.”
- [106] G. M. Del Gobbo, A. Blakeborough, and M. S. Williams, “Improving total-building seismic performance using linear fluid viscous dampers,” *Bulletin of Earthquake Engineering*, vol. 16, no. 9, pp. 4249–4272, Sep. 2018, doi: 10.1007/s10518-018-0338-4.